ESTIMATION OF DIFFUSE SOLAR IRRADIATION AND ITS EFFECTS ON PV POWER PLANT PRODUCTION AT METU NCC

A THESIS SUBMITTED TO
THE BOARD OF GRADUATE PROGRAMS
OF
MIDDLE EAST TECHNICAL UNIVERSITY NORTHERN CYPRUS CAMPUS

BY

GENCO KAVAS

IN PARTIAL FULFILLMENT OF THE REQUIREMENTS
FOR
THE DEGREE OF MASTER OF SCIENCE
IN
SUSTAINABLE ENVIRONMENT AND ENERGY SYSTEMS PROGRAM

AUGUST 2019

Approval of the Board of Graduate Program

Prof. Dr. Gürkan Karakaş
Chairperson

I certify that this thesis satisfies all the requirements as a thesis for the degree of Master of Science

Asst. Prof. Dr. Ceren İnce Derogar
Program Coordinator

This is to certify that we have read this thesis and that in our opinion it is fully adequate, in scope and quality, as a thesis for the degree of Master of Science.

Asst. Prof. Dr. Onur Taylan
Supervisor

Examining Committee Members

Assoc. Prof. Dr. Murat Fahrioğlu	Electrical and Electronics Engineering, METU NCC	
Asst. Prof. Dr. Onur Taylan	Mechanical Engineering, METU NCC	
Prof. Dr. Serkan Abbasoğlu	Energy Systems Engineering, Cyprus International University	
Asst. Prof. Dr. Canraş Batunlu	Electrical and Electronics Engineering, METU NCC	
Asst. Prof. Dr. Tuğçe Yüksel Bediz	Mechatronics Engineering, Sabanci University	

I hereby declare that all information in this document has been obtained and presented in accordance with academic rules and ethical conduct. I also declare that, as required by these rules and conduct, I have fully cited and referenced all material and results that are not original to this work.

Name, Last name: Genco KAVAS

Signature:

ABSTRACT

ESTIMATION OF DIFFUSE SOLAR IRRADIATION

AND ITS EFFECTS ON PV POWER PLANT PRODUCTION AT METU NCC

Kavas, Genco

M.Sc., Sustainable Environment and Energy Systems

Supervisor: Assist. Prof. Dr. Onur Taylan

August 2019, 84 pages

Excess amount of greenhouse gas (GHG) emission is the main reason of global warming. Renewable energy systems are one possible way to decrease GHG emission and solar energy is one of options; however, fluctuations on solar energy production is one of the main drawbacks. Accurate estimation of energy production from a solar power plant, such as PV-based plant is important to satisfy energy demand successfully. To be able to estimate energy production in advance, solar energy incident on PV modules should be known first. For this thesis, the most accurate model is sought to estimate solar energy on a tilted surface in Cyprus. To be able to estimate total solar energy on a tilted surface GHI, DNI and DHI values should be known; however, DHI measurement is available for some parts of the World for a limited period. There are some models to estimate DHI and as a first step the most accurate model is found to estimate DHI for Cyprus. Different models from the literature have been checked and models which give accurate results in the locations which are close Cyprus are determined and these models are checked for Cyprus. According to this comparison Bailek's 23rd model is selected as the most accurate model to estimate for

Cyprus. For the second part of this thesis, different models to estimate total solar energy on a tilted surface are checked. Estimation results were compared with measurements collected with a 30° tilted pyranometer in METU NCC. Liu-Jordan, Perez, Muneer, Skartveit-Olseth- Hay and Davies- Reindl, HDKR and Badescu models were checked and according to comparison results simple, isotropic models like Liu-Jordan and Badescu gave more accurate results than most sophisticated model Perez. %RMSE between tilted measurement and isotropic models (Badescu and Liu-Jordan) were 17%. Same steps were repeated with DHI estimated with Bailek's 23rd model and some equations are suggested according to DHI measurements collected in METU NCC. %RMSE between measured tilted irradiation and tilted irradiation calculated with DHI estimated with Bailek's 23rd model was 68%. Additionally, %RMSE for total tilted energy calculated with equation created for this study was 72%. Energy production from a PV power plant with this tilted estimation was compared with actual production of METU NCC PV power plant. %RMSE between actual production and estimation with measured DHI was about 20% for all the models, but Badescu model gave the most accurate estimation with 18%. %RMSE calculated for the same models, but instead of measured DHI, DHI estimated with Bailek's 23 model was used and results were within 24%, Badescu model gave the most accurate estimation with 22%. %RMSE calculated energy production from tilted measurement which has the same tilt angle with PV modules of METU NCC PV power plant. %RMSE was 20.3% and this showed that energy production estimation with measured or estimated DHI was very close to energy estimation amount with measured titled irradiation. These results showed that DHI can be estimated with Bailek's 23 model accurately, simple isotropic models such as Badescu or Liu-Jordan can be used to estimate total irradiation on a tilted surface accurately. When these

estimations are used to estimate energy production of PV power plant, they would work with a high accuracy.

Keywords: solar energy, DHI estimation, estimation of total solar energy on a tilted surface, energy production with PV systems.

ÖZ

YAYILI GÜNEŞ IŞINIMI TAHMİNİ VE

FOTOVOLTAİK ENERJİ SANTRALİ ÜRETİMİNE OLAN ETKİLERİ

Kavas, Genco

Yüksek Lisans, Sürdürülebilir Çevre ve Enerji Sistemleri

Tez Yöneticisi: Dr. Öğr. Üyesi Onur Taylan

Ağustos 2019, 84 sayfa

Sera gazı salınımı, küresel ısınmanın başlıca sebeplerinden birisi ve bu salınımı azaltma yollarından birisi de güneş enerjisi gibi temiz enerji kaynaklarının kullanımının arttırılmasıdır. Güneş enerjisi ile üretim yapmanın bazı olası problemleri var ve bunların başında enerji üretim miktarının gün içindeki dalgalanmaları geliyor. Bunlar göz önünde bulundurularak enerji üretimi daha önceden tahmin edilerek enerji tüketim ihtiyacının karşılanıp karşılanamayacağının bilinmesi önemlidir. Tüm bunları sağlamanın başında fotovoltaik (PV) modüllerinin üzerine düşen toplan enerji miktarının bilinmesi geliyor. Eğimli modül üzerine ulaşacak olan toplam güneş enerji miktarını hesaplamaya yardımcı olan birçok modeller literatürde mevcut fakat bunların hepsi her lokasyon için doğru sonuçları veremiyor. Bu tez kapsamında literatürdeki modeller incelenip Kıbrıs için uygun olabilecek modeller belirlendi ve bu modeller ODTÜ KKK güneş istasyonundan toplanan verilerle karşılaştırıldı. Ayrıca güneşten gelen toplam ışınımın 2 şeklinden biri olan yayılı gelen ışığın (DHI) doğru tahmini bu tezin amaçlarından birisidir. Güneş ışığı doğrudan ve yayılı ile gelen olmak üzere ikiye ayrılır ve yayılı gelen güneş enerjisinin ölçümü, ölçüm işleminin zor ve

çok pahalı cihazlar gerektirmesi nedeni ile Dünya'nın birçok yeri için mevcut değildir. DHI değerinin doğru tahmini için de birçok model mevcuttur ve bu tezde ayrıca mevcut modelleri incelenip Kıbrıs için uygun olabilecek modeller belirlendikten sonra bu modeller toplanmış olan DHI ölçümleri ile karşılaştırılmıştır. Bu karşılaştırma sonuçlarına göre Kıbrıs için en uygun DHI tahmin modeli, Bailek'in 23. Modeli olarak belirlenmiştir. Eğimli yüzey üzerindeki toplam güneş enerjisi miktarını tahmin etmek için Liu-Jordan, Perez, Munner, Skartveit-Olseth, Hay and Davies, Reindl, HDKR ve Badescu modelleri kullanıldı. Bu modellerin vermiş olduğu değer ODTÜ KKK'den toplanan 30°'lik eğime sahip piranometre yardımı ile toplanan verilerle karşılaştırıldı. Eğimli yüzey üzerindeki toplam güneş enerjisi 3 farklı şekilde hesaplandı; (i) ölçülmüş DHI ile, (ii) Bailek'in 23. modeli ile hesaplanan DHI ile ve (iii) ODTÜ KKK'de toplanan DHI ölçümleri yardımıyla çıkarılan 2 denklemi kullanarak. Sırasıyla bu yöntemlerin vermiş olduğu %RMSE değerleri %18, 70% ve %74 civarlarındadır. Bu değerler 8 farklı model için dörder kez hesaplandı ve bu sonuçlara göre Liu-Jordan ve Badescu modelleri izotopik ve basit modeller olmalarına rağmen, anizotrop olan gelişmiş modellerden gerçeğe daha yakın tahmin sonuçları verdiler. Bu sonuçlara göre, Kıbrıs şartları için, izotropic modeller kullanarak eğimli yüzey üzerine düşen toplam güneş enerjisi tahmini yapmak en iyisi olacaktır. Ayrıca tüm bu modeller ve sonuçlar kullanılarak enerji üretim tahmini üzerinde karşılaştırmalar yapıldı. Tahmini üretim değerleri ODTÜ KKK da bulunan 1 MW kurulu gücündeki güneş enerji santralinin gerçek üretimiyle kıyaslandı ve her bir yöntemde çıkan %RMSE değerinin enerji üretimindeki %RMSE değerlerinden düşük çıktığı görüldü. Tüm bunlar yorumlandığında sonuç olarak Bailek'in 23. modellinin DHI tahmini için en iyi model olduğu, Badescu modelinin eğimli yüzeyde ki toplam güneş enerjisi tahmini için en

iyi model olduğu söylenebilir. Ayrıca, bu değerler kullanarak enerji üretimi kontrol edildiğinde güneş enerjisi tahmininde ki farkların enerji üretiminde daha da azaldı görülmekte. Belirtilen 2 model kullanarak DHI ölçümü olmayan lokasyonlar için sadece GHI ölçümü kullanarak enerji üretim tahmini başarılı bir şekilde yapılabilir.

Anahtar Kelimeler: güneş enerjisi, DHI tahmini, eğimli yüzeyde toplam güneş enerjisi tahmini, PV sistemlerinde enerji üretimi.

DEDICATIONS

To my beloved parents for their continuous support during my whole life. I love you with my whole hearth.

ACKNOWLEDGEMENTS

I would like to thank my advisor Dr. Onur Taylan for his supports throughout my studies at METU NCC. His supports started during my undergraduate education in Mechanical Engineering and in the last 5 years I learned lots of things from him. Also I would like thank Mechanical Engineering department of METU NCC for the education which I get during undergraduate study and for giving me the opportunity of working as a teaching assistant during my graduate study. Thanks to education which I got and working experience as a teaching assistant I believe that I have become a successful engineer and I want to thank all of my professors for that. I especially thank to Dr. Murat Sönmez, Dr. Volkan Esat, Dr. Behzat Kentel and Dr. Eray Uzgoren, Dr. Eşref Eşkinat, they taught me lots of things and they were very helpful whenever I need them. Also I would like to thank Laboratory technicians, especially Hamza Çoban who helped me to prepare my experimental setup for this thesis study. I would like to thank Ahmet Alas for giving me the opportunity of working as a student assistant at Science and Technology Center of METU NCC and helping me when I need.

Besides, I would like to thank my great friends with whom I had lots of unforgettable moments and fun, Sinem, Erim, Kağan, Mustafa, Barış, Koray, Ahmet, Ahmad, Safa. My friends are very important for me and they were like my family here, we spent lots of time together. I want to especially thank to my friends Sinem Balaç, Erim Gürer, Coşkun Kağan Özel, Mustafa Kumbur and Barış Ördek.

My biggest thanks go to my parents Süleyman Kavas, Semra Kavas and my brother Alihan Kavas. Their support is precious to me and I owe everything in my life to their endless support and love.

TABLE OF CONTENT

ABSTRACT iii

ÖZ vi

DEDICATIONS ix

ACKNOWLEDGEMENTS x

TABLE OF CONTENT xii

LIST OF FIGURES xiv

LIST OF TABLES xvi

CHAPTER 1 – INTRODUCTION 1

1.1. Problem Statement 1

1.2. Objective of the Study 2

CHAPTER 2 – LITERATURE REVIEW 5

2.1. Studies in Literature about Accuracy of Estimating Diffuse Radiation with Clearness Index 5

2.2. Studies in Literature about Comparison of Different Solar Models to Estimate Total Solar Energy Which is Incident on a Tilted Surface 22

CHAPTER 3 – METHODOLOGY 39

3.1. Geometrical Relations 39

3.2. Models Used to Estimate Solar Radiation on a Tilted Surface 43

3.2.1. Liu and Jordan’s Isotropic Sky Model 43

3.2.2. HDKR Model 44

3.2.3. Perez Model 45
3.2.4. Muneer Model 47
3.2.5. Skartveit Olseth Model 47
3.2.6. Hay and Davies Model 48
3.2.7. Reindl Model 48
3.2.8. Badescu's Isotropic Model 49
3.3. Energy Production from a PV Power Plant 49
3.4. Data Collection Process and Important Information of METU NCC Solar Power Plant 50
CHAPTER 4 – RESULTS AND DISCUSSION 54
4.1. Results for DHI Estimation with Different Models 54
4.2. Estimation Results of Total Solar Radiation Which is Incident on a Tilted Plate 61
4.3. Energy Production Comparison for 1 MW Solar Power Plant in METU NCC 65
CHAPTER 5 – CONCLUSIONS 72
REFERENCES 77
APPENDIX 84

LIST OF FIGURES

Figure 1. Solar energy components [4] 2

Figure 2. Comparison of the statistical performance of group 1, 2 and 3. (a) U_{95}, 95% uncertainty indicator; (b) R correlation coefficient [8]. 9

Figure 3. Comparison results for 8 new models from literature and models. (a) equation of models; (b) statistical results and accuracy rank [8]. 9

Figure 4. Comparison of values of monthly average DHI measured and estimated for Gebze [22]. 16

Figure 5. Distribution of DHI measurement stations in China [23]. 20

Figure 6. Average daily solar radiation on tilted surface for 6 models and measured data from a tilted surface ($Hgmt$) [47]. 29

Figure 7. Mean Absolute Percentage Error (MAPE) for 6 models [47]. 31

Figure 8. Mean Bias Error (MBE) for 6 models [47]. 31

Figure 9. Root Mean Square Error (RMSE) for 6 models [47]. 31

Figure 10. t-statistics for 6 models [47]. 32

Figure 11. Measured and estimated tilted radiation for different models and tilt angles for April (Beta means tilt angle of plate) [48]. 34

Figure 12. MBE for global radiation on inclined surface [54]. 37

Figure 13. RMSE for global radiation on inclined surface [54]. 37

Figure 14. Monthly averages on 45^{o} tilted surface [54]. 37

Figure 15. Some of the important angles to define geometric relation between the Sun and a surface [55]. 39

Figure 16. Relation between the Sun and earth [55]. 42

Figure 17. Beam, diffuse and ground reflected radiation on a tilted surface [55]. 44

Figure 18. METU NCC solar station without shading ball. 51
Figure 19. METU NCC solar station with manufactured shading ball. 52
Figure 20. METU NCC solar station with manufactured shading ball. 52
Figure 21. Aerial view of METU NCC solar power plant. 53
Figure 22. DHI/GHI ratio vs. clearness index (kt) for November and December of 2017. 55
Figure 23. DHI/Go ratio vs. clearness index (kt) for November and December of 2017. 56
Figure 24. DHI/G_O comparison with clearness index (k_t) according to Bailek's 23rd model for November and December of 2017. 58
Figure 25. Daily sum of measured GHI, measured DHI and DHI values estimated according to Bailek 23 model and derived equations according to collected data from METU NCC solar station. 60
Figure 26. Daily total radiation amounts for estimation models and measured tilted radiation 64
Figure 27. Daily total energy production comparison for different days with $Gtilted$ calculated with measured DHI. 68
Figure 28. Daily total energy production comparison for different days with $Gtilted$ calculated with Bailek's 23rd DHI model. 69

LIST OF TABLES

Table 1. Geographic locations and data collection period of Adrar, Ghardaia and Tamanrasset [8]. 6

Table 2. Equations and coefficients of sun-shine based DHI estimation models [8]... 6

Table 3. Equations and coefficients of clearness index and sunshine duration based DHI estimation models [8]. 7

Table 4. Geographical locations of Ankara, Istanbul and Izmir [18]. 11

Table 5. MBE, RMSE, MAPE, SSRE, RSE, R2 and s-stat values of equations for each city [18]. 13

Table 6. Functions of three groups of Bakirci's study. 14

Table 7. Geographical locations and data measurement periods for 8 cities of Turkey [22]. 14

Table 8. Regression coefficients for models 1-15 [22]. 17

Table 9. Statistical indicators of derived models with Gebze DHI measurements [22]. 17

Table 10. Statistical indicators of derived models with Gebze DHI measurements [22]. 18

Table 11. Iqbal model and A.A. El-Sebaii model parameters at 16 stations in China, the data used are between January 1 1994 and December 1998 [23]. 20

Table 12. Parameters of Liu and Jordan model [23]. 21

Table 13. nMBE results of 26 different models for 4 different locations and 18 different tilt and azimuth angle combinations [25]. 24

Table 14. nRMSE results of 26 different models for 4 different locations and 18 different tilt and azimuth angle combination [25]. 25

Table 15. MBE and RMSE of models which Li et al used on all sky conditions [44]. 26
Table 16. MBE of models which Li et al used on different sky conditions [44]. 27
Table 17. RMSE of models which Li et al used on different sky conditions [44]. 27
Table 18. MBE of models which Li et al. used on different orientations [44]. 28
Table 19. RMSE of models which Li et al. used on different orientations [44]. 28
Table 20. Estimated value of total radiation on a horizontal surface [47]. 30
Table 21. RMSE and MBE results for Circumsolar, Isotropic, Klucher and Hay models [48]. 33
Table 22. Comparison of regression (calculated =a+ b x measured) and correlation coefficient (R), RMSE, MBE for south facing (A) and west facing (B) surface. RMSE and MBE are in units of MJ/m^2 [50]. 35
Table 23. Ratio of monthly average daily radiation on a tilted surface and horizontal surface for experimental, isotropic model and anisotropic model [54]. 38
Table 24. Brightness coefficient for Perez Anisotropic Sky Model [5]. 46
Table 25. RMSE values according to measured DHI and estimated DHI with Bailek (2018) models. 57
Table 26. RMSE values according to measured DHI and estimated DHI with Bakirci (2015) models. 57
Table 27. RMSE values according to measured DHI and estimated DHI with Ulgen (2009) models. 57
Table 28. RMSE values of DHI calculated with trend-line equations of and Figure 22 and Figure 23. 58
Table 29. %RMSE results for 8 different models for 4 different DHI includes sun rise and sun set hours. 63

Table 30. %RMSE results for 8 different models for 4 different DHI without sun rise and sun set hours. 63

Table 31. %RMSE results of energy production from METU NCC solar power plant which are calculated with measured DHI, DHI via Bailek's 23rd model [8] and measured $Gtilted$ 66

Table 32. %RMSE between energy production estimation from G_{tilted} which is calculated with measured DHI and with Bailek's 23rd model [8] and measured energy production..... 71

CHAPTER 1 – INTRODUCTION

1.1. Problem Statement

In today's world living without electrical energy is almost impossible and there are different energy production methods to satisfy this energy demand. Conventional energy production methods such as coal, oil or natural gas based thermal power plants are reliable systems however, these systems cause significant amount of greenhouse gas (GHG) emission which is the main cause of global warming and climate change [1]. To decline the effects of climate change, GHG emission should be decreased. Renewable energy-based power plants do not emit GHG during energy production because they use clean energy resources such as sun, wind, hydro, etc. [2] One of the drawbacks of renewable energy systems is that energy production is not at a constant rate, it fluctuates. Point of interest of this thesis is solar energy and for solar, energy production amount of a solar power plant varies with time-based on the variations in the solar resource. It is important to be able to properly estimate the energy production that will be produced in advance because energy produced should ideally match the energy consumption requirement. To estimate energy production of a photovoltaic (PV) module, solar radiation which is incident on a PV module should be known. PV modules are mostly placed with a tilt angle to increase solar income but estimating solar income on a tilted surface is not an easy task. To estimate total solar energy on tilted PV modules, expensive and sophisticated measurement tools are required but for most of the locations data for these tools are not available [3]. Because of these reasons there are different models to estimate solar energy on a tilted surface, but the estimation accuracy of these models is not high for some locations. Optimum solar

estimation model should be determined for Cyprus because island is not interconnected to mainland and sudden changes at ratio between energy consumption and production may cause fatal system failures. Also estimating solar energy potential of a PV power plant is important for economic aspects.

1.2. Objective of the Study

Estimation of solar energy on a tilted surface is an important task of solar energy-based projects. Energy income on a flat surface can be increased by tilting the surface with an angle. Tilt angle which maximize energy income of these surfaces can be calculated. Calculation of tilt angle is completely another task because this angle should be adjusted according to energy load. However, almost all of the PV modules or solar thermal panels are installed with a tilt angle. For horizontal and tilted surfaces solar energy income has 3 components; direct solar energy, diffuse solar energy and albedo solar energy. Figure 1 shows direct (beam), diffuse and reflected (albedo) solar energy. Albedo solar energy is energy reflected from ground and reaches to flat surface. Albedo can be assumed zero for horizontal surfaces because if a surface is horizontal to ground, energy reflected from ground would not reach to these flat surfaces.

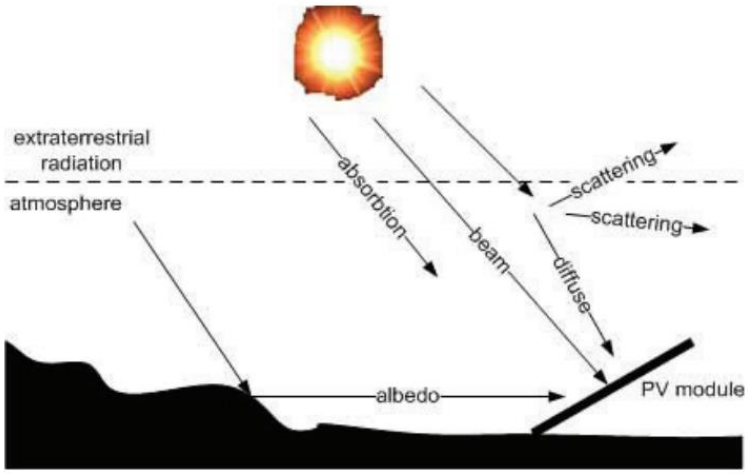

Figure 1. Solar energy components [4]

Calculating solar energy income is important especially for large size solar power plants. Correct estimation of energy production will be helpful to know the financial situation of the project. For investors, correct energy income estimation means good or bad investment and by the help of better estimation, if they see solar power plant will produce more energy than previous estimations, investments in this field will increase. As the investments in this field increase, carbon emission rate will decrease because more investment to solar energy means less investment to conventional power plants which causes lots of GHG emissions. Another importance of correct estimation is that if the correct energy production of solar power plate is known beforehand, backup systems will be prepared according to that. Just like other renewable energy systems solar based power plants do not give power output all the time. Weather conditions and the position of the sun directly affect how much energy reaches flat surfaces and energy output of these power plants changes. Because of these reasons, the correct estimation of power output will be helpful for financial analysis and preparing backup systems according to total energy requirement.

The objective of this thesis is that investigating available studies in the solar energy field and see which models are used to determined total solar radiation on a tilted flat plate. After that models which is more suitable for METU NCC and Cyprus weather conditions will be determined. Total solar radiation on a tilted surface will be calculated with most suitable models and these results will be compared with tilted measurements which were collected from METU NCC solar power plant. As a result of these comparisons most accurate model to estimate total solar radiation on a tilted surface for Cyprus and locations near to Cyprus. Lastly, the amount of theoretical energy production from 1 MW solar power plant of METU NCC will be calculated and compared with the real production amount of same power plant. Purpose of this

comparison is to see when the estimation accuracy for solar radiation on a tilted surface increase, the estimation accuracy of energy production from a PV power plant is increasing or decreasing.

There are lots of different models to calculate solar energy income on a tilted flat plate. Calculation of direct solar energy on a tilted surface is straight forward and same for these models; however, diffuse solar energy calculation is different for each model and it causes the highest computational error during power output estimation. Calculation of ground reflected solar energy which is called albedo may cause computational errors; however, the magnitude of albedo is much less than other two solar energy components and errors in the computation of albedo may be neglected [5][6].

Aim of this thesis is calculating solar energy on a tilted surface with different models and predict how much energy will be produced from METU NCC solar power plant. The power plant is placed in METU NCC and it has 1 Megawatt (MW) power. This power plant was established in March 2016 and hourly energy production from this power plant has been known since that time. This data set will be compared with energy production predictions which were calculated according to total solar energy on a tilted surface. As explained before, solar energy on a tilted surface will be calculated with different models and results will be used in energy production calculations. Models which will be used to compare with measurements are Liu's isotropic sky, HDKR (Combination of Hay and Davies, Klucher and Reindl models) Perez, Muneer, Skartveit Olseth, Hay and Davies, Reindl and Badescu's isotropic models.

CHAPTER 2 – LITERATURE REVIEW

In this part of the thesis, available studies in literature about estimation of diffuse solar radiation from GHI or G_o and some models which estimates total solar irradiation on a horizontal plate with different considerations will be shown. In section 2.1 some of the available studies about estimation of diffuse solar radiation which is incident on a horizontal plate are shown and in section 2.2 different studies from different locations about total solar radiation estimation on a tilted plate are shown.

2.1. Studies in Literature about Accuracy of Estimating Diffuse Radiation with Clearness Index

Estimation of solar energy on a tilted surface requires diffuse horizontal radiation (DHI) and direct normal irradiation (DNI) measurements for most of the models. For most of the locations these measurements are not available because establishment cost of devices for these measurements are very high [7]. Most common measurement is global horizontal irradiation (GHI) and it is available for so many different locations. GHI measurement requires only one pyranometer. There are different models to estimate DHI from GHI. These models typically use clearness index or sunshine duration.

In one of these studies, Bailek et al. (2018) [8] compared different models to estimate DHI for Sahara Desert in Algerian Big South. They measured GHI and DHI for 6 years' period from 2010 to 2015. They applied statistical test methods on their estimation to be able to see accuracies of these models. They divided these models into three groups. Models in group 1 are sunshine duration based, models in group 2 are based on clearness index and models in group 3 are based on sunshine duration and

clearness index. They compared 35 models from group 1, 2 and 3 for Adrar region. After that, they completed comparison and selected most accurate model for Adrar region, they compared this model with 8 different models available in the literature for different time periods of Ghardaia and Tamanrasset regions of Algeria. Table 1 shows geographical locations, data collection period, monthly mean daily sunshine hour (S) and some climatic information for Adrar, Ghardaia and Tamanrasset. Table 2 and Table 3 shows 35 models compared with Adrar measurements. Table 2 shows model equations and coefficients of these equations for sun-shine duration-based models and Table 3 shows for clearness factor-based models and sun-shine duration & clearness factor-based models. In table 2 and 3 S_0 represents maximum possible sun-shine duration and K_t represents clearness index.

Table 1. Geographic locations and data collection period of Adrar, Ghardaia and Tamanrasset [8].

Station	Adrar	Ghardaia	Tamanrasset
Latitude $(°N)$	27.88	32.36	22.78
Longitude $(°N)$	-0.27	3.81	5.51
Elevation (m)	269	450	1378
Data series period	2010-2015	2005-2008	2010-2012
Mean GHI (MJ/m^2day)	6.89	7.44	7.26
Mean S $(Hour)$	9.27	8.68	9.20
Mean T $(°C)$	25.9	21.34	22.71
Mean $Relative\ Humidity$ (%)	23	38.82	28.6

Table 2. Equations and coefficients of sun-shine based DHI estimation models [8].

Models		General forms of the models	Values of coefficients			
			a	b	c	d
D1	Sunshine duration-based models	$H_d/H = a + b(S/S_0) + c(S/S_0)^2 + d(S/S_0)^3$	0.918	−0.786	0.0	0.0
D2			0.137	1.193	−1.244	0.0
D3			7.943	−28.938	37.281	−16.316
D4		$H_d/H = a + blog(S/S_0)$	0.148	−0.617		
D5		$H_d/H = a + bexp(S/S_0)$	1.081	−0.355		
D6		$H_d/H = a + expb(S/S_0)$	−0.075	−1.272		
D7		$H_d/H_0 = a + b(S/S_0)$	0.555	−0.447		
D8		$H_d/H_0 = a + blog(S/S_0) + c(S/S_0)^2$	−0.104	1.225	−1.051	
D9		$H_d/H_0 = a + b(S/S_0) + c(S/S_0)^2 + d(S/S_0)^3$	7.206	−26.993	35.028	−15.280
D10		$H_d/H_0 = a + blog(S/S_0)$	0.118	−0.350		
D11		$\frac{H_d}{H_0} = a + bexp(S/S_0)$	0.649	−0.203		
D12		$H_d/H_0 = a + expb(S/S_0)$	−0.307	−0.852		

D1 is taken from [9], D2 is taken from [10], D3 is taken from [11], D4 is taken from [12], D7 is taken from [13] , D9 is taken from [14], and D10 is taken from [12], D13 is taken from [15], D14 is taken from [16] , D15 is taken from [17], D19 is taken from [13], D20 is taken from [11], D21 is taken from [18], D25 is taken from [19], D26 is taken from [3], D27 is taken from [15], and D32 is taken from [3].

Table 3. Equations and coefficients of clearness index and sunshine duration based DHI estimation models [8].

Models	Regression equation	Values of coefficients						
		a	*b*	*c*	*d*	*e*	*f*	*g*
clearness index-based models (Category II)								
D13	$H_d/H = a + bK_t + cK_t^2 + dK_t^3$	0.797	−0.734	0.0	0.0			
D14		−4.612	15.113	−11.580	0.0			
D15		−15.724	64.032	−83.180	34.845			
D16	$H_d/H = a + blog(K_t)$	0.109	−0.486					
D17	$H_d/H = a + bexp(K_t)$	1.042	−0.377					
D18	$H_d/H = a + expb(K_t)$	−0.008	−1.451					
D19	$H_d/H_0 = a + bK_t + cK_t^2 + dK_t^3$	0.341	−0.206	0.0	0.0			
D20		−3.780	11.868	−8.823	0.0			
D21		−4.101	13.282	−10.892	1.007			
D22	$H_d/H_0 = a + blog(K_t)$	0.150	−0.130					
D23	$H_d/H_0 = a + bexp(K_t)$	0.417	−0.109					
D24	$H_d/H_0 = a + expb(K_t)$	−0.387	−0.765					
Sunshine duration and clearness index-based models (Category III)								
D25	$H_d/H = a + bK_t + c(S/S_0)$	0.529	0.867	−1.047				
D26	$\frac{H_d}{H} = a + bK_t + cK_t^2 + d(S/S_0) + e(S/S_0)^2$	−2.657	8.511	−5.609	0.420	−0.907		
D27	$\frac{H_d}{H} = a + bK_t + cK_t^2 + dK_t^3 + e(S/S_0) + f(S/S_0)^2 + g(S/S_0)^3$	21.898	−91.591	140.845	−71.227	−6.262	7.268	−3.322
D28	$H_d/H = a + blog(K_t) + clog(S/S_0)$	0.321	0.585	−0.819				
D29	$H_d/H = a + bexp(K_t) + cexp(S/S_0)$	0.474	0.437	−0.473				
D30	$H_d/H = a + exp(bK_t) + exp(cS/S_0)$	−0.967	−0.162	−1.246				
D31	$H_d/H_0 = a + bK_t + c(S/S_0)$	0.159	0.884	−0.713				
D32	$H_d/H_0 = a + bK_t + cK_t^2 + d(S/S_0) + e(S/S_0)^2$	−2.487	7.160	−4.605	0.568	−0.793		
D33	$\frac{H_d}{H_0} = a + bK_t + cK_t^2 + dK_t^3 + e(S/S_0) + f(S/S_0)^2 + g(S/S_0)^3$	21.229	−88.295	134.985	−67.857	−6.929	8.446	−3.781
D34	$H_d/H_0 = a + blog(K_t) + clog(S/S_0)$	0.294	0.598	−0.556				
D35	$H_d/H_0 = a + bexp(K_t) + cexp(S/S_0)$	0.029	0.446	−0.323				

Figure 2 shows the minimum and maximum certainty indicators at 95% and R values among all the considered estimations. According to these results group 1 models have the highest R value and the lowest U_{95} values. Group 2 models have the lowest R value and the highest U_{95} values among these three groups. As a conclusion of Figure 2, it can be said that group 1 has the most accurate models and group 3 has the least accurate models. Figure 3 shows statistical results for 35 different models. Bailek et al. [8] checked mean percentage error (MPE), root mean square error (RMSE), U95, R, t-stat (showed as TS in the table) and global performance indicator (GPI). Last column of Figure 3 shows rank of accuracy for 35 models and most accurate model was D2.

Bailek et al. [8] compared D2 with 8 other models with using Adrar, Ghardaia and Tamanrasset data. Figure 3 shows the 8 models from literature and statistical results for them. These models compared with D2 for 3 different locations in Sahara Desert in Algeria and D2 model is the most accurate among these 9 models. To conclude, Bailek et al. [8] compared DHI estimation models for 3 different locations in Sahara Desert in Algeria for different time periods and they found that most accurate model to estimate DHI from GHI was in group 1 which use only sunshine duration. Models use clearness index showed worse accuracy than models use sun-shine duration for Sahara Desert climatic conditions [8].

There are explanations for some statistical comparison methods which is used in this study and in other studies. Mean Absolute Percentage Error (MAPE), Mean Bias Error (MBE), Root Mean Square Error (RMSE) and t-statistic. MAPE indicates accuracy of results as percentage. MBE provides information on the long-term performance of models. Normally low value of MBE is desired. Positive value of MBE gives average of over-estimation and negative MBE values give average under-estimations. A drawback of this test is that some under and over estimations will cancel each other. Other test methods are required to get actual accuracy of models. RMSE gives information on short-term performance of models. This term is always positive; zero value is desired. Lower RMSE means that better performance for solar model.

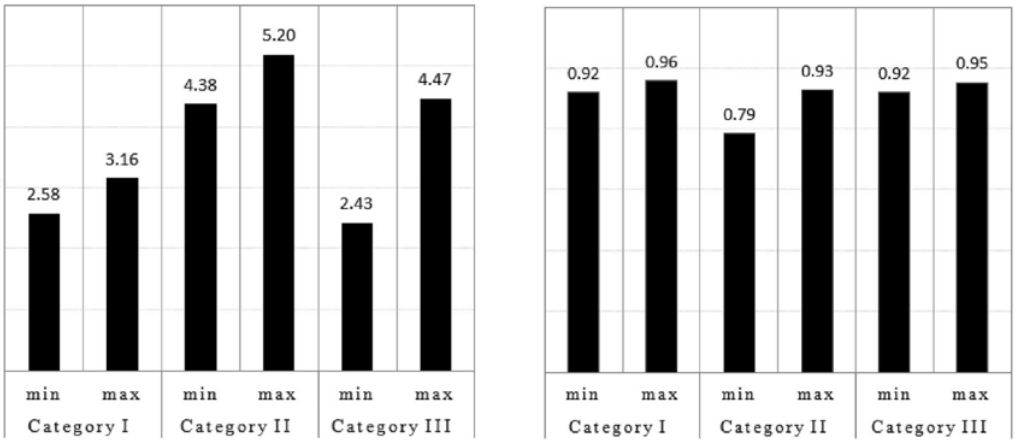

(a) (b)

Figure 2. Comparison of the statistical performance of group 1, 2 and 3. (a) U_{95}, 95% uncertainty indicator; (b) R correlation coefficient [8].

$$H_d/H = -0.59276 + 4.60382(S/S_0) - 6.85670(S/S_0)^2 + 3.06795(S/S_0)^3 \quad (9)$$

$$H_d/H = 0.888 - 0.737K_t - 0.176(S/S_0) \quad (10)$$

$$H_d/H = 0.79 - 0.59(S/S_0) \quad (11)$$

$$H_d/H = 0.927 - 0.595(S/S_0) - 0.164K_t \quad (12)$$

$$H_d/H = 0.798 - 0.0702(S/S_0) - 0.7475K_t \quad (13)$$

$$H_d/H = 3.494 - 9.025K_t + 6.224\,K_t^2 \quad (14)$$

$$H_d/H_0 = 0.311 + 0.078(S/S_0) - 0.314(S/S_0)^2 \quad (15)$$

$$H_d/H_0 = -2.313 + 7.393(S/S_0) - 5.314(S/S_0)^2 \quad (16)$$

(a)

Models	MPE	RMSE	U95	R	TS	GPI	Rank
Adrar site							
D2	−0.010	0.935	2.578	0.951	1.657	0.943	1
Eq (9)	0.152	2.510	6.190	0.917	5.162	−1.937	5
Eq (10)	0.198	2.517	5.973	0.967	6.497	−2.155	6
Eq (11)	−0.088	1.049	2.905	0.943	1.769	0.464	2
Eq (12)	−0.151	1.121	2.892	0.959	3.751	−0.138	3
Eq (13)	0.238	2.892	6.814	0.959	6.778	−2.755	8
Eq (14)	0.170	2.798	6.897	0.876	5.184	−2.447	7
Eq (15)	0.169	1.901	4.469	0.951	6.872	−1.551	4
Eq (16)	0.266	2.942	7.399	0.684	4.548	−3.554	9
Tamanrasset site							
D2	−0.056	1.163	3.245	0.906	0.287	0.659	1
Eq (9)	0.330	4.775	12.075	0.258	4.377	−3.341	9
Eq (10)	0.282	3.606	8.867	0.471	5.269	−2.530	7
Eq (11)	−0.177	1.363	3.352	0.929	5.261	−0.039	2
Eq (12)	−0.213	1.717	4.210	0.887	5.361	−0.224	3
Eq (13)	0.330	3.926	9.445	0.402	6.006	−2.965	8
Eq (14)	−0.235	4.619	12.848	−0.021	0.704	−2.030	5
Eq (15)	0.125	2.046	5.278	0.783	3.769	−0.856	4
Eq (16)	0.273	3.532	9.181	0.617	3.526	−2.068	6
Ghardaia site							
D2	0.137	2.071	5.156	0.825	4.997	1.068	1
Eq (9)	0.225	4.768	12.490	0.147	4.157	0.030	7
Eq (10)	0.207	3.971	10.284	0.259	4.633	0.156	6
Eq (11)	−0.196	3.762	10.378	0.411	1.480	1.060	2
Eq (12)	−0.256	4.077	11.154	0.388	2.061	1.050	3
Eq (13)	0.280	4.008	9.989	0.270	6.183	−0.182	8
Eq (14)	−0.284	3.910	10.703	0.161	2.026	0.744	5
Eq (15)	0.069	3.355	9.106	0.372	2.533	0.856	4
Eq (16)	2.409	31.756	84.292	0.168	3.597	−2.447	9

(b)

Figure 3. Comparison results for 8 new models from literature and models. (a) equation of models; (b) statistical results and accuracy rank [8].

In another study, Ulgen and Hepbasli (2009) investigated DHI estimation models for Turkey's big cities [18]. They used clearness index and sunshine duration to estimate DHI separately. They used monthly averages of daily diffuse and global solar radiation for 16 years, starting from 1990 to 2006. They divided their investigation to four groups. Group 1 and 3 are function of clearness index. Group 2 and 4 are functions of sunshine duration. For group 1, ratio between DHI and GHI is a function of clearness

index. For group 2, ratio between DHI and GHI is a function of sunshine duration. For group 3, ratio between DHI and extraterrestrial radiation (I_o) is a function of clearness index (k_t) [11] and for group 4, ratio between DHI and extraterrestrial radiation (I_o) is a function of sun-shine duration (S). S_o represents maximum possible daily sunshine hour.

Group 1 [20]; $$K_d = \frac{DHI}{GHI}) \approx f\left(k_t = \frac{GHI}{I_o}\right)$$

Group 2 [21]; $$(K_d = \frac{DHI}{GHI}) \approx f\left(\frac{S}{S_o}\right)$$

Group 3 [11]; $$(K_{dd} = \frac{DHI}{I_o}) \approx f\left(k_t = \frac{GHI}{I_o}\right)$$

Group 4 [21]; $$(K_{dd} = \frac{DHI}{I_o}) \approx f\left(\frac{S}{S_o}\right)$$

There are 17 different models under group 1, 6 different models under group 2, 3 different models under group 3 and 6 different models under group 4 category. For example, Equations (1), (2), (3), and (4) show one example for group 1, 2, 3 and 4, respectively [18].

$$K_d = 1.1244 - 1.5582k_t + 0.3635k_t^2 \quad (1)\ [11]$$

$$K_d = 0.663 - 0.4883 \cdot \frac{S}{S_o} \quad (2)\ [11]$$

$$K_{dd} = 0.331 - 0.233k_t \quad (3)\ [11]$$

$$K_{dd} = 0.2205 - 0.0126 \cdot \frac{S}{S_o} - 0.1292 \cdot \left(\frac{S}{S_o}\right)^2 \quad (4)\ [21]$$

Ulgen and Hepbasli compared these DHI estimation models for Ankara, Istanbul and Izmir in Turkey [18]. Geographical locations of these cities are shown in Table 4. They checked accuracy of DHI estimation models from the years of 1990-2006. Extraterrestrial radiation (I_o) and maximum possible sun-shine duration (S_o) were calculated from fundamental mathematical expressions and they are shown in equation (38) and (40) respectively. Since DHI measurements for these 3 cities were not available for that time period, Ulgen and Hepbasli used average of these 32 models to calibrate new correlation models. 8 new hybrid models were developed by taking linear and polynomial forms of each group. Equations (5)-(12) These equations are developed for whole Turkey region and for places have similar climatic conditions. The authors also checked all these 32 models for these 3 cities individually. Statistical test methods were applied to model results. Most accurate models for each city determined individually for all the groups. According to group 1 results, Equation (5) has the smallest t-stat value for Ankara and Izmir and Equation (6) has the smallest t-stat value for Istanbul. According to group 2 results, Equation (7) has the smallest t-stat value for Ankara, Istanbul and Izmir. According to group 3 results, Equation (9) has the smallest t-stat value for Ankara and Istanbul and Equation (10) gives the smallest t-stat value for Izmir. Lastly, for group 4, Equation (11) gives the smallest t-stat value for Istanbul and Izmir and Equation (12) gives the smallest t-stat value for Ankara. The authors suggested to use models give smallest t-stat values for these cities. Equations (47)-(54) in Table 5 correspond to Equation (5)-(12) in this work [18].

Table 4. Geographical locations of Ankara, Istanbul and Izmir [18].

Station	Longitude	Latitude	Altitude (m)
Ankara	$32°53'$	$39°57'$	894
Istanbul	$29°05'$	$40°58'$	39
Izmir	$27°10'$	$38°24'$	15

Group 1; $$K_d = 0.6772 - 0.4841k_t, \quad R^2 = 0.9707 \tag{5}$$

Group 1; $$K_d = 0.981 - 1.9028k_t + 1.9319k_t^2 - 0.6809k_t^3, \quad R^2 = 0.9979 \tag{6}$$

Group 2; $$K_d = 0.5456 - 0.2242\frac{S}{S_o}, \quad R^2 = 0.9037 \tag{7}$$

Group 2; $$K_d = 0.6595 - 07841\frac{S}{S_o} + 0.7461\left(\frac{S}{S_o}\right)^2 - 0.2579\left(\frac{S}{S_o}\right)^3, \quad R^2 = 0.9722 \tag{8}$$

Group 3; $$K_{dd} = 0.1155 + 0.1958k_t, \quad R^2 = 0.9965 \tag{9}$$

Group 3; $$K_{dd} = 0.0273 + 0.727k_t - 1.0411k_t^2 + 0.6659k_t^3, \quad R^2 = 0.9974 \tag{10}$$

Group 4; $$K_{dd} = 0.1677 + 0.0926\frac{S}{S_o}, \quad R^2 = 0.9662 \tag{11}$$

Group 4; $$K_{dd} = 0.1437 + 0.2151\frac{S}{S_o} - 0.1748\left(\frac{S}{S_o}\right)^2 + 0.0697\left(\frac{S}{S_o}\right)^3, \quad R^2 = 0.9820 \tag{12}$$

Table 5. MBE, RMSE, MAPE, SSRE, RSE, R2 and s-stat values of equations for each city [18].

Eqs. No.	ANKARA							ISTANBUL							IZMIR						
	MBE	RMSE	MPE	MAPE	SSRE	RSE	R^2	t^a	MBE	RMSE	MPE	MAPE	SSRE	RSE	R^2	t^a	MBE	RMSE	MPE	MAPE	SSRE	RSE	R^2	t^a
Group I																								
10	−0.653	1.253	−5.295	5.295	0.293	0.156	1.000	2.024	−0.151	0.739	1.873	1.873	0.170	0.119	1.000	0.693	−1.044	1.456	−12.501	12.501	0.334	0.167	1.000	3.412
11	−1.592	2.315	−18.317	18.317	0.880	0.271	0.999	3.141	−0.880	1.523	−8.428	8.428	0.418	0.187	1.000	2.350	−2.165	2.680	−28.418	28.418	1.218	0.319	1.000	4.547
12	−1.649	2.047	−22.407	22.407	0.744	0.249	1.000	4.505	−1.215	1.538	−17.136	17.136	0.441	0.192	1.000	4.270	−1.995	2.309	−27.680	27.680	1.001	0.289	1.000	5.687
13	−1.583	2.302	−18.157	21.386	0.873	0.270	0.999	3.140	−0.875	1.524	−8.223	15.422	0.424	0.188	1.000	2.324	−2.156	2.663	−28.340	28.340	1.206	0.317	1.000	4.576
14	1.106	1.748	26.352	31.499	1.662	0.372	0.999	2.710	1.909	2.080	38.765	38.765	2.232	0.431	0.999	7.666	0.520	1.398	14.184	22.972	0.802	0.259	1.000	1.330
15	0.368	0.835	12.008	16.605	0.540	0.212	1.000	1.627	0.857	1.055	21.713	22.135	1.001	0.289	1.000	4.621	−0.032	0.573	2.284	8.411	0.109	0.095	1.000	0.185
16	−0.586	0.903	−6.297	8.487	0.137	0.107	1.000	2.827	−0.287	0.579	−2.063	6.347	0.068	0.075	1.000	1.892	−0.821	1.041	−10.570	10.570	0.180	0.122	1.000	4.256
17	−1.270	1.605	−16.777	16.777	0.449	0.193	1.000	4.292	−0.898	1.198	−11.667	11.951	0.255	0.146	1.000	3.753	−1.566	1.815	−21.703	21.703	0.617	0.227	1.000	5.662
18	−0.540	0.979	−4.613	10.187	0.180	0.122	1.000	2.192	−0.154	0.604	1.184	8.769	0.118	0.099	1.000	0.876	−0.841	1.131	−10.343	10.501	0.204	0.130	1.000	3.682
19	−1.916	3.256	−17.766	33.181	2.095	0.418	0.930	2.414	−0.366	1.863	9.788	33.702	2.520	0.458	0.857	0.665	−2.914	3.990	−36.779	36.779	2.483	0.455	0.995	3.546
20	1.689	2.170	29.675	30.429	1.581	0.363	0.999	4.110	2.066	2.563	29.397	35.442	1.762	0.383	0.997	4.515	1.504	1.952	29.217	30.736	1.642	0.370	1.000	4.007
21	0.751	1.146	8.915	8.988	0.206	0.131	1.000	2.878	0.359	0.590	4.154	4.612	0.057	0.069	1.000	2.544	1.034	1.396	12.937	12.937	0.306	0.160	1.000	3.656
22	−0.501	0.831	−4.950	7.997	0.119	0.100	1.000	2.504	−0.202	0.509	−0.691	6.150	0.061	0.072	1.000	1.430	−0.732	0.961	−9.179	9.179	0.149	0.112	1.000	3.895
23	−0.068	0.912	3.627	13.355	0.258	0.147	1.000	0.247	0.396	0.663	10.043	12.259	0.239	0.141	1.000	2.468	−0.406	0.977	−2.606	10.627	0.181	0.123	1.000	1.515
24	−0.649	1.286	−4.972	4.972	0.316	0.162	1.000	1.939	−0.124	0.760	2.574	2.574	0.193	0.127	1.000	0.550	−1.059	1.491	−12.573	12.573	0.350	0.171	1.000	3.343
25	−0.642	1.275	−4.756	14.073	0.321	0.163	1.000	1.934	−0.120	0.783	2.991	12.160	0.219	0.135	1.000	0.514	−1.058	1.470	−12.658	13.358	0.342	0.169	1.000	3.433
26	−0.637	1.282	−4.490	14.315	0.335	0.167	1.000	1.898	−0.090	0.789	3.928	12.939	0.260	0.147	1.000	0.383	−1.063	1.483	−12.725	13.329	0.346	0.170	1.000	3.408
47	**−0.017**	**0.118**	**−0.106**	**1.318**	**0.003**	**0.015**	**1.000**	**0.481**	**0.024**	**0.076**	**−0.040**	**1.177**	**0.004**	**0.017**	**1.000**	**1.085**	**−0.023**	**0.139**	**0.151**	**1.746**	**0.004**	**0.019**	**1.000**	**0.557**
48	**−0.005**	**0.024**	**−0.071**	**0.381**	**0.000**	**0.005**	**1.000**	**0.770**	**−0.004**	**0.023**	**−0.066**	**0.423**	**0.000**	**0.005**	**1.000**	**0.537**	**0.006**	**0.023**	**0.105**	**0.279**	**0.000**	**0.003**	**1.000**	**0.898**
Group II																								
27	−1.103	1.648	−12.533	12.533	0.451	0.194	1.000	2.986	−0.749	1.176	−8.589	8.589	0.230	0.139	1.000	2.739	−1.613	2.243	−19.231	19.231	0.779	0.255	1.000	3.432
28	−1.072	1.638	−11.497	11.497	0.467	0.197	1.000	2.874	−0.724	1.216	−7.290	7.290	0.260	0.147	1.000	2.461	−1.565	2.136	−18.733	18.733	0.720	0.245	1.000	3.569
29	−1.222	1.759	−13.028	13.028	0.620	0.227	1.000	3.203	−1.237	1.702	−14.445	14.445	0.500	0.204	1.000	3.511	−1.692	2.095	−21.747	21.747	0.745	0.249	0.999	4.543
30	−0.687	1.183	−6.726	6.726	0.244	0.143	1.000	2.367	−0.410	0.793	−3.694	3.694	0.112	0.096	1.000	2.004	−1.112	1.702	−12.239	12.239	0.446	0.193	1.000	2.864
31	−0.688	1.191	−6.783	6.783	0.244	0.143	1.000	2.349	−0.405	0.785	−3.731	3.731	0.108	0.095	1.000	2.001	−1.123	1.736	−12.287	12.287	0.462	0.196	1.000	2.814
32	−0.697	1.194	−7.020	7.020	0.241	0.142	1.000	2.382	−0.429	0.821	−4.234	4.234	0.115	0.098	1.000	2.035	−1.072	1.637	−11.706	11.706	0.419	0.187	1.000	2.875
49	**0.023**	**0.114**	**0.335**	**0.335**	**0.003**	**0.015**	**1.000**	**0.673**	**−0.023**	**0.091**	**−1.187**	**1.187**	**0.010**	**0.028**	**1.000**	**0.878**	**−0.012**	**0.281**	**1.046**	**1.046**	**0.021**	**0.042**	**1.000**	**0.138**
50	**0.017**	**0.055**	**0.385**	**0.385**	**0.002**	**0.014**	**1.000**	**1.046**	**−0.071**	**0.079**	**−1.336**	**1.336**	**0.003**	**0.015**	**1.000**	**6.945**	**0.036**	**0.072**	**0.998**	**0.998**	**0.004**	**0.018**	**1.000**	**1.939**
Group III																								
33	−0.598	1.249	−3.129	3.129	0.398	0.182	1.000	1.807	−0.045	0.942	6.804	6.804	0.512	0.207	1.000	0.157	−1.059	1.389	−13.146	13.146	0.315	0.162	1.000	3.906
34	−0.640	1.276	−4.681	4.681	0.323	0.164	1.000	1.923	−0.112	0.783	3.216	3.216	0.227	0.138	1.000	0.479	−1.057	1.472	−12.637	12.637	0.342	0.169	1.000	3.421
35	−0.630	1.280	−4.311	4.311	0.340	0.168	1.000	1.875	−0.074	0.797	4.463	4.463	0.288	0.155	1.000	0.310	−1.058	1.479	−12.657	12.657	0.344	0.169	1.000	3.399
51	**−0.005**	**0.026**	**−0.101**	**0.101**	**0.000**	**0.006**	**1.000**	**0.684**	**−0.002**	**0.029**	**0.017**	**0.017**	**0.000**	**0.006**	**1.000**	**0.195**	**0.009**	**0.023**	**0.131**	**0.131**	**0.000**	**0.003**	**1.000**	**1.467**
52	**−0.006**	**0.024**	**−0.076**	**0.076**	**0.000**	**0.004**	**1.000**	**0.802**	**−0.005**	**0.022**	**−0.085**	**0.085**	**0.000**	**0.005**	**1.000**	**0.731**	**0.006**	**0.024**	**0.102**	**0.102**	**0.000**	**0.003**	**1.000**	**0.850**
Group IV																								
36	−1.225	1.864	−12.562	12.562	0.648	0.232	1.000	2.892	−0.689	1.408	−3.787	3.787	0.496	0.203	1.000	1.861	−1.788	2.241	−23.019	23.019	0.838	0.264	1.000	4.391
37	−0.299	1.156	2.433	2.433	0.508	0.206	1.000	0.888	0.217	0.963	11.769	11.769	0.694	0.241	1.000	0.769	−0.835	1.351	−8.509	8.509	0.301	0.158	1.000	2.605
38	−1.683	2.336	−19.894	19.894	0.928	0.278	1.000	3.444	−1.094	1.750	−11.089	11.089	0.567	0.217	1.000	2.656	−2.320	2.870	−30.392	30.392	1.387	0.340	1.000	4.559
39	−0.622	1.212	−4.030	4.030	0.351	0.171	1.000	1.983	−0.174	0.908	3.749	3.749	0.371	0.176	1.000	0.646	−1.072	1.450	−12.938	12.938	0.337	0.167	1.000	3.642
40	−0.627	1.236	−4.540	4.540	0.316	0.162	1.000	1.952	−0.155	0.841	3.051	3.051	0.271	0.150	1.000	0.624	−1.116	1.608	−13.011	13.011	0.399	0.182	1.000	3.199
41	−0.622	1.236	−4.359	4.359	0.325	0.165	1.000	1.930	−0.141	0.829	3.433	3.433	0.286	0.154	1.000	0.572	−1.141	1.655	−13.304	13.304	0.419	0.187	1.000	3.156
53	**−0.029**	**0.040**	**−0.405**	**0.405**	**0.001**	**0.007**	**1.000**	**3.477**	**0.042**	**0.060**	**1.117**	**1.117**	**0.004**	**0.018**	**1.000**	**3.323**	**0.001**	**0.106**	**−0.563**	**0.563**	**0.004**	**0.019**	**1.000**	**0.033**
54	**−0.027**	**0.058**	**−0.480**	**0.480**	**0.001**	**0.009**	**1.000**	**1.786**	**0.055**	**0.064**	**1.008**	**1.008**	**0.002**	**0.012**	**1.000**	**5.363**	**−0.009**	**0.047**	**−0.463**	**0.463**	**0.002**	**0.012**	**1.000**	**0.629**

Additionally, Bakirci (2015) [22] established new solar models to estimate DHI after he checked several different models in the literature. Bakirci [22] used measurements from different cities of Turkey and established new models for different cities of Turkey. He used monthly average daily values of GHI and sunshine duration between the years of 1975 and 2007. He compared results of 15 different DHI estimation models and came up with 18 new DHI estimation models. He grouped models into three groups. In group 1; monthly mean diffuse fraction is a function of monthly mean clearness index. In group 2; monthly mean diffuse fraction is a function of the monthly mean sunshine duration and in group 3; monthly mean diffuse fraction is a function of monthly mean clearness index and monthly mean sunshine duration. Table 7 shows the cities Bakirci considered, geographical location and data collection period.

Table 6. Functions of three groups of Bakirci's study.

Group 1; $\frac{DHI}{GHI} = f(k_t)$	Group 2; $\frac{DHI}{GHI} = f(S)$	Group 3; $\frac{DHI}{GHI} = f(k_t, S)$

Table 7. Geographical locations and data measurement periods for 8 cities of Turkey [22].

Location	Longitude ($°E$)	Latitude ($°N$)	Elevation (m)	Measured data	
				Period	Total years
Adana	35.18	36.59	20	1975-2007	33
Ankara	32.53	39.57	894	1975-2006	32
Diyarbakır	40.12	37.55	660	1975-2007	33
Erzurum	41.16	39.55	1869	1975-2007	33
Istanbul	29.05	40.58	39	1975-2006	32
Izmir	27.10	38.24	25	1975-2006	32

Samsun	36.20	41.17	44	1975-2006	32
Trabzon	39.43	41.00	30	1975-2005	31

Bakirci [22] derived 18 new models to estimate DHI. He used GHI, I_o, sunshine duration and maximum possible sunshine duration measurements supplied by Turkish State Meteorological Service for 8 typical meteorological stations in Turkey. Bakirci [22] applied MBE, MABE and RMSE statistical test methods and calculated R value for these models. According to his results, all of the 18 derived models show very good accuracy for average of Turkey. Also, some models that Bakirci used to derive new models showed good accuracy for Turkey. According to Bakirci's result, most accurate model for average of the eight cities is found and this model is shown as Equation (13). This model uses both clearness index and sunshine duration. Bakirci had more 5 years of DHI data for Gebze city and he compared some models from the literature and some models that he derived with these data. He applied statistical test methods to models that he collected from literature and choose the most accurate models for Gebze and Turkey. Figure 4 shows comparison results between measured DHI values from Gebze and estimated DHI values from 5 different models. Figure 4 contains Eq. 24, M1, M4, M15 and E-2 which correspond to Equations (13), (14), (15), (16) and (17) respectively, in this study. MABE and RMSE values for 18 new derived models are shown in Table 9 and Table 10. Also, Table 8 shows regression coefficients for these models. MABE and RMSE values for these models are higher than acceptable range except for eq. 24 which is shown as Equation (13) in this study. According to Bakirci's work it can be concluded that to estimate DHI from GHI clearness index is not enough by itself. Models which are function of clearness index and sun-shine duration showed better accuracies [22].

$$K_d = 0.8130 - 0.2041k_t - 0.8108k_t^2 + 0.5217k_t^3 - 0.0491\frac{S}{S_0} - 0.5646\left(\frac{S}{S_0}\right)^2 - 0.3961\left(\frac{S}{S_0}\right)^3, \quad R = 1 \tag{13}$$

$$K_d = 1.0 - 1.13k_t \tag{14}$$

$$K_d = 0.583 - 0.9985k_t - 5.24k_t^2 + 5.322k_t^3 \tag{15}$$

$$K_d = 0.7463 + 1.2922k_t - 3.7966k_t^2 - 0.7285\frac{S}{S_0} + 1.0592\left(\frac{S}{S_0}\right)^2 \tag{16}$$

$$K_d = 1.0087 - 1.0779k_t - 0.1058k_t^2 \tag{17}$$

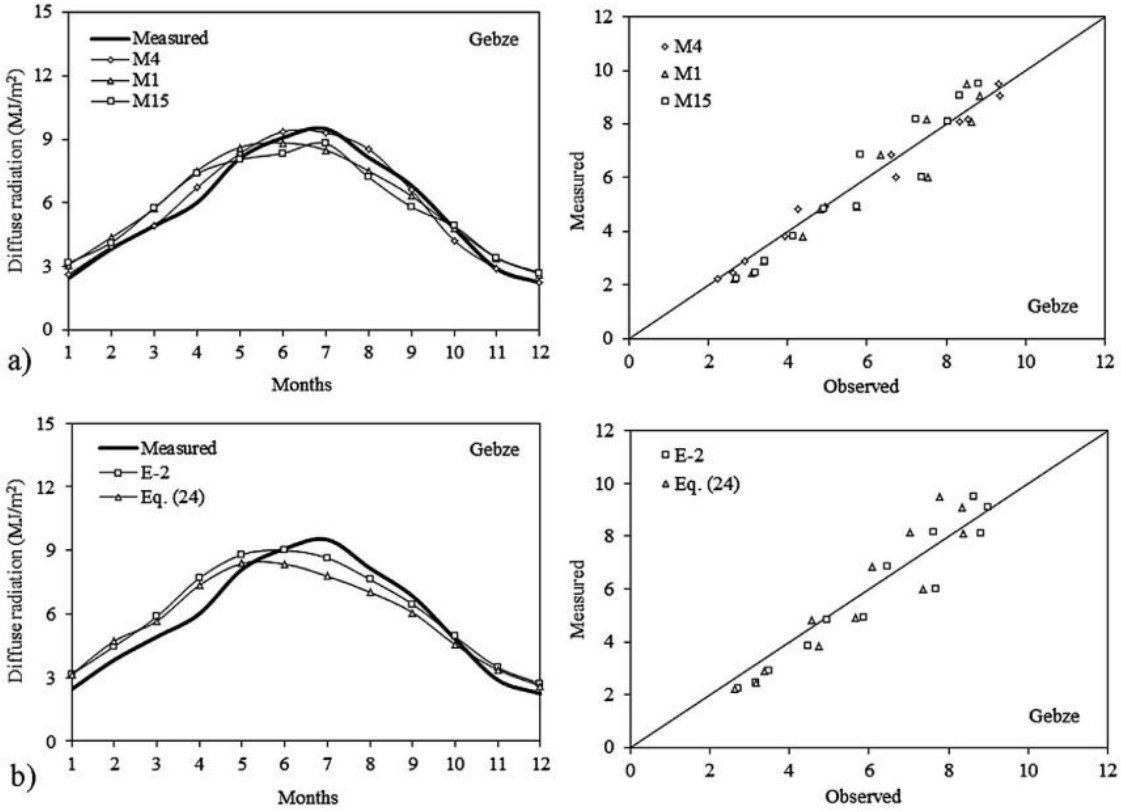

Figure 4. Comparison of values of monthly average DHI measured and estimated for Gebze [22].

Table 8. Regression coefficients for models 1-15 [22].

Function	Equations	a	b	c	d	R^2
$K_d = f(k_t)$	E-1. Linear	1.0328	−1.1801	–	–	0.9332
	E-2. Quadratic	1.0087	−1.0779	−0.1058	–	0.9333
	E-3. Cubic	0.7385	0.6507	−3.7177	2.4684	0.9335
$K_d = f(S/S_0)$	E-4. Linear	0.7379	−0.5268	–	–	0.9408
	E-5. Quadratic	0.7715	−0.6632	0.1241	–	0.9423
	E-6. Cubic	0.8042	−0.8704	0.5278	−0.2449	0.9424
$K_{dd} = f(k_t)$	E-7. Linear	0.2684	−0.1079	–	–	0.2312
	E-8. Quadratic	−0.0072	1.0640	−1.2132	–	0.4399
	E-9. Cubic	−0.1173	1.7684	−2.6850	1.0058	0.4411
$K_{dd} = f(S/S_0)$	E-10. Linear	0.2581	−0.0800	–	–	0.6420
	E-11. Quadratic	0.2031	0.1436	−0.2034	–	0.7583
	E-12. Cubic	0.1467	0.5005	−0.8989	0.4219	0.7723

Table 9. Statistical indicators of derived models with Gebze DHI measurements [22].

	E-1	E-2	E-3	E-4	E-5	E-6	E-7	E-8	E-9
Adana									
MBE	0.38033	0.38667	0.38333	0.21489	0.38308	0.38134	−0.23354	−0.25782	−0.24875
MABE	0.38492	0.38995	0.38539	0.28268	0.38693	0.38411	0.23880	0.25782	0.24875
RMSE	0.48580	0.49164	0.48117	0.35331	0.48777	0.47998	0.28878	0.29826	0.28469
Ankara									
MBE	0.18373	0.18578	0.17875	0.11478	0.18356	0.17921	−0.07850	−0.07713	−0.07283
MABE	0.25872	0.26010	0.24947	0.26469	0.25819	0.25042	0.10568	0.09874	0.09204
RMSE	0.33725	0.33715	0.32080	0.34902	0.33515	0.32321	0.15315	0.12732	0.12355
Diyarbakir									
MBE	−0.17535	−0.18998	−0.16833	0.04746	−0.18535	−0.17163	0.29463	0.33021	0.31353
MABE	0.21015	0.21531	0.21106	0.44750	0.21284	0.21182	0.32587	0.33340	0.32574
RMSE	0.25767	0.26072	0.25994	0.53241	0.26021	0.26065	0.39256	0.40029	0.39430
Erzurum									
MBE	−0.25393	−0.25249	−0.26653	−0.31410	−0.25510	−0.26512	0.36230	0.35766	0.36092
MABE	0.51347	0.51199	0.50838	0.58379	0.51215	0.50957	0.43189	0.40951	0.40865
RMSE	0.64603	0.64553	0.64719	0.67653	0.64601	0.64713	0.57150	0.56746	0.56313
Istanbul									
MBE	0.16705	0.16910	0.16151	0.12465	0.16698	0.16001	−0.10022	−0.11483	−0.10663
MABE	0.19015	0.19142	0.17810	0.23540	0.18951	0.17709	0.12680	0.12043	0.11765
RMSE	0.28515	0.28892	0.27656	0.26712	0.28586	0.27632	0.14433	0.14443	0.13559
Izmir									
MBE	0.06852	0.06296	0.05950	0.13665	0.06331	0.06098	0.07828	0.10112	0.09333
MABE	0.15640	0.14567	0.14516	0.35819	0.14893	0.14838	0.18344	0.14740	0.16012
RMSE	0.19965	0.18636	0.18879	0.44355	0.19019	0.19190	0.21468	0.16783	0.18253
Samsun									
MBE	−0.02558	−0.02214	−0.01781	−0.12007	−0.02388	−0.01887	−0.00223	−0.02217	−0.02434
MABE	0.09349	0.09591	0.08973	0.14515	0.09399	0.08926	0.08435	0.06507	0.06583
RMSE	0.12682	0.12779	0.11733	0.20139	0.12667	0.11718	0.09964	0.07446	0.07813
Trabzon									
MBE	0.06011	0.05648	0.06536	0.14983	0.05807	0.06709	−0.22134	−0.21427	−0.22100
MABE	0.11065	0.11042	0.11660	0.16079	0.11071	0.11685	0.22134	0.21427	0.22107
RMSE	0.13145	0.13119	0.14048	0.18378	0.13158	0.14101	0.25142	0.25728	0.26855
Gebze									
MBE	0.32987	0.32974	0.32055	0.34813	0.32839	0.31933	−0.24432	−0.24729	−0.23961
MABE	0.64577	**0.64156**	0.64704	0.77035	0.64362	0.64559	0.79647	0.80695	0.79867
RMSE	0.75881	**0.75599**	0.76184	0.86774	0.75735	0.76076	0.98986	0.98897	0.97877

Table 10. Statistical indicators of derived models with Gebze DHI measurements [22].

	E-10	E-11	E-12	Eq. (22)	Eq. (23)	Eq. (24)	Eq. (25)	Eq. (26)	Eq. (27)
Adana									
MBE	0.00787	0.09606	0.06420	0.03029	0.01291	**0.00015**	−0.17563	−0.01719	−0.02962
MABE	0.08488	0.10057	0.06808	0.03029	0.02431	**0.00015**	0.17563	0.02156	0.03104
RMSE	0.10247	0.11014	0.09153	0.03830	0.02809	**0.00016**	0.18538	0.02605	0.03587
Ankara									
MBE	**0.00008**	0.00030	−0.01675	0.00822	0.00827	0.00015	−0.05400	0.01081	0.00532
MABE	0.13315	0.05865	0.04403	0.03003	0.02117	**0.00015**	0.10528	0.02279	0.00786
RMSE	0.14625	0.06571	0.05146	0.04001	0.02464	**0.00015**	0.12489	0.02653	0.01001
Diyarbakir									
MBE	−0.01294	−0.09057	−0.04648	−0.04524	−0.02329	**0.00012**	0.19614	−0.00303	0.01348
MABE	0.26339	0.11759	0.09198	0.09046	0.04521	**0.00012**	0.27312	0.04259	0.01913
RMSE	0.30442	0.14717	0.11875	0.13018	0.06454	**0.00013**	0.36671	0.05997	0.02179
Erzurum									
MBE	−0.25347	−0.23296	−0.24538	0.01581	0.01398	**0.00016**	−0.02831	0.00560	−0.00176
MABE	0.31212	0.26249	0.24538	0.02740	0.02166	**0.00016**	0.07695	0.03619	0.02554
RMSE	0.38261	0.37104	0.35702	0.03782	0.02858	**0.00016**	0.10833	0.04652	0.03322
Istanbul									
MBE	0.06649	0.10347	0.07173	0.02558	0.01469	**0.00017**	−0.03283	0.01033	−0.00285
MABE	0.17197	0.10890	0.07751	0.03329	0.02822	**0.00017**	0.16549	0.02583	0.01047
RMSE	0.22395	0.13478	0.10393	0.04565	0.03251	**0.00017**	0.17996	0.02863	0.01340
Izmir									
MBE	−0.00476	−0.05233	−0.03293	−0.02235	−0.00843	**0.00012**	0.06308	0.00605	0.01866
MABE	0.18310	0.06960	0.03827	0.07179	0.03243	**0.00012**	0.15891	0.03730	0.01866
RMSE	0.20623	0.09239	0.04383	0.09882	0.04590	**0.00013**	0.18596	0.04993	0.02007
Samsun									
MBE	−0.05768	0.00397	0.01183	0.01019	−0.00337	**0.00019**	−0.07065	0.00644	0.01139
MABE	0.14622	0.06339	0.05461	0.03226	0.01677	**0.00019**	0.11239	0.01791	0.01236
RMSE	0.16844	0.07659	0.06389	0.04155	0.02071	**0.00020**	0.13114	0.02199	0.01589
Trabzon									
MBE	0.22509	0.19254	0.21824	−0.01585	−0.01357	**0.00021**	0.04252	−0.02709	−0.00953
MABE	0.22509	0.19852	0.22914	0.01606	0.02094	**0.00021**	0.09963	0.04689	0.01903
RMSE	0.24096	0.22560	0.26889	0.01874	0.02382	**0.00022**	0.12487	0.05380	0.02270
Gebze									
MBE	0.20757	0.21281	0.18399	0.02913	0.02488	0.01264	−0.01234	**−0.01002**	−0.01787
MABE	0.88859	0.88904	0.91283	0.77153	0.77263	0.78322	0.88148	0.77435	0.78604
RMSE	0.99405	0.99582	1.02490	0.87735	0.87427	0.89012	0.98949	0.87833	0.89328

Until this point results of studies completed for the locations which are close to Cyprus were shown. These studies gave promising results for locations close to Cyprus and findings of these models will be used in further calculations steps; however, there are some similar studies which were completed for locations which are not close to Cyprus. These studies are also investigated, and it is seen that it is better to use models gave accurate results in the areas which are geographically close to Cyprus. Some of studies far from Cyprus will be shown after this point.

In Rensheng et al.'s study [23], they checked 3 different groups of models to estimate DHI for overall China. The first group is Iqbal's group of models [24]. For these groups of models, ratio between DHI and GHI is based on a polynomial equation which uses sunshine duration and different coefficients. Equation (1818) shows Iqbal's [24] group of models. In the second group of models, El-Sabaii and Trabea's models [14] are used. For this group, ratio between DHI and I_o is calculated as a

polynomial equation based on sunshine duration. Equation (1919) shows El-Sabaii and Trabea's model [14] For the third group, they used Liu and Jordan's model [17] to estimate ratio between DHI and GHI. Equation (2020) shows Liu and Jordan's DHI estimation model. In this equation, Y_0 represents the ratio of DHI/GHI when $k_t < 0.2$. According to that value of X_0 is 0.2. Value of 0.2 is calculated from readings collected from 14 different locations in China for 5 years.

$$\frac{DHI}{GHI} = a + b\left(\frac{S}{S_o}\right) + c\left(\frac{S}{S_o}\right)^2 \tag{18}$$

$$\frac{DHI}{I_o} = a + b\left(\frac{S}{S_o}\right) + c\left(\frac{S}{S_o}\right)^2 \tag{19}$$

$$\begin{aligned} \frac{DHI}{GHI} &= Y_0 \quad for\ k_t < X_0 \\ \frac{DHI}{GHI} &= a + b \cdot k_t \quad for\ k_t > X_0 \end{aligned} \tag{20}$$

Figure 5. Distribution of DHI measurement stations in China [23]. Figure 5 shows distribution of DHI measurement stations in China, and the data from these stations were used in Rensheng et al.'s study [23]. Table 11 shows calculated coefficients and R^2 values for the models of Iqbal [24] and El-Sebaii [14] for different locations in China and mean value and standard deviation (SD) of them. According to the results in Table 11, Iqbal's model [24] gave promising results for China but El-Sebaii's model [14] did not. R^2 values for El-Sebaii's model [14] was very low which showed that this model would not give accurate DHI estimation for China. However, R^2 values for Iqbal's model [24] was about 0.85 and mean value of R^2 was 0.84 which could be used to estimate DHI value for any location in China.

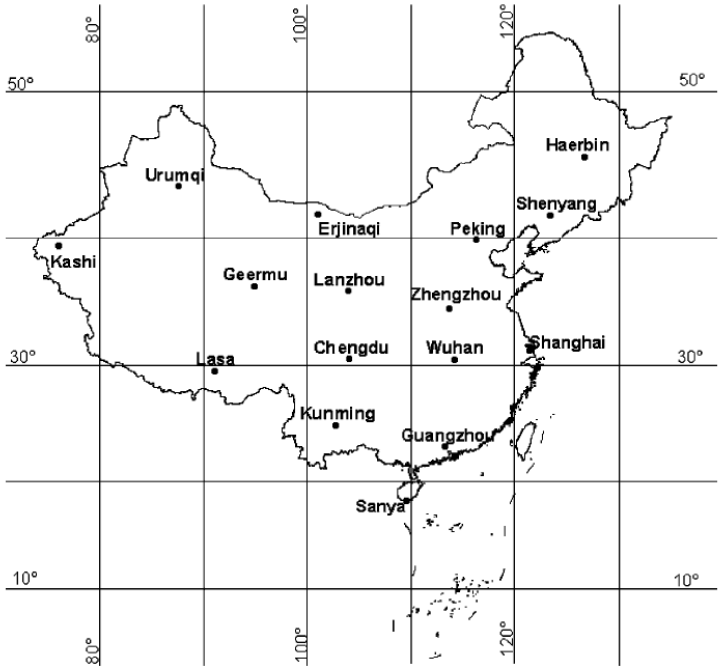

Figure 5. Distribution of DHI measurement stations in China [23].

Table 11. Iqbal model and A.A. El-Sebaii model parameters at 16 stations in China, the data used are between January 1 1994 and December 1998 [23].

Stations	$DHI/GHI = a + b(n/N) + c(n/N)^2$				$DHI/I_0 = a + b(n/N) + c(n/N)^2$			
	a	b	c	R^2	a	b	c	R^2
Haerbin	0.9369	−0.865	0.1109	0.87	0.2085	0.3121	−0.4138	0.44
Urumuqi	0.8623	−0.7202	−0.0109	0.74	0.1793	0.3323	−0.4308	0.26
Erjinaqi	0.9609	−0.4929	−0.4022	0.80	0.2436	0.4801	−0.6661	0.54
Shenyang	0.9349	−0.5678	−0.2174	0.82	0.1744	0.4586	−0.5362	0.32
Peking	0.9584	−0.3067	−0.5735	0.90	0.158	0.6288	−0.7226	0.53
Kashi	0.9608	−0.3474	−0.4936	0.77	0.2293	0.4496	−0.584	0.39
Geermu	0.9674	−0.5578	−0.3553	0.80	0.2241	0.5459	−0.7234	0.59
Lanzhou	0.9826	−0.575	−0.2016	0.85	0.1498	0.5346	−0.5541	0.41
Zhengzhou	0.9727	−0.3823	−0.4426	0.92	0.1558	0.6819	−0.7563	0.54
Shanghai	0.9733	−0.7686	0.0202	0.91	0.1507	0.6081	−0.6553	0.46
Chengdu	0.9833	−0.4262	−0.2645	0.83	0.1351	0.7095	−0.7144	0.56
Wuhan	0.9723	−0.3211	−0.4002	0.83	0.1172	0.6736	−0.654	0.56
Lhasa	0.9063	−0.8837	0.0163	0.80	0.2741	0.1828	−0.4242	0.66
Kunming	0.8714	−0.8109	−0.0555	0.93	0.1658	0.574	−0.6823	0.56
Guangzhou	0.9755	−0.6951	−0.0618	0.92	0.1346	0.6099	−0.6759	0.47
Sanya	0.9074	−0.9492	0.2074	0.81	0.2035	0.2967	−0.4266	0.29
Mean	0.95	−0.60	−0.20	0.84	0.18	0.50	−0.60	0.47
SD	0.04	0.21	0.23	0.06	0.04	0.16	0.12	0.11

Table 12 shows X_0, a and b coefficients and R^2 values for Liu and Jordan's DHI estimation model [17]. R^2 results were higher than El-Sebaii model [14]; however, they were slightly lower than R^2 results of Iqbal's [24] model. Liu and Jordan's DHI

estimation model [23] was also a good option to estimate DHI for all over the China. As a conclusion, Iqbal's model [24] was the best option, and Liu and Jordan's DHI estimation model [23] was the second best model to estimate DHI for all over the China [23] among the investigated options.

Table 12. Parameters of Liu and Jordan model [23].

Stations	$DHI/GHI = Y_0$	$DHI/GHI = a + b(K_t)$		
	X_0	a	b	R^2
Haerbin	0.186	1.2635	−1.5152	0.81
Urumuqi	0.168	1.2411	−1.5463	0.75
Erjinaqi	0.310	1.5698	−1.8935	0.85
Shenyang	0.217	1.3450	−1.6752	0.79
Peking	0.238	1.4044	−1.7723	0.86
Kashi	0.261	1.4321	−1.7216	0.77
Geermu	0.309	1.544	−1.8209	0.84
Lanzhou	0.215	1.3251	−1.5995	0.81
Zhengzhou	0.257	1.4394	−1.7775	0.85
Shanghai	0.239	1.3844	−1.6857	0.88
Chengdu	0.239	1.3417	−1.5019	0.73
Wuhan	0.222	1.3421	−1.6193	0.79
Lhasa	0.217	1.3107	−1.5135	0.82
Kunming	0.227	1.3495	−1.6180	0.90
Guangzhou	0.190	1.2933	−1.638	0.65
Sanya	0.225	1.3803	−1.7674	0.87
Mean	0.233	1.3729	−1.6666	0.81
SD	0.04	0.09	0.12	0.06

In another study, Pandey and Katiyar tried to see the most accurate DHI estimation model for the whole India region [7]. They collected DHI, GHI and sunshine duration data from different cities of India; Jodhpur (Latitude 26.30°N, Longitude 73.03°E), Calcutta (Latitude 22.65°N, Longitude 88.35°E), Bombay (Latitude 19.12°N, Longitude 72.85°E) and Pune (Latitude 18.53°N, Longitude 73.91°E) for 5 years (2001-2005). Their aim was to establish a model which estimates DHI for the whole India with a high accuracy. Least square regression analysis was used to determine coefficients of third-degree polynomial equations of models. Four equations were created with the collected data; Equations (21)-(24). Pandey and Katiyar [7] created another model and called that model AIC(I), this model is shown as Equation (25), and they also tested this model to see the estimation accuracy. They applied statistical test methods to see accuracy of their models. For the first 4 models, differences

between estimated and measured DHI values were about 10%, but the difference for AIC(I) model was less than 5% for all cities. Pandey and Katiyar [7] suggested the AIC(I) model to estimate DHI for the whole India, and suggested to use this model in the locations which have similar weather conditions with India.

$$\frac{DHI}{GHI} = -2.887 + 17.95\left(\frac{S}{S_0}\right) - 29.4\left(\frac{S}{S_0}\right)^2 + 14.92\left(\frac{S}{S_0}\right)^3 \quad (21)$$

$$\frac{DHI}{GHI} = 3.419 - 15.03\left(\frac{S}{S_0}\right) + 25.18\left(\frac{S}{S_0}\right)^2 - 13.86\left(\frac{S}{S_0}\right)^3 \quad (22)$$

$$\frac{DHI}{GHI} = 0.8384 - 0.2841\left(\frac{S}{S_0}\right) - 0.8208\left(\frac{S}{S_0}\right)^2 + 0.4315\left(\frac{S}{S_0}\right)^3 \quad (23)$$

$$\frac{DHI}{GHI} = 1.033 + 0.9107\left(\frac{S}{S_0}\right) - 0.1288\left(\frac{S}{S_0}\right)^2 + 0.0972\left(\frac{S}{S_0}\right)^3 \quad (24)$$

$$\frac{DHI}{GHI} = 0.09781 + 4.763\left(\frac{S}{S_0}\right) - 11.32\left(\frac{S}{S_0}\right)^2 + 7.167\left(\frac{S}{S_0}\right)^3 \quad (25)$$

2.2. Studies in Literature about Comparison of Different Solar Models to Estimate Total Solar Energy Which is Incident on a Tilted Surface

Solar energy is popular at least for last 50-60 years. As the negative effects of conventional carbon based fules understand better and these effects become more and more visible, investments and research & development projects to solar energy and other renewable energy projects are increasing. For instance, before calculating energy production from a PV module, total solar radiation reaches on this module should be calculated correctly. There are lots of different studies about estimating solar incident radiation on a tilted surface, such as a surface of PV modules. In these studies, total solar energy on a tilted surface was calculated with different models and these results were compared with solar measurements on a tilted surface. To the best of my knowledge, there is not any publication for Cyprus; however, there are lots of

publications for different locations. In some models, for the same location different models were suggested for different weather conditions.

For instance, Yang (2016) [25] compared 26 solar models for 4 different locations. Yang [25] collected data from Singapore ($1.30°N; 103.77°E$), Golden (Colorado, US) ($39.74°N; 105.18°W$), Oldenburg (Germany) ($53.15°N; 8.17°E$) and Eugene (Oregon, US) ($44.05°N; 127.07°W$) for one year period and calculated total solar energy on tilted surfaces for different tilt angles and different azimuth angles combinations. Yang [25] compared data from different continents and locations far from each other to generalize a universal model to calculate solar energy on a tilted surface. Yang [25] applied normalized mean bias error (nMBE) and normalized root mean square error (nRMSE) on calculated results to compare accuracy of these models. Table 13 and Table 14 show results for nMBE and nRMSE, respectively, for 18 different cases are shown. Yang calculated solar energy on tilted surfaces for different tilt and azimuth angles combinations and compared these results with measured results. For example, nMBE is 2.2 for Eugene if tilt angle is $30°$ and azimuth angle is $180°$ using Liu and Jordan's isotropic model and nMBE is -21.2 for Eugene if tilt angle is $90°$ and azimuth angle is $0°$ using Klucher's anisotropic model. Original sources of models which are shown in following tables from Yang's [25] study are stated here. Liu [17], Temps [26], Bugler 1 [27], Bugler 2 [28], Klucher [29], Steven 1 [30], Steven 2 [31], Hay 2 [32], Willmott [33], Koronakis [34], Perez 1 [35], Perez 2 [5], Perez 4 [36], Skartveit [37], Gueymard [38], Muneer1 [39], Reindl [40], Olmo 1 [41], Tian [42], Badescu [43].

Table 13. nMBE results of 26 different models for 4 different locations and 18 different tilt and azimuth angle combinations [25].

Model	Eugene (44.05°, −127.07°)			Oldenburg (53.15°, 8.17°)		Singapore (1.30°, 103.77°)			
	(30, 180)	(90, 180)	(90, 0)	(45, 180)	(45, 135)	(10, 64)	(20, 64)	(30, 64)	(40, 64)
Liu	2.2	3.6	−11.1	5.6	3.7	0.3	1.7	0.7	1.0
Temps	−5.3	−11.1	−30.0	−8.3	−9.6	−5.0	−4.0	−5.7	−6.8
Bugler1	−0.5	1.9	−11.2	3.3	1.5	−1.5	−0.1	−1.0	−0.8
Bugler2	2.3	4.5	−5.1	5.1	3.4	0.7	2.2	1.2	1.4
Klucher	−1.1	−3.1	−21.2	−0.7	−2.3	−2.3	−1.1	−2.5	−2.9
Steven1	−4.3	−11.9	6.4	−10.5	−10.4	0.0	1.0	−0.7	−1.4
Steven2	−4.6	−12.2	7.8	−10.8	−10.5	0.0	1.0	−0.7	−1.2
Steven3	3.1	9.1	1.5	8.0	6.2	0.5	2.4	2.1	3.3
Steven4	−1.3	−3.3	5.4	−4.3	−4.2	−0.0	1.0	−0.3	−0.5
Hay1	0.3	1.4	6.3	1.1	0.2	0.2	1.7	0.8	1.3
Hay2	0.2	1.3	7.0	1.0	0.1	0.2	1.7	0.8	1.3
Willmott	1.5	1.3	7.0	3.1	2.3	1.0	3.5	3.2	4.0
Koronakis	1.5	−6.0	−29.1	3.0	1.0	0.2	1.2	−0.5	−1.4
Perez1	−2.0	−5.0	2.6	−2.9	−3.1	−0.1	1.0	−0.1	0.1
Perez2	−2.2	−5.0	1.8	−3.2	−3.4	−0.3	0.7	−0.4	−0.1
Perez3	−1.4	−2.9	3.9	−1.9	−2.3	−0.1	1.1	0.2	0.7
Perez4	−1.2	−2.8	4.0	−1.2	−1.5	0.0	1.3	0.4	0.9
Skartveit	0.6	5.3	19.9	2.1	1.2	0.2	1.9	1.3	2.1
Gueymard	0.6	0.6	−5.2	2.2	1.1	−0.0	1.4	0.5	1.0
Muneer1	0.0	0.2	10.7	0.2	−0.9	0.1	1.2	−0.2	−0.4
Muneer2	−0.4	−2.4	9.9	−0.2	−1.3	0.1	1.1	−0.4	−0.8
Reindl	0.1	−1.8	−3.1	0.4	−0.6	0.2	1.6	0.5	0.5
Olmo1	−7.4	−17.4	−44.2	−10.2	−10.4	−1.9	−0.4	−1.3	−1.1
Olmo2	−4.6	−13.7	−6.4	−7.5	−6.8	4.5	5.8	4.6	4.5
Tian	5.9	3.6	−11.1	11.4	9.7	3.0	6.6	7.0	7.9
Badescu	4.3	3.6	−11.1	11.4	9.7	0.7	3.4	4.3	6.8

Model	Singapore				Golden (39.74°, −105.18°)					Rank
	(90, 90)	(90, 180)	(90, 270)	(90, 0)	(40, 180)	(90, 0)	(90, 90)	(90, 180)	(90, 270)	
Liu	−2.6	−13.8	−5.3	−14.3	3.9	−8.5	2.5	1.6	1.2	15
Temps	−20.7	−30.0	−23.8	−29.9	−3.0	−24.2	−9.3	−9.1	−12.4	26
Bugler1	−3.7	−14.0	−6.1	−14.5	1.1	−8.5	0.6	−0.3	−0.5	12
Bugler2	−1.7	−11.7	−4.0	−12.4	3.6	−3.2	3.2	1.9	2.7	16
Klucher	−12.0	−22.3	−14.7	−22.5	0.2	−17.8	−4.3	−4.3	−6.6	19
Steven1	−11.6	−10.9	−12.3	−9.7	−2.9	5.0	−4.2	−8.8	−6.7	18
Steven2	−10.9	−10.1	−11.6	−8.6	−3.2	6.3	−3.8	−9.0	−6.3	20
Steven3	5.9	−4.0	4.0	−4.9	5.1	1.2	7.4	5.6	6.8	17
Steven4	−6.6	−7.3	−5.7	−7.6	−0.9	4.8	−0.8	−5.0	−3.4	11
Hay1	−0.8	−6.3	−1.1	−7.2	1.0	7.7	2.3	−1.3	1.6	6
Hay2	−0.8	−6.0	−1.0	−7.0	0.9	8.3	2.3	−1.4	1.6	5
Willmott	−0.8	−6.0	−1.0	−7.0	2.1	8.3	2.3	−1.4	1.6	13
Koronakis	−16.4	−28.6	−19.9	−28.7	2.7	−23.4	−6.0	−5.5	−8.7	21
Perez1	−3.1	−5.9	−2.2	−5.7	−1.2	1.8	−1.2	−5.5	−2.9	8
Perez2	−2.8	−5.4	−1.9	−5.4	−1.4	1.2	−1.3	−5.4	−2.7	10
Perez3	−0.9	−3.4	0.0	−3.8	−0.5	3.0	0.1	−3.8	−1.4	2
Perez4	−0.6	−4.1	0.0	−4.4	−0.3	2.9	0.5	−3.7	−0.8	1
Skartveit	5.0	1.3	5.5	−0.0	1.4	15.5	5.1	0.8	5.0	14
Gueymard	−2.3	−9.3	−3.4	−10.2	1.5	−4.8	−0.0	−1.9	−1.4	7
Muneer1	−1.4	−7.3	−1.3	−7.1	0.4	7.7	1.6	−2.9	−0.0	3
Muneer2	−2.0	−7.6	−1.7	−8.0	−0.3	7.1	−0.2	−5.1	−1.5	4
Reindl	−7.0	−13.9	−8.0	−14.6	0.7	−0.3	−0.9	−3.8	−2.1	9
Olmo1	−13.2	−22.8	−16.4	−20.4	−7.4	−32.6	−9.4	−10.0	−15.5	25
Olmo2	−10.2	−10.8	−9.3	−9.8	−3.0	2.4	−5.1	−9.9	−7.3	24
Tian	−2.6	−13.8	−5.3	−14.3	7.4	−8.5	2.5	1.6	1.2	23
Badescu	−2.6	−13.8	−5.3	−14.3	6.8	−8.5	2.5	1.6	1.2	22

These results show that most of models struggle with vertical surfaces' calculations. Yang aimed to be able to suggest a universal model after this work; however, nMBE and nRMSE results showed that it is not possible to suggest a universal solar model. Order of accuracy of models are shown in Table 13 and Table 14, while clarifying accuracy of models, effect of nRMSE is more important than nMBE and Yang suggested using Perez family models. Accuracy of Perez models for each combination are in an acceptable limit [25].

Table 14. nRMSE results of 26 different models for 4 different locations and 18 different tilt and azimuth angle combination [25].

Model	Eugene (44.05°, −127.07°)			Oldenburg (53.15°, 8.17°)		Singapore (1.30°, 103.77°)			
	(30, 180)	(90, 180)	(90, 0)	(45, 180)	(45, 135)	(10, 64)	(20, 64)	(30, 64)	(40, 64)
Liu	5.5	14.1	31.3	11.9	13.2	4.3	7.1	11.0	13.0
Temps	8.1	17.0	46.0	12.4	13.6	7.3	7.2	10.2	11.7
Bugler1	4.7	12.3	31.1	9.7	11.2	4.9	6.2	10.1	11.6
Bugler2	4.9	13.1	30.6	11.0	11.9	3.9	6.5	10.0	11.7
Klucher	4.4	11.5	39.2	6.7	8.5	5.3	5.8	9.0	10.3
Steven1	7.6	20.3	23.9	15.1	15.6	3.7	6.1	8.6	10.8
Steven2	7.5	20.0	23.0	15.1	15.4	3.6	6.0	8.4	10.8
Steven3	6.0	17.2	27.1	13.8	14.5	4.3	7.3	11.3	13.4
Steven4	5.1	13.2	20.8	10.4	10.2	3.0	4.7	6.5	8.3
Hay1	4.0	9.1	29.1	6.8	7.2	3.0	4.5	6.8	7.7
Hay2	4.1	9.0	29.5	6.7	7.1	3.0	4.5	6.7	7.6
Willmott	4.8	9.0	29.5	7.8	7.9	3.3	5.7	7.5	8.6
Koronakis	5.0	15.4	45.4	10.5	12.4	4.3	6.9	11.0	13.1
Perez1	4.3	9.2	20.5	6.6	6.2	2.7	3.4	4.9	5.2
Perez2	4.3	9.3	19.2	6.7	6.4	2.9	3.4	4.9	5.3
Perez3	3.9	8.3	19.8	6.1	5.9	2.8	3.6	5.0	5.3
Perez4	3.8	8.4	20.1	6.3	6.1	2.8	3.6	5.1	5.3
Skartveit	4.2	11.4	32.3	7.1	7.3	3.0	4.6	6.8	7.9
Gueymard	4.2	10.7	26.1	7.4	8.0	3.3	4.7	7.2	8.1
Muneer1	4.0	10.0	25.6	6.3	7.1	3.0	4.5	7.0	8.2
Muneer2	4.4	12.2	24.5	7.2	7.8	3.1	4.4	7.0	8.1
Reindl	4.0	9.1	30.7	6.5	7.1	3.0	4.5	6.7	7.7
Olmo1	10.8	26.1	53.9	16.8	17.6	5.0	7.5	10.1	12.7
Olmo2	8.1	22.4	24.7	13.4	13.6	7.6	9.6	9.9	12.3
Tian	8.6	14.1	31.3	16.9	17.1	5.6	10.3	13.7	15.8
Badescu	7.1	14.1	31.3	16.9	17.1	4.3	7.8	12.1	15.1

Model	Singapore				Golden (39.74°, −105.18°)					Rank
	(90, 90)	(90, 180)	(90, 270)	(90, 0)	(40, 180)	(90, 0)	(90, 90)	(90, 180)	(90, 270)	
Liu	25.0	24.2	24.6	23.8	7.6	24.5	14.1	9.8	14.8	19
Temps	30.1	39.0	33.1	38.5	6.9	38.7	16.4	13.2	20.0	25
Bugler1	23.2	24.3	23.3	23.8	5.8	24.4	12.2	9.0	13.1	15
Bugler2	23.1	22.3	22.9	22.2	6.9	26.7	13.1	9.0	14.3	14
Klucher	25.7	33.3	27.8	32.3	4.4	30.7	13.0	9.5	14.7	16
Steven1	24.1	22.8	25.4	18.9	7.4	19.7	15.0	14.9	19.2	18
Steven2	23.7	23.2	25.2	18.8	7.3	19.3	14.4	14.7	18.5	17
Steven3	25.8	18.7	24.1	17.6	8.5	19.2	15.5	11.6	15.6	20
Steven4	19.7	21.2	20.4	17.7	5.1	19.4	11.4	11.3	15.7	13
Hay1	16.1	18.5	17.0	18.2	5.3	31.3	11.8	8.7	14.7	7
Hay2	16.0	18.4	16.9	18.2	5.2	31.9	12.0	8.9	15.0	6
Willmott	16.0	18.4	16.9	18.2	6.0	31.9	12.0	8.9	15.0	12
Koronakis	31.0	38.0	33.3	37.7	6.8	38.0	17.0	12.0	19.9	24
Perez1	12.6	17.3	12.8	14.9	4.3	13.8	8.5	9.0	9.2	3
Perez2	12.9	16.8	12.5	14.8	4.2	13.7	8.5	8.8	9.1	4
Perez3	12.6	16.2	12.2	14.3	4.1	14.1	8.2	7.7	8.8	2
Perez4	12.6	16.7	12.5	14.6	4.0	13.8	8.2	7.6	7.9	1
Skartveit	16.6	17.9	17.1	15.8	5.4	29.4	12.7	9.8	14.6	10
Gueymard	17.1	21.1	17.3	19.4	5.1	18.4	9.8	8.5	9.7	8
Muneer1	16.0	22.4	17.1	19.1	4.8	19.2	10.4	9.6	12.6	5
Muneer2	17.2	24.2	18.3	20.6	5.2	19.0	11.7	11.9	13.9	11
Reindl	18.0	23.7	19.7	23.3	5.0	31.3	11.7	9.2	15.0	9
Olmo1	25.6	29.5	26.7	28.1	14.2	38.5	23.5	20.9	29.7	26
Olmo2	21.7	22.3	22.8	21.3	9.0	28.7	16.9	17.6	24.1	21
Tian	25.0	24.2	24.6	23.8	10.6	24.5	14.1	9.8	14.8	23
Badescu	25.0	24.2	24.6	23.8	10.1	24.5	14.1	9.8	14.8	22

In another study, Li et al (2017) compared 7 different solar model to verify which solar model fits with highest accuracy for Beijing, China. Li et al. [44] aimed to estimate total solar irradiance on building facades. Beijing is one of the most populated cities in the World and energy consumption of the city is very high. Industrial activities and excess amount of energy consumption causes excess amount of carbon emission in Beijing. To be able to decrease carbon emission in Beijing, covering building facades with solar modules is advertised by government. In this case, it is important to estimate energy produced by solar modules to create a high performance and efficient energy

systems for buildings. For urban areas, estimation of solar energy potential is quite complex especially for diffuse radiance. One of the reasons is that when building facades are covered with solar modules, these modules will be perpendicular to ground, and this makes diffuse component hard to estimate. Li et al. [44] compared different models to determine most accurate model for urban areas in Beijing, China. They compared Bugler [27], Klucher [29], Skartveit-Olseth [37], Perez (1987) [5], Muneer [39], Yao [45] and Igawa [46] models. Li et al. [44] compared these models results for different orientations (West, East, North, South facing facades) and for different weather conditions. Coordinate of Beijing is $39°55'N; 116°23'E$ and data collected was from 17 December 2016 to 12 February 2017. Li et al. [44] calculated MBE and RMSE for their results to evaluate accuracy of models which they compared. They also calculated coefficient of determination of linear regression analysis of data (R^2). Table 15 shows MBE, RMSE and R^2 for all sky conditions. According to Table 15 results, they recommended Muneer and Iwaga models for all sky conditions for Beijing.

Table 15. MBE and RMSE of models which Li et al used on all sky conditions [44].

Model	MBE (W/m^2)	MBE (%)	RMSE (W/m^2)	RMSE (%)	R^2
Bugler	-4.59	6.31	11.84	20.16	0.9326
Iwaga	-1.39	6.63	5.40	13.43	0.9487
Klucher	-0.41	15.79	14.38	28.09	0.9177
Muneer	0.93	5.63	6.38	11.88	0.9378
Perez	5.11	7.48	13.72	23.06	0.9261
Skartveit-Olseth	-12.71	-35.41	15.22	39.41	0.8520
Yao	0.58	8.48	7.17	16.26	0.9210

Li et al. [44] also investigated models under different sky conditions, such as overcast (O), intermediate (I), and clear (C) sky conditions. Table 16 and

Table 17 show MBE and RMSE results for these sky conditions. According to these results it can be said that performance of models highly variable to sky conditions. For example, Skartveit-Olseth model gives accurate results for overcast sky conditions; $RMSE_{overcast}$=2.44%; however, for clear sky conditions this model is highly unreliable; $RMSE_{clear}$=128.63%. When the results were investigated it can be concluded that Muneer and Yao models performs better others. For overcast and intermediate-overcast sky conditions Skartveit-Olseth, Iwaga and Muneer models show more accurate result than others for intermediate-clear and clear sky conditions. Table 6 and 7 show MBE and RMSE results of the models for different orientations, respectively.

Table 16. MBE of models which Li et al used on different sky conditions [44].

Model	MBE (W/m^2)					MBE (%)				
	O	I-O	I	I-C	C	O	I-O	I	I-C	C
Bugler	0.52	0.20	12.78	16.65	21.18	4.31	30.30	24.21	-11.11	10.81
Iwaga	0.14	-0.35	0.95	-5.24	-9.17	2.43	15.94	17.54	11.54	5.17
Klucher	0.53	3.23	-1.53	-4.76	-2.23	4.32	31.38	43.69	32.66	50.37
Muneer	0.16	-1.29	-3.21	6.45	5.17	2.56	8.79	20.04	-2.79	9.69
Perez	0.48	0.31	14.08	19.96	21.81	4.22	29.41	23.53	-1.36	21.09
Skart. -Ol	0.37	11.75	26.97	45.17	52.05	0.59	-8.98	32.83	154.65	103.1
Yao	0.67	4.51	5.63	-5.02	12.38	8.74	49.13	26.96	-24.00	-7.50

Table 17. RMSE of models which Li et al used on different sky conditions [44].

Model	RMSE (W/m^2)					RMSE (%)				
	O	I-O	I	I-C	C	O	I-O	I	I-C	C
Bugler	0.76	17.44	36.73	39.51	36.71	4.79	57.78	59.58	49.19	30.04
Iwaga	0.40	7.65	10.57	17.80	19.53	3.07	35.75	25.38	22.42	32.36
Klucher	0.77	18.35	40.61	49.83	48.25	4.80	58.52	73.77	77.97	67.3
Muneer	0.44	10.80	19.23	19.15	19.15	3.24	38.60	38.37	29.76	8.22
Perez	0.75	18.65	39.54	46.72	45.15	4.71	57.35	61.57	59.00	46.64
Skart. -Ol.	0.49	15.72	28.96	53.61	58.97	2.44	39.76	52.38	39.67	128.6
Yao	1.40	15.58	16.70	18.95	21.42	9.52	57.97	36.00	21.11	11.00

In addition to the effects of sky conditions, Li et al. [44] analyzed the effects of orientation of building facades on the amount diffuse irradiance reaching surface. Performance of models for different orientations usually steady with respect to other orientations. For example, Iwaga model shows the most accurate performance for West facade and this model shows quiet reliable results for other facades as well. According to Table 18 and

Table 19, it can be concluded that Muneer and Iwaga model shows better performance on East facade. Iwaga, Yao and Muneer models give smaller MBE and RMSE results on west, north, south facades respectively. To sum up, Iwaga model was identified as most accurate solar model for Beijing after a 3-month investigation and data collection. It is logical that Iwaga model shows the most accurate results for Beijing because origin of this model is Kyoto, Japan. Kyoto, Japan and Beijing, China are close geographic locations to each other and it is logical to recommend Iwaga solar model for Beijing [44].

Table 18. MBE of models which Li et al. used on different orientations [44].

Model	**MBE (W/m^2)**				**MBE (%)**			
	E	S	W	N	E	S	W	N
Bugler	-3.91	-21.36	-0.72	7.64	4.01	-14.32	5.63	29.90
Iwaga	-2.93	-6.46	1.02	2.83	2.11	3.94	5.17	15.32
Klucher	0.15	-19.77	3.72	14.25	11.65	-12.69	15.24	48.98
Muneer	-1.55	-2.23	3.26	4.21	2.21	-5.07	8.36	17.01
Perez	-4.00	-25.01	-0.53	9.10	4.64	-15.71	6.97	34.04
Skart. -Ol.	-13.32	-9.42	-7.84	-20.28	-33.10	-12.07	-28.69	-67.78
Yao	-4.20	-0.28	0.91	1.26	6.02	11.27	6.55	10.07

Table 19. RMSE of models which Li et al. used on different orientations [44].

Model	**RMSE (W/m^2)**				**RMSE (%)**			
	E	S	W	N	E	S	W	N
Bugler	10.61	22.72	6.32	7.72	18.53	15.22	16.30	30.57
Iwaga	6.33	8.99	3.27	3.00	11.63	15.89	10.12	16.09
Klucher	12.37	21.02	9.76	14.36	24.01	15.04	24.12	49.17
Muneer	5.60	9.60	5.87	4.45	10.25	4.93	14.03	18.30
Perez	11.75	26.10	7.81	9.22	20.48	18.60	18.76	34.39
Skart. -Ol.	14.70	12.98	11.66	21.55	35.76	5.72	38.30	77.88
Yao	8.84	12.68	4.98	2.19	18.82	19.08	13.92	13.22

In another study, Shukla et al. (2015) [47] compared 3 isotropic and 3 anisotropic model for Bhopal, India. Location of Bhopal, India is $23°26'N; 77°36'E$. Bhopal is under the effect of Monsoons and usually Monsoon rains start in June and lasts till September. As mentioned earlier, Shukla et al. compared 3 isotropic models namely

Liu and Jordan (LJ) (1960) [17], Koronakis (KO) (1986) [34] and Badescu (BA) (2002) [43], and 3 anisotropic models namely Hay and Davies (HD) (1980) , Reindl (RE) et al. (1990) [40] and HDKR (2006) models. Shukla used several different models to calculate daily global irradiation, diffuse and beam solar radiation on a horizontal surface for Bhopal, India. After they calculated radiation values for horizontal surface, they calculated total radiation on surface tilted 23.26° (latitude of Bhopal) with the above mentioned 6 different solar models. Calculated tilted radiation values were compared with data collected with a pyranometer tilted at same angle. Shukla et al. applied 4 statistical tests to their results to determine accuracy results. Figure 6 shows calculated solar radiation for 6 models and measured tilted solar radiation. As it is shown in Figure 6, Liu and Jordan model and Koronakis model almost give same results. Hay and Davies, Reindl et al. and HDKR models give slightly higher results than isotropic models because these anisotropic models consider circumsolar components in diffuse radiation.

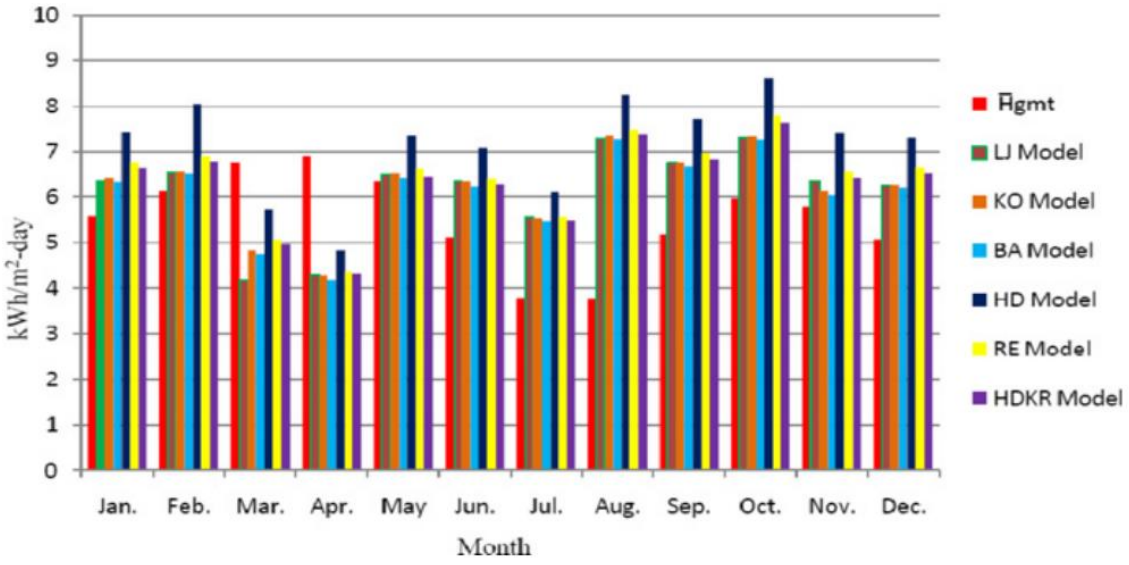

Figure 6. Average daily solar radiation on tilted surface for 6 models and measured data from a tilted surface ($\bar{H}_{gmt}$) [47].

Table 20 shows estimated value of total radiation on a horizontal surface, measured total radiation on a tilted surface and estimated daily solar radiation on tilted surface for 6 different models for 12 months and yearly average. This table helps to follows numerical results easier. Tilted measurement and estimations are higher than estimated values of horizontal radiation as expected for each month. Except April, monthly averages of estimated tilted radiation values are higher than measured tilted radiation values for each month. Figure 7, Figure 8, Figure 9 and Figure 10 show results of MAPE, MBE, RMSE and t-stat for 6 models respectively. For these values, they are desired to be small as possible, especially for t-stat values. Smaller the t-stat value, more accurate the model. Figure 10 shows yearly average of t-stat for each model and according to this figure, isotropic models are more accurate than anisotropic models because t-stat results are lower for isotropic models.

Table 20. Estimated value of total radiation on a horizontal surface [47].

Month	$\bar{H}_{gm}\left(\frac{kWh}{m^2}\right)$	$\bar{H}_{gmt}\left(\frac{kWh}{m^2}\right)$	Estimated daily solar radiation on tilted surface (kWh/m^2)					
			LJ	KO	BA	HD	RE	HDKR
Jan	4.38	5.59	6.36	6.41	6.33	7.43	6.75	6.63
Feb	5.21	6.12	6.54	6.56	6.51	8.04	6.90	6.77
March	6.62	6.75	4.18	4.82	4.74	5.73	5.06	4.95
April	6.97	6.90	4.28	4.27	4.18	4.82	4.36	4.31
May	6.78	6.34	6.50	6.52	6.42	7.33	6.62	6.44
June	5.57	5.12	6.35	6.35	6.24	7.08	6.40	6.28
July	4.03	3.78	5.56	5.52	5.46	6.10	5.56	5.47
Aug	3.91	3.77	7.28	7.34	7.26	8.24	7.49	7.36
Sep	5.11	5.18	6.75	6.75	6.66	7.71	6.97	6.83
Oct	5.33	5.97	7.30	7.32	7.25	8.62	7.78	7.63
Nov	4.70	5.79	6.36	6.12	6.04	7.42	6.56	6.41
Dec	4.49	5.07	6.26	6.27	6.22	7.29	6.64	6.52
Average	5.22	5.33	6.14	6.18	6.10	7.15	6.42	6.30

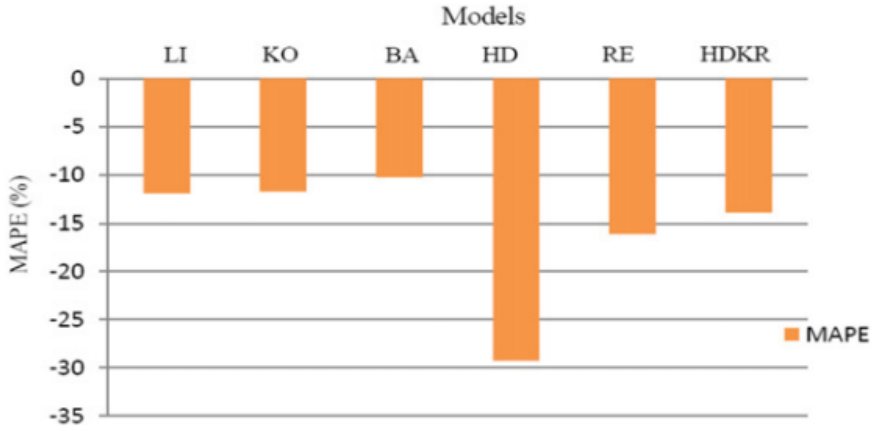

Figure 7. Mean Absolute Percentage Error (MAPE) for 6 models [47].

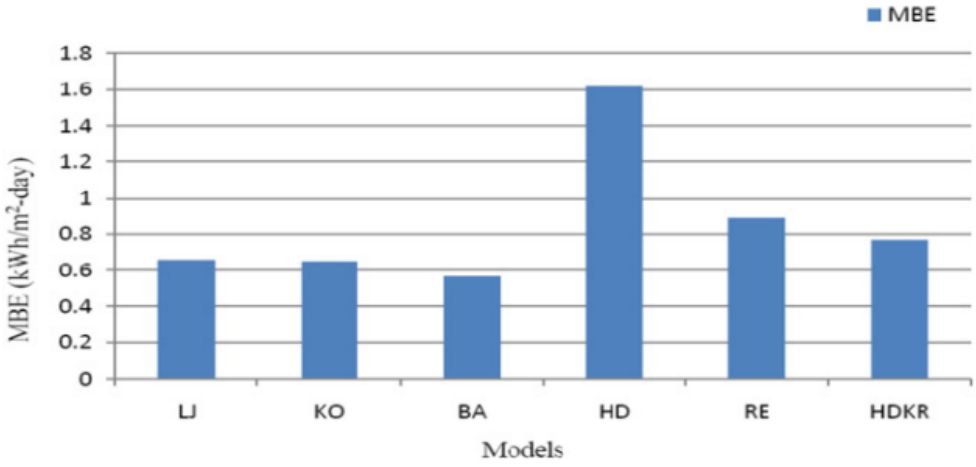

Figure 8. Mean Bias Error (MBE) for 6 models [47].

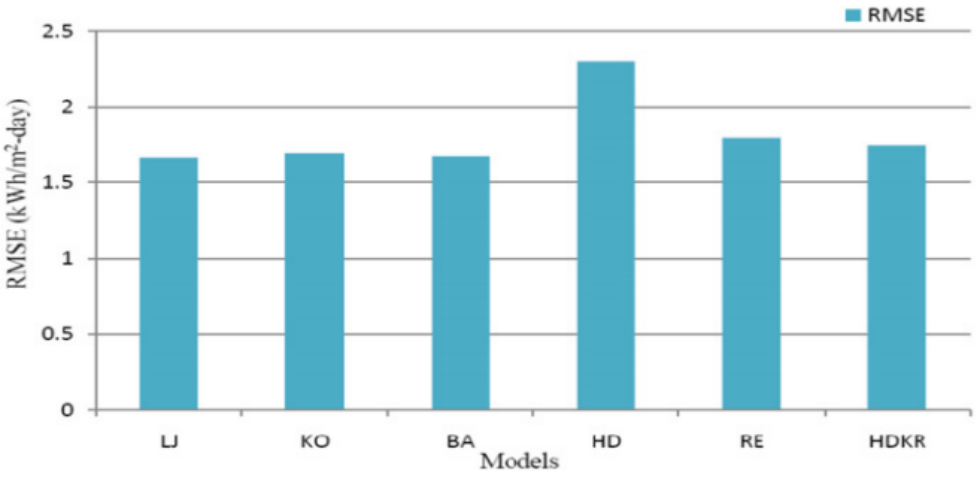

Figure 9. Root Mean Square Error (RMSE) for 6 models [47].

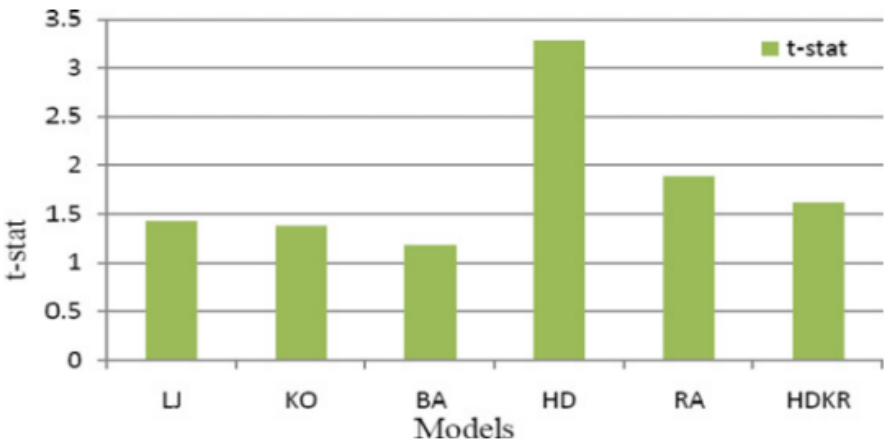

Figure 10. t-statistics for 6 models [47].

To sum up, Shukla et al. [47] compared 6 different solar models for Bhopal, India for one-year period. They collected tilted measurement data from a surface tilted with 23.26°. According to the results that they get, Hay and Davies model estimates the highest amount of solar energy on tilted surface and Badescu's isotropic model estimated the lowest. Most of the isotropic models estimated lower solar radiation on tilted surface in overcast weather conditions and estimated higher results than tilted measurement in good weather conditions from August to February. Liu and Jordan's and Koronakis' isotropic models estimated almost the same total radiation on tilted surfaces for each month. Badescu model estimated closer total radiation to measured radiation on tilted surface. Additionally, statistical error results for Badescu are smaller than other models' results. By the light of these information, Shukla et al. suggest Badescu's isotropic model to estimate total solar radiation on a tilted surface for Bhopal, India weather conditions [47].

Moreover, Pandey and Katiyar (2014) [48] compared circumsolar model, isotropic model suggested by Liu and Jordan and isotropic models of Klucher [29] and Hay [49] with measurement from Lucknow, Uttar Pradesh, India ($26.75°N; 80.85°E$). Pandey and Katiyar measured global and diffuse radiation on horizontal surface and south

facing ($\gamma = 0°$) surfaces inclined at $15°, 30°, 45°$ and $60°$. Data collection period was one-year period, from January to December in 2007. Because of lack of space, Pandey and Katiyar [48] could only showed results for 5 different months. However, according to them the results of months that they coincided with other months. As shown in Table 21, order of accuracy of models does not vary much with inclination angle except slight variation for high angles $45°$ and $60°$. RMSE and MBE results in Table 21 show that Isotropic model suggested by Liu and Jordan and anisotropic models of Hay and Klucher perform better accuracy than circumsolar model for Indian climatic conditions.

Table 21. RMSE and MBE results for Circumsolar, Isotropic, Klucher and Hay models [48].

Slope	Month	Circumsolar		Isotropic		Klucher		Hay	
		RMSE	MBE	RMSE	MBE	RMSE	MBE	RMSE	MBE
15°	February	166.19	149.17	31.16	17.55	79.08	67.78	105.88	81.29
	April	33.36	−19.02	33.56	−26.99	27.11	−9.89	32.92	−23.56
	June	69.27	−53.49	56.1	−44.36	48.85	−31.38	60.68	−47.78
	September	129.95	95.15	116.39	76.99	134.37	99.79	121.84	84.51
	December	57.64	51.88	5.19	2.85	36.35	30.67	19.87	17.98
30°	February	91.48	60.37	70.28	−9.61	86.78	29.47	72.37	18.78
	April	55.96	−31.45	50.87	−40.29	42.67	−22.67	52.2	−36.33
	June	93.29	−85.72	64.43	−60.13	55.92	−47.89	74.99	−70.19
	September	29.11	15.91	22.1	−12.68	22.83	11.8	20.92	−0.82
	December	91.31	75.73	24.11	−14.52	31.87	23.63	23.25	58.08
45°	February	109.07	104.86	28.6	14.36	66.47	57.73	59.93	50.94
	April	95.68	−88.97	93.16	−91.34	75.73	−72.06	93.35	−89.97
	June	157.2	−153.07	107.02	−104.79	93.28	−89.88	126.53	−124.28
	September	28.19	4.03	34.79	−26.52	23.57	−0.52	28.05	−13.74
	December	109.64	102.66	48.75	−36.12	22.2	9.03	26.14	0.94
60°	February	101.67	58.58	18.84	−0.69	50.37	43.73	46.94	39.24
	April	121.45	−117.37	109.04	−106.31	87.24	−83.46	113.37	−110.29
	June	225.7	−222.69	149.94	−147.07	128.92	−125.67	180.41	−178.09
	September	33.62	−29	57.43	−52.94	29.83	−24.89	46.71	−42.77
	December	112.28	78.47	76.05	−60.22	27.69	−12.72	39.4	−17.88

To further illustrate the results of Pandey and Katiyar [48], Figure 11 shows measured and estimated values of radiation on tilted surfaces with different inclination angles. April data are shown in Figure 11 because radiation magnitudes and order of magnitudes of model estimations are very close to yearly average. According to this figure, to get maximum amount of radiation tilt angle should be $30°$ which is logical because to get yearly maximum radiation for any location, tilt angle should be latitude of that location. Latitude of Lucknow is $26.75°$ and getting highest of radiation at $30°$

tilt angle is logical for this location. According to these results, the authors suggested Liu and Jordan's isotropic model for Lucknow, Uttar Pradesh, India because of good accuracy and simplicity of the model [48].

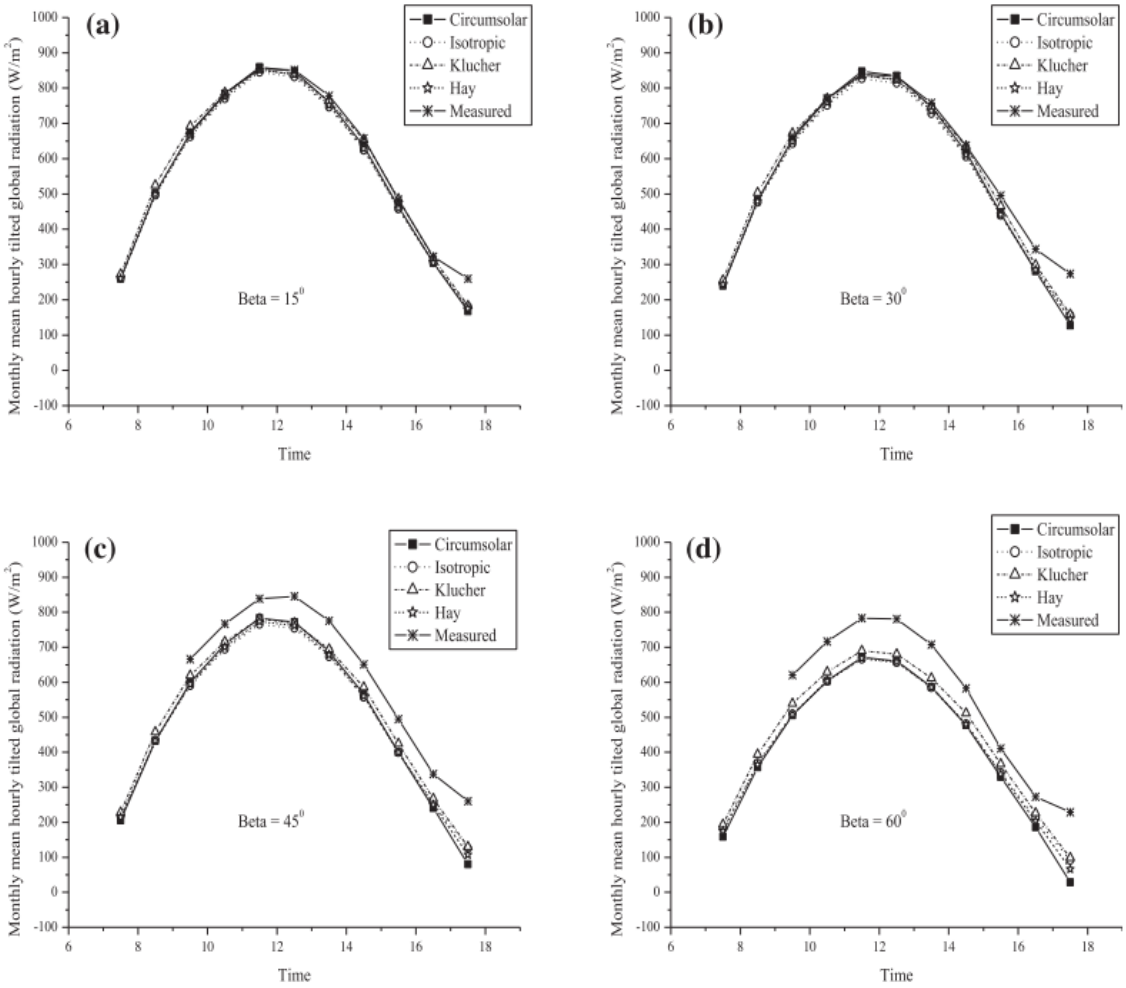

Figure 11. Measured and estimated tilted radiation for different models and tilt angles for April (Beta means tilt angle of plate) [48].

Furthermore, Noorian et al (2007) evaluated 12 different models for Karaj, Iran ($35°55'N; 50°56'E$) [50]. They measured total radiation on horizontal surface and two different tilted surface using a solar station on the roof of thr Faculty of Agriculture, University of Tehran. One of the surfaces was tilted with $45°$ and this was faced through South ($\gamma = 0°$). Second surface was tilted with $40°$ and this surface was faced through West ($\gamma = 90°$). As mentioned earlier 12 models were investigated in Noorian et al (2007) and these models are Badescu [Ba] [43], Tian et al. [Ti] [42],

Perez et al. (1990) [P9] [36], Reindl et al. [Re] [40], Koronakis [Kr] [34], Perez et al. (1986) [P8], Skartveit and Olseth [SO] [37], Steven and Unsworth [SU] [31], Hay [Ha] [51], Klucher [Kl] [29], Temps and Coulson [TC] [52], and Liu and Jordan [LJ] [53]. Total solar radiation on tilted surface was calculated with these models for south facing ($\gamma = 0°$) and west facing ($\gamma = 90°$) plates. Evaluation of results carried out on a semi-hourly basis and data collection period was from February 2002 to June 2002. To be able compare experimental and calculated results, Root Mean Square Error (RMSE) and Mean Bias Error (MBE) test were applied on results. Table 22 shows statistical results for the models for both south and west facing surfaces. For south facing surface, MBE and RMSE values are very close in each model, except SU and TC models where MBE and RMSE values were significantly higher in magnitude. SO, Ha, Re and P9 models predicts solar radiation on tilted surfaces better than other models for south facing surface. For west facing surface MBE values were very close to each other except SU and TC model. RMSE values did not differ so much from each other. Perez (1990) was most accurate model for west facing surfaces and Skartveit and Olseth, Hay, Reindl and Perez are most accurate models for Karaj, Iran according to Noorian et al [50].

Table 22. Comparison of regression (calculated =a+ b x measured) and correlation coefficient (R), RMSE, MBE for south facing (A) and west facing (B) surface. RMSE and MBE are in units of MJ/m^2 [50].

Model	*a*	*b*	*R*	RMSE	MBE	%RMSE	%MBE
LJ	0.07	0.93	0.99	0.07	0.03	13.4	6.16
Kr	0.08	0.95	0.99	0.08	0.05	14.89	9.54
Ba	0.06	0.88	0.99	0.08	−0.01	13.95	−1.00
Ti	0.06	0.88	0.99	0.08	−0.01	13.95	−1.00
Ha	0.06	0.94	1.00	0.06	0.02	10.37	4.47
SO	0.06	0.94	1.00	0.06	0.02	10.16	4.27
Re	0.06	0.95	1.00	0.06	0.03	10.87	6.07
SU	0.09	1.23	0.99	0.26	0.22	47.18	40.62
P8	0.02	0.94	0.99	0.07	−0.01	12.44	−2.07
P9	0.04	0.94	0.99	0.06	0.01	11.17	1.44
Kl	0.08	0.96	0.99	0.08	0.06	15.43	10.40
TC	0.1	0.5	0.94	0.3	−0.18	54.89	−31.86

(A)

Model	*a*	*b*	*R*	RMSE	MBE	%RMSE	%MBE
LJ	0.12	0.72	0.89	0.24	−0.04	42.49	−7.70
Kr	0.12	0.74	0.89	0.24	−0.03	42.10	−5.20
Ba	0.1	0.69	0.89	0.25	−0.08	44.17	−13.45
Ti	0.1	0.68	0.89	0.26	−0.08	44.57	−14.46
Ha	0.08	0.76	0.92	0.21	−0.06	37.18	−10.04
SO	0.08	0.76	0.92	0.21	−0.06	37.25	−10.23
Re	0.09	0.76	0.92	0.21	−0.05	36.85	−8.95
SU	0.13	1.03	0.95	0.24	0.15	40.90	26.26
P8	−0.02	0.76	0.95	0.24	−0.16	41.80	−28.23
P9	0.05	0.81	0.95	0.18	−0.07	30.71	−11.50
Kl	0.11	0.78	0.91	0.22	−0.01	37.97	−2.43
TC	0.07	0.5	0.89	0.37	−0.22	63.53	−38.52

(B)

In another study, Nijmeh and Mamlook (2000) compared Liu and Jordan's isotropic model with Hay's anisotropic model for Amman, Jordan ($31°59'N; 35°59'E$) [54]. They measured global radiation on a horizontal surface, global radiation on a $45°$ tilted surface and diffuse radiation on a horizontal surface for one-year period. Tilted surface which was used for this experiment was facing towards south ($\gamma = 0°$). Nijmeh and Mamlook [54] compared Liu and Jordan's isotropic model and Hay's anisotropic model because these two models' only difference from each other is calculation of diffuse component of global insolation. Nijmeh and Mamlook [54] used statistical error methods of RMSE and MBE to evaluate accuracy of measurements for 12 months separately. Figure 12 shows MBE of isotropic and anisotropic for 12 months. Positive MBE means overestimation and negative MBE means underestimation. According to these results, both models overestimated during summer period and underestimated during winter period. Figure 13 shows results of RMSE for 12 months. According to results showed in Figure 12 and Figure 13 , these two models were in good agreement during whole year. RMSE of isotropic model changes between 3.6% and 25.7% and RMSE of anisotropic model changed between 3.5% and 25.6%. Isotropic model showed slightly better performance; it was 2% more accurate than anisotropic model during summer period. For rest of the year, anisotropic model showed more accurate performance than isotropic model. Radiation on $45°$ tilted surface was showed on Figure 14 for these two models and measured tilted results. According to Figure 14, difference between tilted measurement and anisotropic and isotropic models' estimations were close to each other.

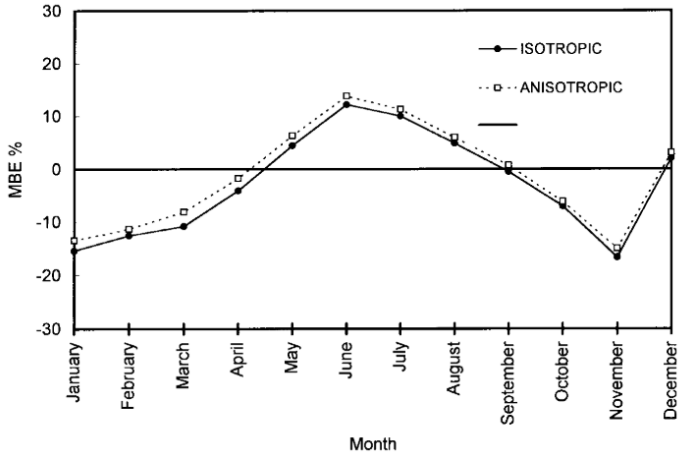

Figure 12. MBE for global radiation on inclined surface [54].

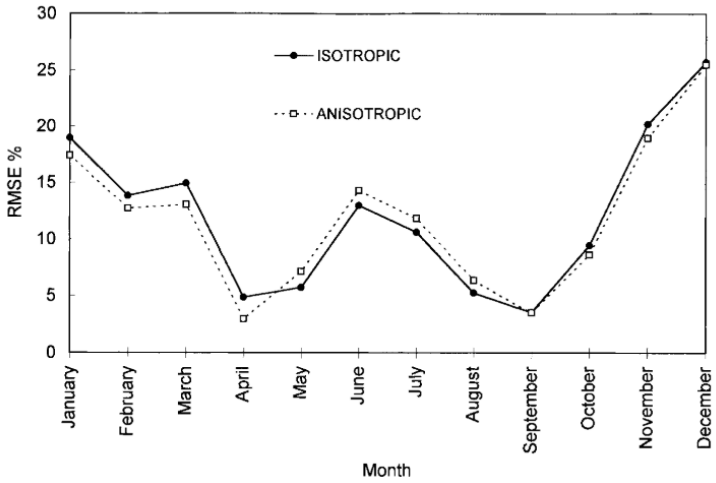

Figure 13. RMSE for global radiation on inclined surface [54].

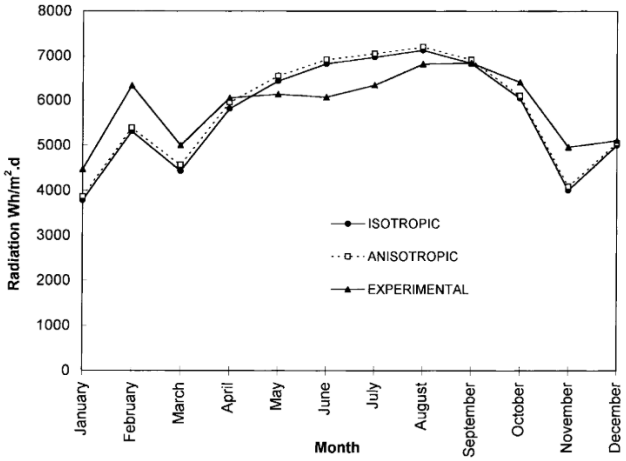

Figure 14. Monthly averages on 45º tilted surface [54].

Additionally, Table 23 shows ratio of monthly average daily radiation on a tilted surface and radiation on a horizontal surface. According to this table R values were

close to each other for each month, both of the Liu and Jordan's isotropic model's and Hay's anisotropic model's accuracies were both satisfactory and both of these models could be used to estimate solar radiation on tilted surfaces in Amman, Jordan [54].

Table 23. Ratio of monthly average daily radiation on a tilted surface and horizontal surface for experimental, isotropic model and anisotropic model [54].

Month	Experimental	Isotropic	Anisotropic
January	1.65	1.39	1.42
February	1.58	1.33	1.35
March	1.22	1.08	1.11
April	1.03	0.99	1.01
May	0.86	0.90	0.91
June	0.76	0.85	0.87
July	0.80	0.88	0.89
August	0.93	0.97	0.98
September	1.11	1.11	1.12
October	1.39	1.31	1.32
November	1.72	1.39	1.41
December	1.63	1.60	1.61

In this section results of some models were shown to be able to understand which models can be applied to Cyprus. Some of these models gave accurate estimations for the locations which are close to Cyprus. However, some models in the literature created with data collected from locations far away from Cyprus and it is expected that these models won't give estimation results. For example, Iwaga model [44] created with readings from Japan and this model was not modified by other researchers to increase estimation accuracy for another location. Results for this model calculated during model selection period and this model's estimation accuracy much lower than other models for Cyprus as expected. Solar income, seasonal conditions, and geographic conditions of Japan very different than Cyprus and a model created for Japan did not accurate estimation results for Cyprus.

CHAPTER 3 – METHODOLOGY

In this chapter of this thesis, geometrical relations between sunlight and horizontal/tilted surfaces will be explained. Section 3.1 explains important and required angles and parameters which will be to estimate G_{tilted}. In Section 3.2, models which will be used to estimate total solar energy which is incident on tilted plate will be explained. For this thesis 8 different models will be explained. In Section 3.3, energy production estimation of a PV power plant will be explained. In last section of Chapter 3, data collection process from METU NCC solar station and some important information about METU NCC solar power plant will be shown.

3.1. Geometrical Relations

The geometric relation between a surface and beam radiation coming from sun is described with several angles. Between sun rise and sun set time, as the sun moves these angles change. Figure 15 shows some of these important angles.

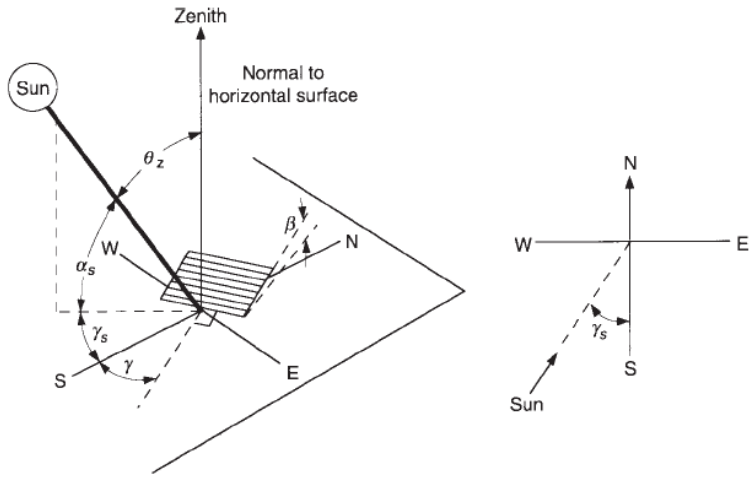

Figure 15. Some of the important angles to define geometric relation between the Sun and a surface [55].

Equation (26) shows how to calculate declination angle. Declination angle changes with number of days. Declination angle represents angular positions of the sun at solar noon with respect to the axis of the Earth, and it changes between $-23.45°$ and $23.45°$.

$$\delta = 23.45 \cdot \sin\left(360\frac{284+n}{365}\right) \tag{26}$$

where; n is the number of days.

Solar time (t_s) is another term which is used in solar radiation calculations. Solar time is based on the angular position of the sun over the sky hemisphere. Usually there is a small difference between local time (t_{std}) and solar time because local time is identified for a meridian and a time zone close to this meridian. Equation (27) shows relation between solar and local time. In this equation, E is referred as the equation of time in minutes and, Equation (28) shows how to calculate it; L_{st} is standard meridian for local time zone and L_{loc} is longitude of location. Another important point during calculation of solar time is consideration of daylight saving. In case of daylight-saving time, 1 hour should be subtracted from local time before calculating solar time. Equations (30) and (31) shows how to calculate standard meridian (L_{st}) and longitude of location (L_{loc}) respectively [55].

$$t_s - t_{std} = 4 \cdot (L_{st} - L_{loc}) + E \tag{27}$$

$$\begin{aligned} E = 229.2 \cdot (&0.000075 + 0.001868 \cdot \cos B - 0.032077 \cdot \sin B \\ &- 0.014615 \cdot \cos 2B - 0.04089 \cdot \sin 2B) \end{aligned} \tag{28}$$

$$B = (n-1)\frac{360°}{365} \tag{29}$$

$$L_{st} = \begin{cases} 360° - TZ \cdot 15° & if \;\; TZ > 0 \\ -TZ \cdot 15° & if \;\; TZ < 0 \end{cases} \tag{30}$$

$$L_{loc} = \begin{cases} L_{loc} & if\ location\ is\ in\ West \\ 360° - L_{loc} & if\ location\ is\ in\ East \end{cases} \quad (31)$$

Another important parameter which is required for solar radiation calculations is the hour angle. Equation (32) shows how to calculate it. Hour angle gives negative results in mornings and positive results for afternoon. Equation (33) shows how to calculate cosine of zenith angle [55]. Zenith angle is the angle between beam radiation and normal of horizontal ground surface. Zenith angle reaches its minimum value at solar noon and from sun set to sun rise its value is higher than 90°.

$$\omega = (t_s - 12) \cdot 15°/hour \quad (32)$$

$$\cos\theta_z = \cos\phi \cdot cos\delta \cdot cos\omega + sin\phi \cdot sin\delta \quad (33)$$

Equation (34) and (35) show how to calculate solar azimuth angle. Solar azimuth angle is the angle between projection of beam radiation on ground and south. To be able to calculate solar azimuth angle zenith angle for a specific time, declination angle and hour angle should be calculated for that time and also latitude (ϕ) of the location should be known. Latitude describes angular position of a location according to equator. If latitude is positive; location is at north of equator, if it is negative; location is at the south of equator. Equation (36) shows how to calculate cosine of incidence angle (θ). Incidence angle is the angle between beam radiation and surface normal of a horizontal surface. Incidence angle calculation gives positive results for from sun rise to sun set, otherwise it is negative [55].

$$\gamma_s = \begin{cases} sign(\omega) \cdot |\cos^{-1}(\gamma_s')| & if \quad \gamma_s' \neq 1 \\ 0 & if \quad \gamma_s' = 1 \end{cases} \quad (34)$$

$$\gamma_s' = \begin{cases} \dfrac{cos\theta_z \cdot sin\phi - sin\delta}{sin\theta_z \cdot cos\phi} & if \quad \theta_z \neq 0 \\ 1 & if \quad \theta_z = 0 \end{cases} \quad (35)$$

$$\cos\theta = cos\theta_z \cdot cos\beta + sin\theta_z \cdot sin\beta \cdot \cos(\gamma_s - \gamma) \quad (36)$$

Extraterrestrial normal radiation is another important term which is used for solar radiation calculations. Equation (37) shows how to calculate extraterrestrial normal radiation on a plane. Extraterrestrial normal radiation is calculated daily and depends on number of day and solar constant (G_{sc}). To be able to calculate G_{on}, solar constant value should be determined. Some portion of the energy emitted from the Sun receives outside of earth's atmosphere. Calculation of G_{sc} is based on heat transfer through radiation theory. Figure 16 basically explains the Sun-earth relationship. According to World Radiation Center's calculations and measurements from outer space, solar constant is accepted as 1367 W/m^2 [55].

$$I_{on} = G_{sc} \cdot \left(1 + 0.033 \cdot \cos\left(\frac{360° \cdot n}{365}\right)\right) \tag{37}$$

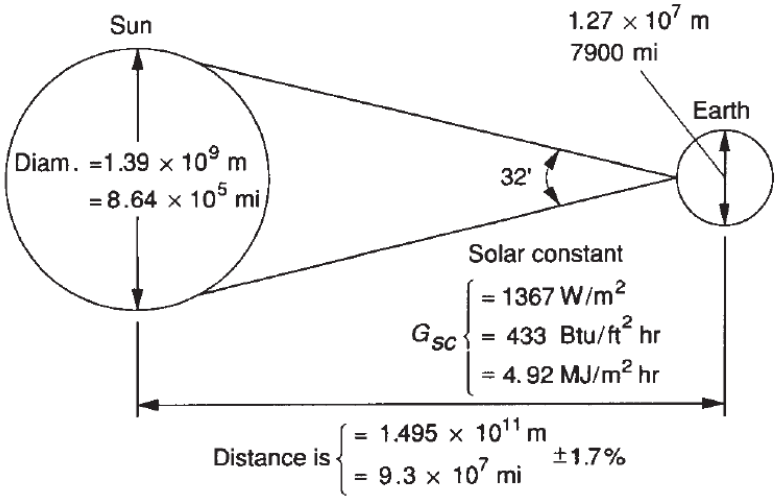

Figure 16. Relation between the Sun and earth [55].

$$I_o = I_{on} \cdot \cos\theta_z \tag{38}$$

Equation (39) shows how to calculate the main sunshine hour angle (ω_s) and equation (40) shows how to calculate the maximum possible sunshine duration day length (S_o) [55].

$$\omega_s = \cos^{-1}(-\tan\phi \tan\delta) \quad (39)$$

$$S_o = \frac{2}{15}\omega_s \quad (40)$$

3.2. Models Used to Estimate Solar Radiation on a Tilted Surface

As mentioned earlier to increase solar income on a horizontal surface, solar plates are placed with a tilt angle. There are lots of different models to calculate total solar energy on a tilted plate. These models can be divided into two main chapter; isotropic sky model and anisotropic sky models. In this section 2 isotropic and 6 anisotropic models will be explained.

3.2.1. Liu and Jordan's Isotropic Sky Model

Isotropic model is one of the simplest models to calculate total solar energy on a tilted surface. This model derived from the simplest and earliest solar model assumption which treats all radiation on a flat plate is direct solar radiation. Isotropic sky model improved this earliest model and considered diffuse and albedo components as well. This model can be understood easily and required calculation steps are simple and straight forward, however, it does not take consider the circumsolar diffuse and horizon brightening components [56]. Figure 17 shows horizon brightening, diffuse from horizon, isotropic diffuse and beam radiation components schematically.

$$I_T = I_{bn} \cdot \cos\theta + I_d \cdot \frac{1+\cos\beta}{2} \quad (41)$$

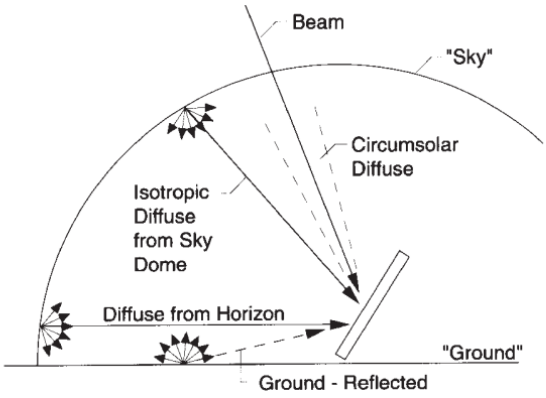

Figure 17. Beam, diffuse and ground reflected radiation on a tilted surface [55].

As explained before, Equation (42) gives monthly total radiation on a tilted surface. To be able to calculate monthly average radiation on a tilted surface Equation (43) can be used. Equation (43) is integrated from Equation 11 which is incidence angle equation. When Equation (36) is integrated from true sunrise to sunset for a surface which has 0° degree zenith angle ($\gamma = 0$). To simplify calculation of $\bar{R}_b$ Duffie and Beckman created some tables for different difference between latitude of the location and tilt angle of surfaces. In Appendix A, $\bar{R}_b$ table which was used for calculation of monthly average radiation on a tilted surface can be seen.

$$\bar{H}_T = \bar{H}_b \bar{R}_b + \bar{H}_d \left(\frac{1+\cos\beta}{2}\right) \tag{42}$$

$$\bar{R}_b = \frac{\cos(\emptyset-\beta)\cos\delta\sin\omega_s' + (\pi/180)\omega_s'\sin(\emptyset-\beta)\sin\delta}{\cos\emptyset\cos\delta\sin\omega_s + (\pi/180)\omega_s\sin\emptyset\sin\delta} \tag{43}$$

$$\omega_s' = min\begin{bmatrix}\cos^{-1}(-\tan\emptyset\tan\delta)\\ \cos^{-1}(-\tan(\emptyset+\beta)\tan\delta)\end{bmatrix} \tag{44}$$

3.2.2. HDKR Model

Klucher (1979) started to work on anisotropic models because Liu and Jordan's model was assuming diffuse solar energy has an isotropic distribution over the sky hemisphere; however, it is not [56], and the first time, he proposed creating and anisotropic model. Hay and Davies (1980) worked on to estimate diffuse energy on a

tilted surface and they assumed circumsolar diffuse radiation is the same in all directions just like beam radiation; however, they did not consider horizon brightening during creating their model. Reindl et al. (1991b) improved this model and add horizon brightening term to Hay and Davies model. Equation 1 shows diffuse radiation on a tilted surface and equation and equation 5 shows total radiation on a tilted surface [56].

$$I_{d_T} = I_d \left\{ (1 - A_i) \left(\frac{1 + \cos\beta}{2} \right) \left[1 + \sin^3 \left(\frac{\beta}{2} \right) \right] + A_i R_b \right\} \tag{45}$$

where;

$$A_i = \frac{I_{bn}}{I_{on}} = \frac{I_b}{I_o} \tag{46}$$

$$R_b = \frac{\cos\theta}{\cos\theta_z} \tag{47}$$

$$\begin{aligned} I_T = I_{bn} \cdot \cos\theta \\ + I_d \left\{ (1 - A_i) \left(\frac{1 + \cos\beta}{2} \right) \left[1 + f \sin^3 \left(\frac{\beta}{2} \right) \right] \right. \\ \left. + A_i R_b \right\} \end{aligned} \tag{48}$$

3.2.3. Perez Model

Perez et al. [5] worked on anisotropic sky diffuse models and enhanced HDKR model by considering both circumsolar diffuse and horizon brightening. Shortly, Perez divided sky into two pieces to check diffuse component of solar radiation. Perez model is more complex than previous models because of circumsolar diffuse and horizon brightness terms. Equation (49) shows diffuse radiation on a tilted surface and equation (54) shows total solar radiation on a tilted surface for Perez model.

Table 24. Brightness coefficient for Perez Anisotropic Sky Model [5].

Range of ε	f_{11}	f_{12}	f_{13}	f_{21}	f_{22}	f_{23}
1-1.065	-0.008	0.588	-0.062	-0.060	0.072	-0.022
1.065-1.230	0.130	0.683	-0.151	-0.019	-0.066	-0.029
1.230-1.5	0.330	0.487	-0.221	0.055	-0.064	-0.026
1.5-1.95	0.568	0.187	-0.295	0.109	-0.152	0.014
1.95-2.8	0.873	-0.392	-0.362	0.226	-0.462	0.001
2.8-4.5	1.132	-1.237	-0.412	0.288	-0.823	0.056
4.5-6.2	1.060	-1.600	-0.359	0.264	-1.127	0.131
6.2-∞	0.678	-0.327	-0.250	0.156	-1.377	0.251

$$I_{d_T} = I_d \left[(1 - F_1) \left(\frac{1 + \cos \beta}{2} \right) + F_1 \frac{a}{b} + F_2 \sin \beta \right] \tag{49}$$

where;

$$a = \max(0, \cos \theta), \qquad b = \max(\cos 85 , \cos \theta_z)$$

$$\varepsilon = \frac{\frac{I_d + I_{b_n}}{I_d} + 5.535x10^{-6}\theta_z^3}{1 + 5.535x10^{-6}\theta_z^3} \tag{50}$$

where; θ_z terms are in degree.

$$F_1 = max \left[0, \left(f_{11} + f_{12}\Delta + \frac{\pi \theta_z}{180} f_{13} \right) \right] \tag{51}$$

$$F_2 = \left(f_{21} + f_{22}\Delta + \frac{\pi \theta_z}{180} f_{23} \right) \tag{52}$$

where;

$$\Delta = \frac{I_d}{I_{o_n}} \tag{53}$$

$$I_T = I_b R_b + I_d (1 - F_1) \left(\frac{1 + \cos \beta}{2} \right) + I_d F_1 \frac{a}{b} + I_d F_2 \sin \beta \tag{54}$$

3.2.4. Muneer Model

This model derived by Muneer, T. [57] after he checked 5 different models which estimates solar radiation on a tilted surface, and he did this checking for 5 different locations from middle Europe. One of the models that he used was belong to him and after that he derived his own model to find final version of his model. Muneer [57] considers illuminated planes and shaded planes separately. Additionally, he divides illuminated planes according sky cloudiness. Equation (55) shows how to calculate diffuse radiation on a tilted plane according to Muneer model. This equation is for planes illuminated under a cloudy sky. This equation is more sophisticated than Muneer's under cloudy sky model and only this equation will be checked [57].

$$I_{d_T} = I_d \left[cos^2\left(\frac{\beta}{2}\right) + \frac{2b}{\pi(3+2b)}\left(\sin\beta - \beta\cos\beta - \pi sin^2\left(\frac{\beta}{2}\right)\right)\right](1 - A_i) + I_d A_i R_b \quad (55)$$

Where;

$$\frac{2b}{\pi(3+2b)} = 0.04 - 0.82A_i - 2.026A_i^2 \quad (56)$$

3.2.5. Skartveit Olseth Model

Skartveit Olseth model usually works better for overcast weather conditions because creating this model used measurements collected from Bergen, Norway [57]. Equation (57) shows how to calculate diffuse radiation on a tilted surface. Last term of this equation (S) represents possible slashing which may block sunlight. However, this term is usually neglected because most of the solar station or solar data collection devices are placed to open terrains without any blocking item around [57].

$$I_{d_T} = I_d \left[A_i R_b + Z \cos\beta + (1 - A_i - Z) \left(\frac{1 + \cos\beta}{2} \right) - S \right] \qquad (57)$$

where; S will be neglected and

$$Z = \max(0, \quad 0.03 - 2A_i) \qquad (58)$$

3.2.6. Hay and Davies Model

In this model diffuse solar radiation is divided into two portions by Hay and Davies; isotropic and circumsolar portions solar radiation [57]. Horizon brightening term is not considered in this model. A_i term represents transmittance through atmosphere for DNI. Anisotropic portion of this model treats some portion of the DHI is circumsolar and rest of the DHI is assumed isotropic. Equation (59) shows how to estimate DHI on a tilted surface and Equation (60) shows how to estimate total solar irradiation which is incident on a tilted plane.

$$I_{d_T} = I_d \left[A_i R_b + \left(\frac{1 + \cos\beta}{2} \right) (1 - A_i) \right] \qquad (59)$$

$$I_T = I_{bn} \cdot \cos\theta + I_d \left[A_i R_b + \left(\frac{1 + \cos\beta}{2} \right) (1 - A_i) \right] \qquad (60)$$

3.2.7. Reindl Model

Reindl et al. [58] enhanced Hay and Davies [57] by adding horizon brightening term into their model. Reindl model accounts for isotropic diffuse, circumsolar radiation and horizon brightening while estimating solar radiation which is incident on a tilted plate. Equation (61) shows how to estimate DHI on a tilted plate and Equation (63) shows how to estimate total solar radiation which is incident on a plate.

$$I_{d_T} = I_d \left[(1 - A_i) \left(\frac{1 + \cos\beta}{2} \right) \left(1 + f sin^3 \left(\frac{\beta}{2} \right) \right) + A_i R_b \right] \qquad (61)$$

where;

$$f = \sqrt{\frac{I_b}{I}} \tag{62}$$

$$I_T = I_{bn} \cdot \cos\theta + I_d \left[(1 - A_i) \left(\frac{1 + \cos\beta}{2} \right) \left(1 + f sin^3 \left(\frac{\beta}{2} \right) \right) + \right] + I_d A_i R_b \tag{63}$$

3.2.8. Badescu's Isotropic Model

Badescu assumes solar radiation distributes evenly in the sky just like Liu and Jordan and in for his model he proposed a view factor to estimate diffuse solar radiation which is incident on a tilted plate. Equation (64) and equation (65) show how to estimate diffuse and total solar radiation which are incident on a tilted surface respectively [47].

$$I_{d_T} = I_d \left(\frac{3 + \cos 2\beta}{4} \right) \tag{64}$$

$$I_T = I_b R_b + I_d \left(\frac{3 + \cos 2\beta}{4} \right) \tag{65}$$

3.3. Energy Production from a PV Power Plant

PV power plants converts solar energy to electricity and how much energy will be produced directly related with solar income. PV modules can not convert all the energy receives on them; they can only convert some of the solar income to electricity. Ratio between energy receives on a PV module and energy converted to electricity is called conversion efficiency. Energy production from a PV module depend on solar income, conversion efficiency of module and area of module. Efficiency is the most important factor for PV modules because as the efficiency of a module changes, amount of electrical energy production changes. Efficiency of modules depends on temperature of cells of module which is called cell temperature. When cell temperature exceeds reference cell temperature, efficiency of the modules decreases. Equation (66) shows

how to calculate cell temperature, Equation (67) shows how to calculate efficiency of a PV module, and Equations (68) and (69) show how to calculate energy production from a PV module and total energy production of a PV power plant respectively [59].

$$T_{cell} = T_{amb} + \left(NOCT - T_{ref}\right)\frac{G_{tilted}}{G_{ref}} \tag{66}$$

$$\eta = \eta_{ref}[1 - \beta(T_{cell} - T_{stc})] \tag{67}$$

$$E_{generated} = G_{tilted} \cdot \eta \cdot Area\ of\ module \tag{68}$$

$$E_{generated_{total}} = G_{tilted} \cdot \eta \cdot Area\ of\ module \cdot Number\ of\ modules \tag{69}$$

where; T_{cell} is cell temperature, T_{amb} is ambient temperature, $NOCT$ is nominal operating cell temperature, T_{ref} is reference temperature, η_{ref} is reference efficiency of module, β is temperature coefficient and T_{stc} is test temperature. $NOCT$, T_{ref}, G_{ref}, η_{ref}, β and T_{stc} are module properties, these values will be shown is Section 3.4. for PV modules which are used in METU NCC PV power plant.

3.4. Data Collection Process and Important Information of METU NCC Solar Power Plant

To be able to calculate solar energy on tilted surfaces with different solar models, GHI, DNI and DHI readings were collected from METU NCC solar station. Figure 18 shows METU NCC solar station. This station was already available on the campus, and it was consisted of a Kipp & Zonen, SOLYS2 sun tracker, a Kipp & Zonen, CHP 1 pyrheliometer and two Kipp & Zonen CMP-10 pyranometers. Data collected with these devices were recorded for 10 minutes interval with a Campbell Scientific, CR800 data logger. Additionally, in another station in the campus ambient temperature was measured with a Kintech, Galtech KPC 1/5 thermometer with 10 minutes interval and

temperature readings again collected in the same data logger. These recorded data were transferred in Microsoft Excel to calculate the required results. This station was only able to measure DNI and GHI, because the station did not consist a shading ball. Shading ball blocks direct solar radiation (DNI) which is not received by pyranometer, thus, the pyranometer only measures DHI. To be able to measure DHI, a shading ball was added to this solar station. Shading ball system was manufactured in METU NCC machine shop from aluminum profiles according to original shading ball structure dimensions. Figure 19 and Figure 20 show the solar station with the manufactured shading ball assembly. As it is shown in the figures, shading ball blocks DNI and one of the pyranometer of solar station measures only DHI.

Figure 18. METU NCC solar station without shading ball.

Figure 19. METU NCC solar station with manufactured shading ball.

Figure 20. METU NCC solar station with manufactured shading ball.

For this study, after shading ball structure manufactured, the station was able to collect GHI, DNI and DHI data. These data collected during November and December in 2017. Actual intention for data collection period was at least one year but at the beginning of 2018 a storm hit the solar station and damaged the pyranometer which

measures DHI was broken. Because of this reason, the data collection period was limited with 2 months. After shading ball structure completed, for the first two days in every two-hours solar station was checked physically to see whether pyranometer which measured DHI was under the shade due to the shading ball structure. Additionally, all of the GHI and DHI data which were collected with 10-minute intervals checked and none of the DHI readings was higher than GHI readings collected at the same time. Thanks to this double check, it is certain that shade of the added structure was always on pyranometer which measures DHI.

Figure 21 shows aerial view of 1 MW solar power plant in METU NCC. This power plant consists of 4000 Axitec polycrystalline solar modules, each has a rated power of 250 W. The energy production from a PV module is given in the previous section and requires properties, such as $NOCT$ is 45 ℃, T_{ref} is 20 ℃ , G_{ref} is 800 W/m^2, η_{ref} is %15.37, β is 0.0044 and T_{stc} is 25 ℃ [60].

Figure 21. Aerial view of METU NCC solar power plant.

CHAPTER 4 – RESULTS AND DISCUSSION

In Chapter 4, important results of this thesis study are presented. In Section 4.1, results for DHI estimation are shown. DHI is calculated with different models and methods to see which of these models give most accurate estimation for Cyprus. In Section 4.2, results for total solar radiation on a tilted surface estimation are shown. Different isotropic and anisotropic models which give accurate results from different locations on earth used to see which models give accurate results for Cyprus. In Section 4.3, energy production estimations for METU NCC power plant are shown and these results will be compared with actual energy production of the PV power plant at METU NCC.

4.1. Results for DHI Estimation with Different Models

According to literature review findings, most of the researchers estimated DHI values with clearness index (k_t) and/or sunshine duration (S). To be able to estimate DHI with the help of k_t and S, some models were derived. These models approximate the ratio between DHI and GHI or the ratio between DHI and G_o. Before making any comparison between measured DHI and estimated DHI from these models, to clarify the relation between measured DHI at METU NCC solar station and clearness index for the campus for the same period, DHI/GHI vs. k_t plot is investigated. Figure 22 shows the comparison of DHI/GHI vs. k_t using the measurement in November and December 2017. Equation of trend-line of this plot and R^2 value are also shown. As a result, it can be said that trend-line equation of Figure 22 can be used to estimate DHI if GHI is known. Importance of this result is that measuring GHI is much easier, common and cheaper than measuring DHI. GHI measurement is available for most of

the location on earth, though DHI measurement is not. Thanks to Equation (70) DHI value can be calculated easily if GHI measurements exist. This graph is plotted for winter measurements and it works well for Cyprus weather conditions during winter. Figure 23 shows the relation between daily average DHI/G_o and k_t. For this comparison extraterrestrial irradiation used and as expected accuracy of this comparison is lower than DHI/GHI comparison. G_o is approximated using an equation and it is assumed constant for each location on earth per day. As the extraterrestrial irradiation does not account for atmospheric conditions, accuracy of DHI estimation decreases. Equation of trend-line and R^2 value are shown in Figure 23 for DHI/G_o. R^2 value for this comparison is 0.481 and Equation (71) shows trend-line DHI/G_o and k_t. Chauvenet criterion applied for both these graphs data set to see if all of these readings are appropriate to use. All of the readings were in suitable limit and none of the readings were disregarded.

$$\frac{DHI}{GHI} = 9.0629k_t^3 - 11.931k_t^2 + 3.1494k_t + 0.7084 \qquad (70)$$

$$\frac{DHI}{GHI} = 2.8116k_t^3 - 5.3485k_t^2 + 2.7543k_t - 0.159 \qquad (71)$$

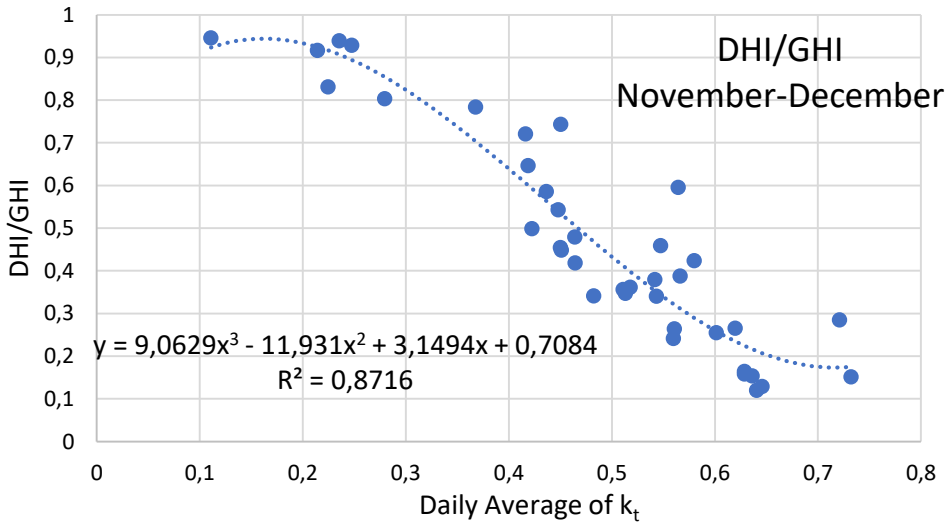

Figure 22. DHI/GHI ratio vs. clearness index (kt) for November and December of 2017.

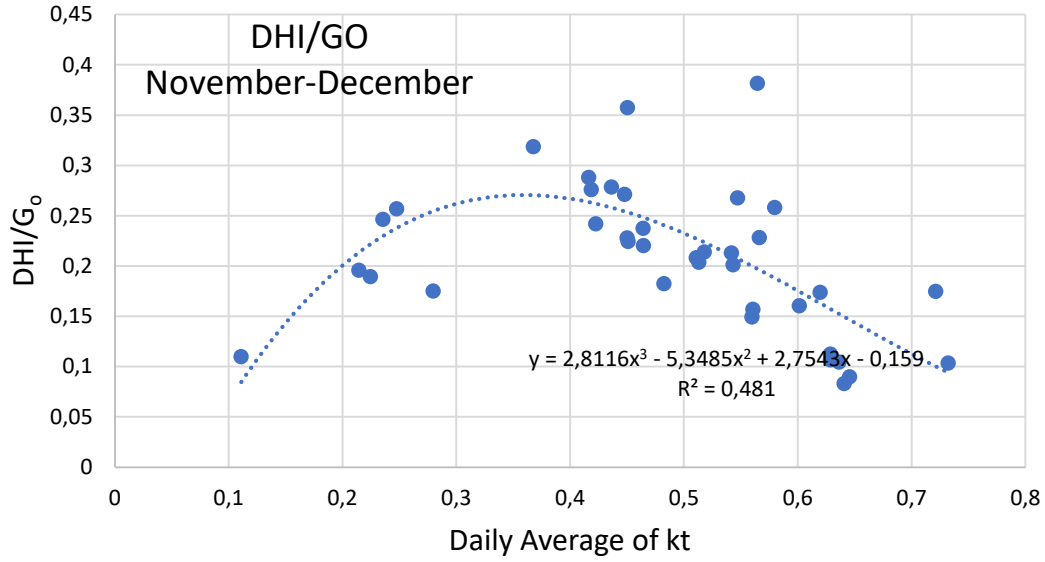

Figure 23. DHI/G_o ratio vs. clearness index (kt) for November and December of 2017.

Table 25, Table 26 and Table 27 show RMSE results between measured DHI and Bailek [8], Bakirci [22] and Ulgen [18] models respectively. Table 28 shows RMSE values for DHI values calculated with Equations (70) and (71). According to these four tables, minimum RMSE among 96 different DHI estimation models belongs to Bailek's 7th model [8] and the second most accurate model is Bailek's 23rd model [8]. Bailek's 7th model use sunshine duration to estimate DHI from G_o; however, for this study there is not enough data to use sunshine duration to estimate DHI, so Bailek's 7th model is not considered. As a result, Bailek's 23rd model is suggested an it will be used in further calculation steps. Bailek's 7th and 23rd models are shown with equation (72) and equation (73) respectively. Figure 24 shows DHI/G_Ovs. k_t in November-December 2017 according to Bailek's 23rd model. As it shown, R^2 value is 0.93 which is higher than R^2 of Figure 22 and Figure 23. Additionally, R^2 value of Bailek's 23rd which is calculated with Cyprus's winter condition is higher than R^2 value of authors of Bailek (2018) got in Algeria weather conditions. As a conclusion Bailek's 23rd model is the second most suitable model to estimate DHI in Cyprus winter conditions,

but this model will be used for further calculations instead of most suitable model which is Bailek's 7th model.

$$\frac{DHI}{G_0} = 0.555 - 0.447\frac{S}{S_0} \quad (72)$$

$$\frac{DHI}{G_0} = 0.417 - 0.109e^{k_t} \quad (73)$$

Table 25. RMSE values according to measured DHI and estimated DHI with Bailek (2018) models.

Bailek 1	2097	**Bailek 2**	2888	**Bailek 3**	1029	**Bailek 4**	3394
Bailek 5	2298	**Bailek 6**	4888	**Bailek 7**	422	**Bailek 8**	32621
Bailek 9	14447	**Bailek 10**	1567	**Bailek 11**	740	**Bailek 12**	7265
Bailek 13	1959	**Bailek 14**	83245	**Bailek 15**	15089	**Bailek 16**	2079
Bailek 17	2123	**Bailek 18**	4863	**Bailek 19**	865	**Bailek 20**	22142
Bailek 21	23292	**Bailek 22**	1249	**Bailek 23**	850	**Bailek 24**	11209
Bailek 25	2992	**Bailek 26**	6669	**Bailek 27**	8305	**Bailek 28**	2579
Bailek 29	3068	**Bailek 30**	1790	**Bailek 31**	3612	**Bailek 32**	16788
Bailek 33	66300	**Bailek 34**	1703	**Bailek 35**	3362		

Table 26. RMSE values according to measured DHI and estimated DHI with Bakirci (2015) models.

Bakirci 1	2367	**Bakirci 2**	2550	**Bakirci 3**	1488
Bakirci 4	61504	**Bakirci 5**	1579	**Bakirci 6**	4950
Bakirci 17	2988	**Bakirci 8**	2420	**Bakirci 9**	1367
Bakirci 10	1238	**Bakirci 11**	2759	**Bakirci 12**	1340
Bakirci 13	2649	**Bakirci 14**	2834	**Bakirci 15**	5369
Bakirci 22	2194	**Bakirci 23**	2152	**Bakirci 24**	8116
Bakirci 25	1344	**Bakirci 26**	2600	**Bakirci 27**	2535

Table 27. RMSE values according to measured DHI and estimated DHI with Ulgen (2009) models.

Ulgen 1	2367	**Ulgen 2**	3243	**Ulgen 3**	3053	**Ulgen 4**	2382
Ulgen 5	3167	**Ulgen 6**	2117	**Ulgen 7**	951	**Ulgen 8**	1933
Ulgen 9	2219	**Ulgen 10**	2250	**Ulgen 11**	7657	**Ulgen 12**	3279
Ulgen 13	2550	**Ulgen 14**	1709	**Ulgen 15**	1932	**Ulgen 16**	2315
Ulgen 17	29748	**Ulgen 18**	2969	**Ulgen 19**	2526	**Ulgen 20**	2579
Ulgen 21	2785	**Ulgen 22**	2567	**Ulgen 23**	2332	**Ulgen 24**	927
Ulgen 25	15438	**Ulgen 26**	1652	**Ulgen 27**	1973	**Ulgen 28**	1115
Ulgen 29	1354	**Ulgen 30**	2653	**Ulgen 31**	1546	**Ulgen 32**	1603
Ulgen 47	1700	**Ulgen 48**	1358	**Ulgen 49**	1580	**Ulgen 50**	1502
Ulgen 51	1225	**Ulgen 52**	1307	**Ulgen 53**	1195	**Ulgen 54**	1140

Table 28. RMSE values of DHI calculated with trend-line equations of and Figure 22 and Figure 23.

RMSE of Equation (70)	RMSE of Equation (71)
1655.0	2220.5

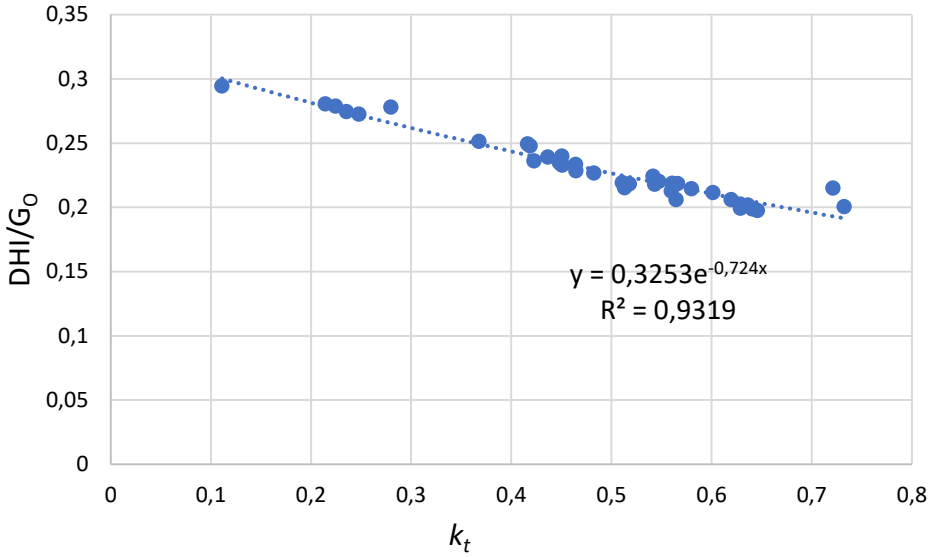

Figure 24. DHI/G_O comparison with clearness index (k_t) according to Bailek's 23rd model for November and December of 2017.

In addition, Figure 25 shows the differences between total daily measured GHI, measured DHI, DHI estimation with Bailek's 23rd DHI estimation model and DHI estimation according to Equations (70) and (71) which are obtained as the trend lines in Figure 22 and Figure 23. According to Figure 25, it can be said that for the days which has minimum 2.5 $\mathrm{kWh/m^2}$ GHI in total, Bailek's 23rd model and models which are shown with Equations (70), (71) overestimates DHI. For sunny days ($GHI > 2.5\,\mathrm{kWh/m^2}$) estimated DHI values are higher than measured DHI value. On the contrary for most of the days which daily total GHI measurement is less than $2.5\,\mathrm{kWh/m^2}$, the same 3 models underestimate DHI value. For most of the days, the closest estimation to measured DHI belongs to Bailek's 23rd model. This model also has the lowest RMSE value among all the DHI models used and derived equation results. It can be seen in Figure 25 if daily total GHI is lower than $2.5\,\mathrm{kWh/m^2}$, the

difference between measured and estimated DHI values is smaller. Estimated DHI values over or underestimating if the daily sum of GHI is higher or lower than $2.5\ \mathrm{kWh/m^2}$, and it should be explained that this threshold value is obtained according to observed data set. For sunny days, DHI component of total solar energy should decrease because there will be less amount of particle in the air to diffuse solar energy and during data collection for model creating, higher DHI values will have higher affect and these models will work better for cloudy or partly cloudy days. DHI estimation is important to calculate total solar energy on a tilted surface if DHI measurements are not available; however, for sunny days, effect of DHI is much less than DNI and GHI components and inaccuracies at DHI estimation will not be too effective on total solar radiation. When all the estimations and measurement results were compared, it is seen that for most of the days models overestimate DHI and overall difference between estimation and actual measurement between DHI is 7%. Also, for sunny days if daily sum of GHI is higher than $2.5\ \mathrm{kWh/m^2}$ models overestimate about 15%, and GHI is lower than $2.5\ \mathrm{kWh/m^2}$, the models underestimate about 9%. If Bailek's model is used to estimate DHI, these differences can be considered to increase estimation accuracy. As a conclusion for this section, 96 models were investigated to estimate DHI from GHI or G_o and most accurate model to estimate DHI was Bailek's 7th model and second most accurate model was Bailek's 23rd model. While calculating total solar energy on a tilted surface, Bailek's 23rd model will be used, not Bailek's 7th model as above mentioned.

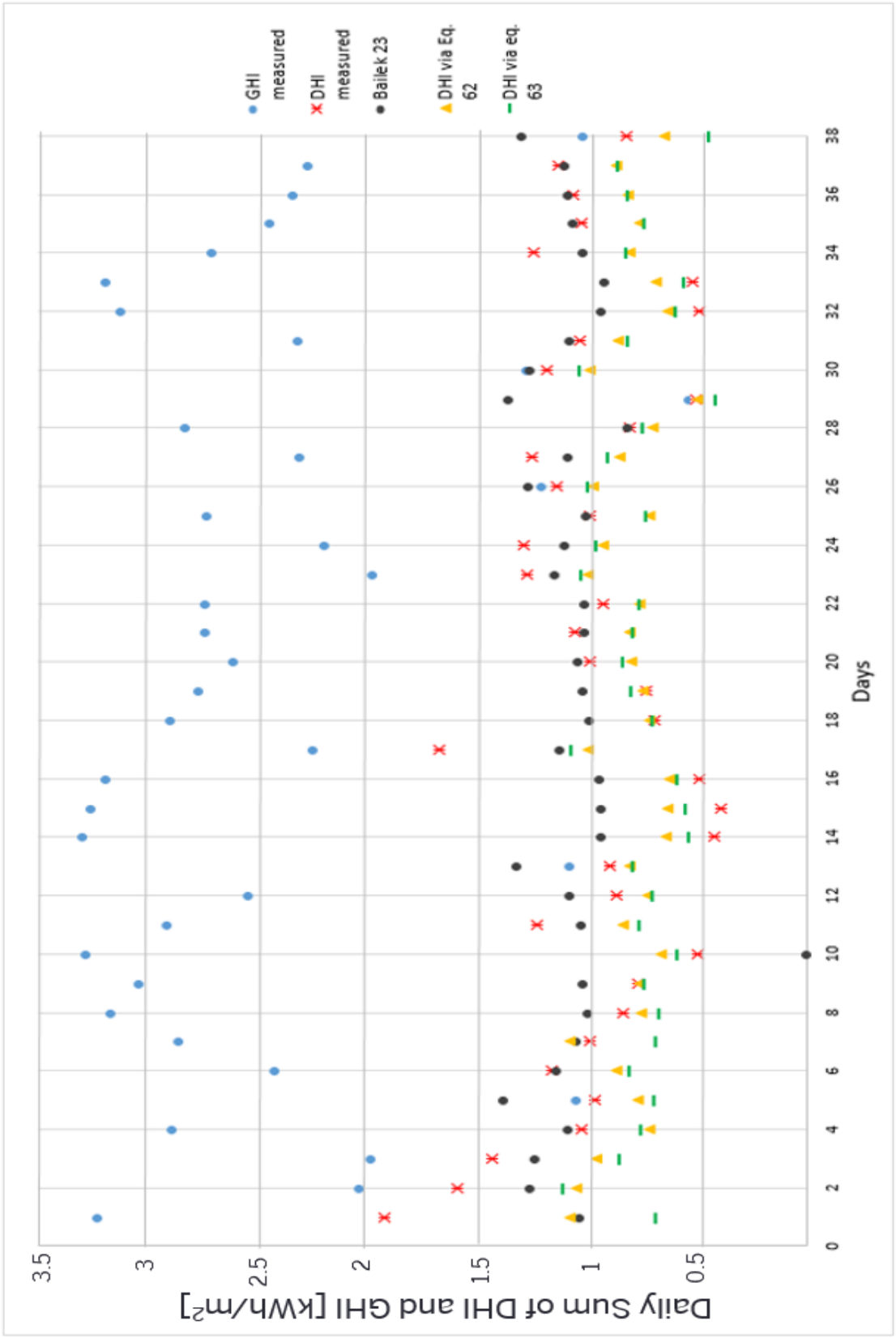

Figure 25. Daily sum of measured GHI, measured DHI and DHI values estimated according to Bailek 23 model and derived equations according to collected data from METU NCC solar station.

4.2. Estimation Results of Total Solar Radiation Which is Incident on a Tilted Plate

Aim of this sectin is to determine accuracies of these models for Cyprus' weather conditions and suggest a model which is suitable to estimate total solar energy which is incident on a tilted plate with a high accuracy. Total solar radiation which is incident on a tilted plate is estimated with 8 different models for weather conditions in Cyprus. To estimate the total tilted solar radiation, DNI and DHI components of solar radiation are required. For this study DNI and GHI and DHI measurements exist, and in addition, DHI is estimated with 3 different ways; Bailek's 23rd model and models created with Equations (70) and (71). Total solar radiation estimations calculated for 8 different models and for each model there are 4 results exist as 4 different DHI data sets exist. For the first method, measured DHI values will be used. For second method, DHI estimation with Bailek's 23rd model will be used. For third and fourth method DHI calculated according to trendline of Figure 22 and Figure 23 will be used.

There are lots of different models and approaches to estimate total solar radiation which is incident on a tilted surface, in this study 2 isotropic models and 6 anisotropic models' results will be compared with solar radiation mesaurement collected in METU NCC with a 30° tilt angle. Isotropic models considered in this study belong to Liu-Jordan [56] and Badescu [47], whereas investigated anisotropic models are Perez [5], Muneer [44], Skartveit-Olseth [57], Hay-Davies [57], Reindll [58], and HDKR . These models were explained in section 3.2. There will be 32 results for 8 different models in total.

To be able to see accuacies of these models, %RMSE values are calculated. Table 29 shows %RMSE results for all hours icluded but Table 30 shows %RMSE results for

without the hours that include sun rise and sun set times. During sun set and sun rise periods, even if there is not DNI or GHI, DHI exists and creates problems during estimation, which is mainly due o the approximation of the sun's position based on mid-hour or end hour considerations in hourly values.. As it is shown in these tables, %RMSE of total solar radiation calculated with $DHI_{measured}$ does not change whether sunrise and sunset hours are included or not but for other DHI methods excluding sunrise and sunset hours decrease %RMSE values.

%RMSE values for each of these 8 models are very close to each other except Muneer model which gives higher %RMSE than others. When sunrise and sunset hours are included to daily total of solar radiation on a tilted surface, %RMSE results are around 18% and when sunset and sunrise hours are not included to daily total of solar radiation on a tilted surface, %RMSE results are around 17% if $DHI_{measured}$ is used in the estimation calculations. If DHI measurements are available along with DNI and GHI measurements, except Muneer model all of these 7 models give almost the same estimation result at winter conditions in Cyprus. Some of these models are much more complex than other however they give almost the same results. For the future studies simpler models like Liu and Jordan's isotropic model [56] or Badescu's isotropic model [47] can be used instead of Perez estimation model [5] which is one of the most sophisticated and complex estimation model.

Table 29. %RMSE results for 8 different models for 4 different DHI includes sun rise and sun set hours.

Models	Type of DHI used			
	$DHI_{measured}$	DHI via Bailek 23rd	DHI via Eqn. (70)	DHI via Eqn. (71)
Liu-Jordan	18%	70%	94%	77%
Badescu	18%	72%	93%	78%
Perez	18%	67%	1374%	71%
Muneer	34%	80%	101%	83%
Skartveit-Olseth	18%	71%	95%	78%
Hay and Davies	18%	71%	95%	78%
Reindl	19%	69%	93%	76%
HDKR	19%	69%	98%	76%

Table 30. %RMSE results for 8 different models for 4 different DHI without sun rise and sun set hours.

Models	Type of DHI used			
	$DHI_{measured}$	DHI via Bailek 23rd	DHI via Eqn. (70)	DHI via Eqn. (71)
Liu-Jordan	17%	68%	72%	74%
Badescu	17%	69%	73%	76%
Perez	17%	65%	68%	68%
Muneer	32%	76%	77%	79%
Skartveit-Olseth	17%	68%	72%	75%
Hay and Davies	17%	68%	72%	75%
Reindl	18%	66%	70%	73%
HDKR	18%	66%	70%	73%

Figure 26 shows daily totals of measured tilted radiation and estimation model results which are calculated with measured DHI. According to the results in the figure, it can be seen most of the models gave close results with the measurements. Muneer model's results are overestimated if daily total tilted radiation measurement is higher than $5\ kWh/m^2$ and underestimated if daily total of tilted radiation is lower than $4\ kWh/m^2$. Muneer model [57] give very close results if daily total of tilted radiaiton is between $4-5\ kWh/m^2$ like other models. For this thesis, lots of different models' estimation results were compared with measurement and almost all of the models gave the same estimation results in daily total base. Some of this models are very complex

and requires lots of calculation steps and data input; however, these complex models give same estimation amount with the simpler models. As a conclusion for this section Liu-Jordan's [56] and Badescu's [47] isotropic models can be used to estimate total solar energy on a a tilted surface with the same accuracy of the most complex models.

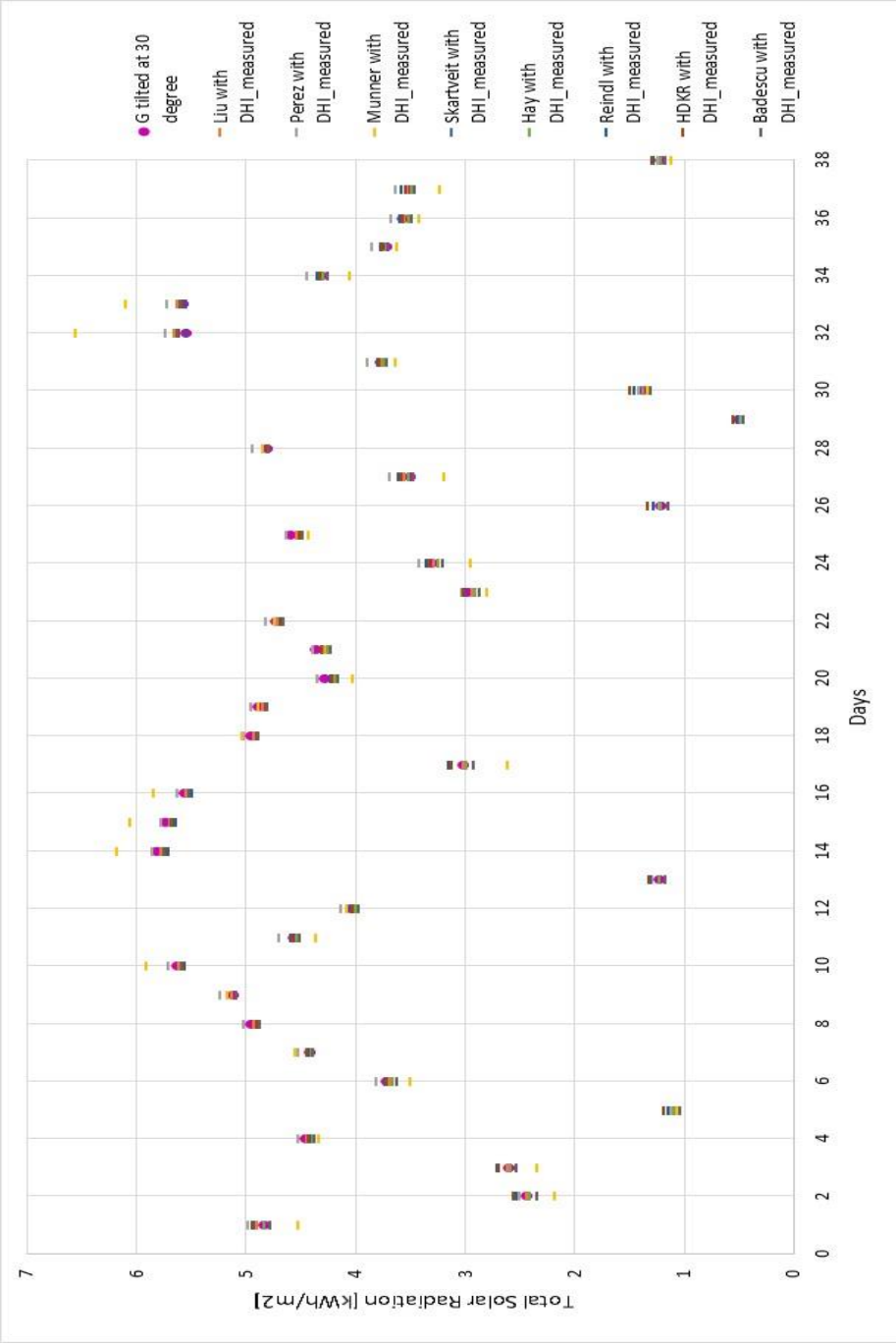

Figure 26. Daily total radiation amounts for estimation models and measured tilted radiation.

4.3. Energy Production Comparison for 1 MW Solar Power Plant in METU NCC

In this section, amount of energy produced from METU NCC PV power plant is compared with energy should be produced according to estimated tilted radiation amount. Energy produced from a PV module is directly related with efficiency of this module. Efficiency of PV modules changes as the cell temperature of PV modules changes. Energy prodction is calculated with 3 different ways; (i) using the measured solar irradiation incident on a 30° tilted pyranometer, (ii) using the estimated solar radiation via Bailek's 23rd model [8], and (iii) using the estimated solar irradiation using the eight different models presented in Section 4.2. First of all, energy production of METU NCC solar power plant is calculated with estimation models of total solar energy on a tilted surface. Total solar energy which is incident on a tilted plate was calculated with 8 different models and T_{cell} and η_{PV} is calculated for each hour for 8 models' results. These calculation steps are repeated for total solar energy on a tilted surface which is calculated with Bailek's 23rd model [3]. Also energy production amount is calculated according to solar energy measured from 30° tilted pyranometer (G_{tilted}) after T_{cell} and η_{PV} values are calculated. All the results are compared with measured energy production and %RMSE value calculated for each model.

Table 31 shows %RMSE values for energy production calculated with three different ways. %RMSE values calculated with measured DHI values are lower than %RMSE values calculated with Bailek's 23rd DHI estimation model. Last coloumn of Table 31 shows %RMSE result of energy production calculated with G_{tilted} measurement collected from a pyranometer tilted 30° in METU NCC solar power plant. %RMSE for this method is 20.34 and models which give a better or very close to this value can

be accepted as accurate models to estimate energy production. Except Perez [5] and Muneer models [57], models give lower %RMSE values than %RMSE value which is showed in Table 31 if G_{tilted} value is calculated with measured DHI however DHI measurement is not available in most of the places on earth. Badescu model [47] gives the lowest %RMSE value for energy production if DHI value is estimated with Bailek's 23rd [8] model. Badescu model [47] is an isotropic model and it is one of the simplest model to estimate total solar energy which is incident on a tilted plate. However, Badescu model [47] shows better accuracy than other models to estimate energy production from a solar power plant. Skartveit [57] and Hay and Davies [57] models also give close results to Badescu model [47], but because of simplicity and better accuracy, Badescu model is suggested rather than other 7 models for winter conditions in Cyprus.

Table 31. %RMSE results of energy production from METU NCC solar power plant which are calculated with measured DHI, DHI via Bailek's 23rd model [8] *and measured* G_{tilted}

Models used to calculate G_{tilted}	%RMSE		
	DHI measured	DHI via Bailek 23rd	Measured G_{tilted}
Liu and Jordan	20.25%	23.73%	
Perez	22.43%	25.75%	
Muneer	21.23%	29.85%	
Skartveit	19.52%	22.87%	20.34%
Hay and Davies	19.52%	22.88%	
Reindl	20.39%	23.23%	
HDKR	20.45%	23.81%	
Badescu	**18.98**%	**22.31**%	

Figure 27 shows daily total energy production amounts for measured energy production and estimation energy production with 8 models. For each day, estiamated energy production amounts are higher than measured energy production. If there will be future investment in METU NCC in energy production from PV power plant and

DHI measurement will be used to to energy production estimation, it should be considered that estimated amount of production will be higher than actual production for all sky conditions (overcast, cloudy and clear). Additionally, Figure 28 shows daily total energy production amounts for measured energy production and estimated energy production which is calculated with G_{tilted} calculated with DHI estimated according to Bailek's 23rd model [8]. Acording to the results shown in this figure, estiamted energy production is usually higher than real production amount. For example, daily summation of GHI is lower than $8\ kWh/m^2$ for days 5, 13, 26, 29, 30 and 38 and estimated energy amount for 8 models' G_{tilted} is higher than measured production in these days. Similar to that, models overestimated the energy production for days 7, 8, 9, 10, 14, 15, 16, 32 and 33 when daily summation of GHI is higher than $16\ kWh/m^2$. Energy prodution is overestimated when G_{tilted} is calculated with DHI estimation of Bailek's 23rd model [8] for overcast and clear sky conditions. However, models give close results measured to actual energy production result for partly cloudy days. For the days which has $8-11\ kWh/m^2$ of daily total GHI is observed, estimated energy production and actual energy production results are close. One possible reason of getting more accurate results during partly cloudy day is that effect of diffuse fraction is mediocre when compared to cloudy and clear days in which effect of diffuse is too much or too less. Thus, this effect drops the accuracy of models during cloudy or clear days.

For estimated energy production with each method, ineffiencies in inverters and losses at cables were not considered, when they considered %RMSE values are expected to decrease more and accuracies of these models will increase.

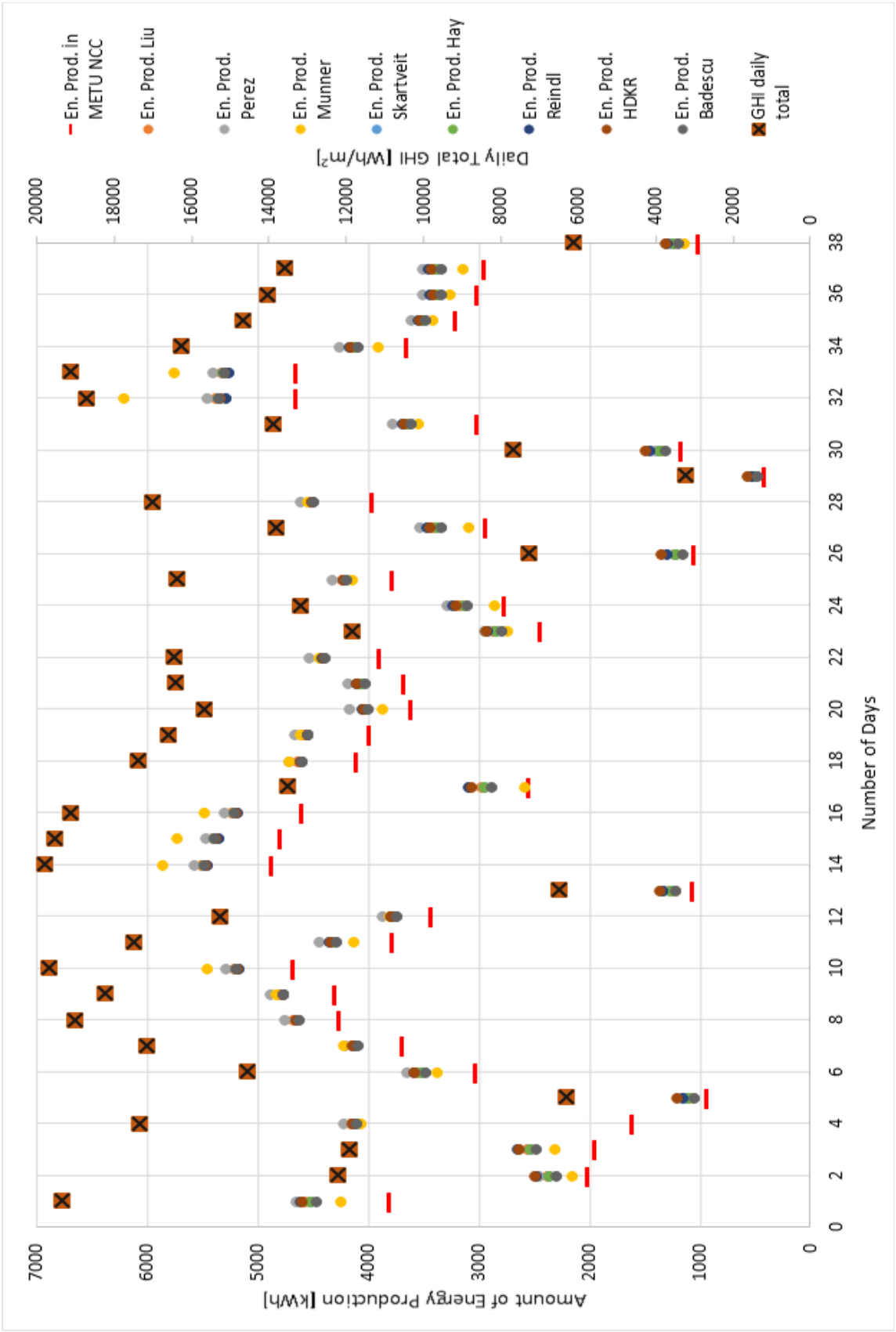

Figure 27. Daily total energy production comparison for different days with G_{tilted} calculated with measured DHI.

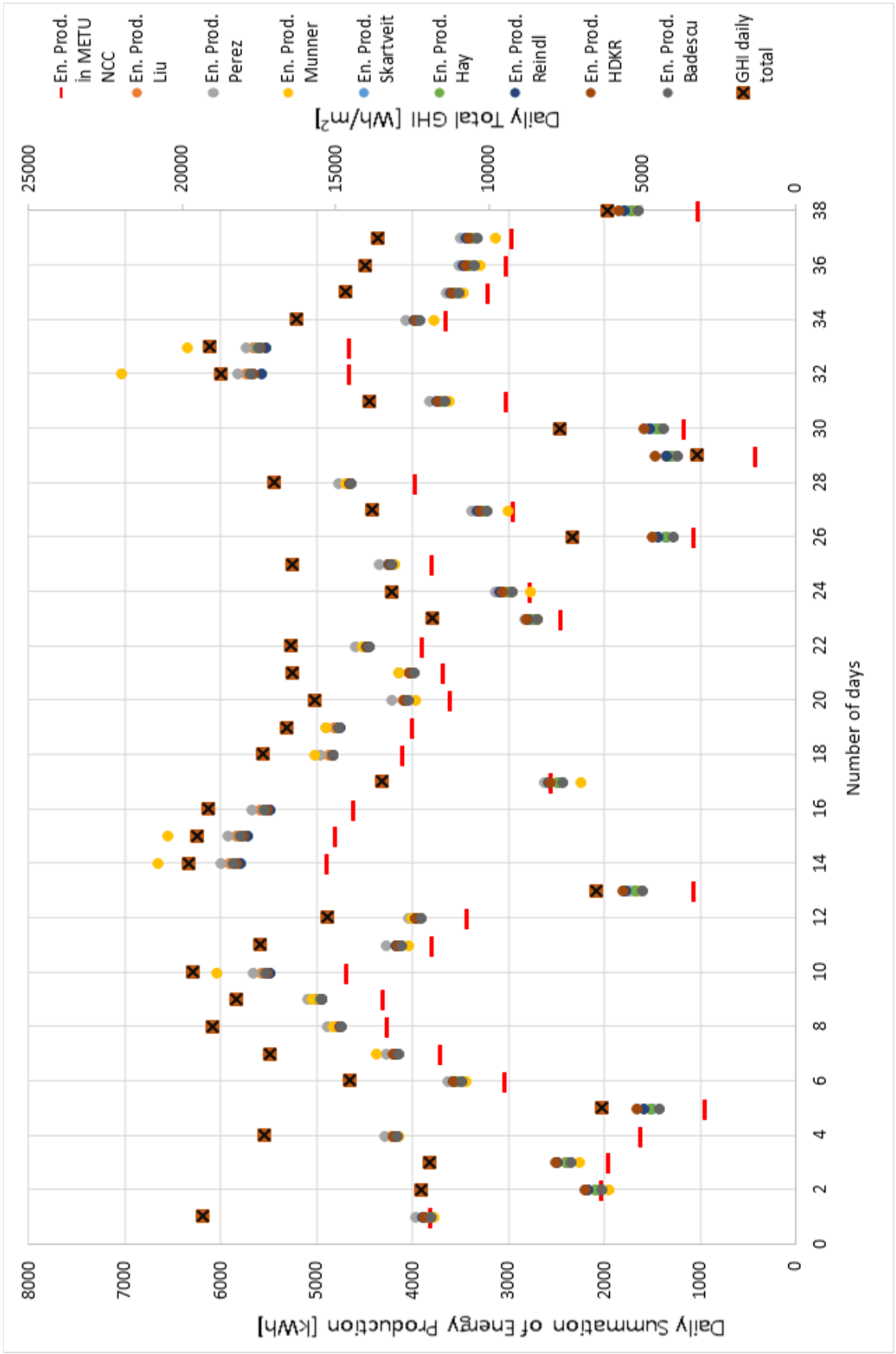

Figure 28. Daily total energy production comparison for different days with G_{tilted} calculated with Bailek's 23rd DHI model.

One of the possible outcome of this thesis is to see how accuracy changes while estimating energy production from estimated total radiation on a tilted PV module. To see that, %RMSE values are calculated between measured energy production and energy production estimation according to estimated total radiation on a tilted PV module. Table 32 shows %RMSE values in two coloumns. First coloumn shows %RMSE values which are calculated between energy production estimation calculated with measured G_{tilted} and energy production estimation with G_{tilted} calculated with $DHI_{measured}$. Second coloumn shows %RMSE values which are calculated between energy production estimation with measured G_{tilted} and energy production estimation with G_{tilted} calculated using DHI estimated with Bailek's 23rd model [13]. Table 29 and Table 30 show %RMSE values between total irradiation measurement from a 30° tilted pyranometer and estimations for same measurement with different models. %RMSE values in Table 32 are much lower than %RMSE showed in Table 29 and Table 30. This comparision shows that even if there is a difference between estimated radiation which is incident on a tilted plate and total radiation measurement from a tilted surface, these difference gets smaller when these values are used for energy production estimation. Total radiation which is incident on a tilted plate changes efficiency of PV modules. Losses on cables and on other devices which are placed in a solar power plant systems cause energy loss but these losses did not include to calculations in this study. According to Table 32 if DHI measurements from a horizontal surface are available, Liu and Jordan's isotropic model [56] gives the most accurate result while calculating energy production. If DHI measurements are not available it should be estimated with Bailek's 23rd model because it gives the most accurate result among the models which are compared in this study. After DHI estimation is completed, Reindl [58] or Badescu [8] models can be used to get most

accurate energy production estimation. Badescu model is one of the simplest model to estimated total radiation which is incident on a tilted plate, however this model usually gives the most accurate results for winter weather conditions in Cyprus.

Table 32. %RMSE between energy production estimation from G_{tilted} which is calculated with measured DHI and with Bailek's 23rd model [8] *and measured energy production.*

Model	Type of DHI used	
	Measured DHI	DHI via Bailek 23rd
Liu-Jordan	0.97%	7.87%
Badescu	1.81%	7.52%
Perez	2.4%	8.31%
Muneer	6.63%	15.1%
Skartveit-Olseth	1.28%	7.66%
Hay and Davies	1.28%	7.66%
Reindl	1.76%	7.44%
HDKR	1.79%	8.22%

As a conclusion for this section, Bailek's 23rd model [13] is the most accurate model to estimate DHI and Liu and Jordan [56] and Badescu [47] isotropic models give very accurate and close results to each other. One of these two models can be used to estimate total solar radiation which is incident on a tilted plate for winter weather conditions in Cyprus. After these estimations are done, energy production estimation from a PV solar power plant can be completed succesfully.

CHAPTER 5 – CONCLUSIONS

Solar energy is a clean and reliable source to satisfy some portion of the total energy demand of the World but energy production and solar income should be determined in advance to maintain energy stability. To maintain this stability estimating energy producting with a high accuracy is a must. For this study, the main point of interest is estimation of the energy production of PV solar power plants. PV modules produce electrical energy after some chemical reactions but to do that they need solar energy. Amount of total radiation which is incident on a plate directly affect energy production. To be able to estimate energy production, solar radiation which is incident on plate should be known. Solar radiation on a plate has three components; Direct normal irradiation, global irradiation and diffuse irradiaiton. Global radiation measurement is usually available from different locations on earth but direct and diffuse component usually are not available. To fiil this gap, it has been tried to find most accurate estimation way for Cyprus weather conditions. Thanks to this experimental setup, METU NCC solar station collects GHI, DNI and DHI readings. In addition to this setup, METU NCC has a 1 MW solar power plant which has 4000 250W PV modules in it. PV modules in this power plant has a constant tilt angle which is 30° and looking directly thorugh south in this power plant there is a pyranometer placed with 30° and this pyranometer measures total solar radiation which incident on these PV modules. These measurements are not available for most of the locations on earth and to be able to estimate solar radiation which is incident on horizontal or tilted plate there are models which estimates DHI and total radiation on a tilted surface.

There are lots of different models to estimate diffuse component of solar radiation on a horizontal plate. Models in the literature has been searched and most appliacable models for Cyprus has been determined. These models use clearness index or sun shine duration to find the ratio between diffuse component of solar irradiation and global horizontal irradiation or the ratio between diffuse component of solar irradiation and extraterrestrial irradation. Estimated DHI values were compared with DHI measurement collected from METU NCC solar station. %RMSE values were calculated for this models and most accurate model to estimate DHI was Bailek's 23rd model for Cyprus winter weather condition. In addition to literature research to determine models can be applied for Cyprus weather conditions to estiamte DHI, with collected DHI measurements from METU NCC solar station, two different models have been established. These two models created with 38 days data. %RMSE values of these two models were around 70% which is considereded inaccurate. These models created with 38 days measurement this time period is not enough to establih an accurate model we could not do it. Expectation was to collect than more than 1.5 year DHI data from this solar station however, the solar station was damaged in a storm and pyranometer which measures DHI was out of order. If there was a longer period of to measure DHI, created model would be much more accurate than present accuracy which is around 70%.

For the second part of this thesis, models to estimate total solar irradiation which is incident on a tilted plate were checked. There are lots of models to estimate total solar radiation on a tilted plate however some of this model are not very accurate for Cyprus weather conditions. Lots of models from literature have been found and accuracy of this models for Cyprus has been determined. After the required literature research have been completed, it is decided to use Liu and Jordan, Badescu, Perez, Skartveit and

Olseth, Muneer, Hay and Davies, Reindl and HDKR model because these models are reliable, used by lots of researcher for different locations and gave accurate results. Some of this models are very complex compare to others. %RMSE values for these models have been calculated and it is observed that for some days simpliest model gave more accurate results than most complicated model which is Perez model. %RMSE for Liu and Jordan model and Badescu were 17% and for Perez model it was slightly higher than 17.1%. While calculating tilted irradiation for Cyprus winter weather conditions isotropic models Liu-Jordan and Badescu gave more accurate results than other models and these isotropic models are very easy to calculate, reliable, easy to follow. In future, these isotropic models can be used to estimate total radiation which is incident on a tilted plate.

For the last part of this thesis study energy production from a solar power plant is checked. Hourly energy production of METU NCC solar power plant is known and these measured production was compared with estimated energy production. Estimated energy production values were calculated for 8 different models' total solar energy which is incident on a tilted surface. According to this comparision just like total solar radiation estimation model results, simpler isotropic models are sightly more accurate than sophisticated anisotropic models. Without considering cables losses, inverter losses and other losses, most accurate model to estimate energy production of a solar power plan in Cyprus during winter time is Badescu model. %RMSE value for this model was around 18% and if we considered mentioned losses, %RMSE for Badescu model should be decreased because real production consider inclued all of the losses but these losses were not considered while calculating theoretical/estimated production amount and result of estimated energy amount was higher than what it should be. If all of these losses should considere %RMSE for all

of these models might decrease at least 5 points. According results all of the models overestimates energy production this result supports than if losses would considered, energy production estimations would be more accurate and for example badescu model's %RMSE value might be 13% or less. As mentioned earlier METU NCC solar station has a tilted pyranometer and energy production amount is calculated for these measurement and compared with estimated production amount which are calcualted according to the 8 models' total titled radaition estimation. %RMSE difference between tilted irradaiation measurement and models' estimation was changing between 17% and 32% however, %RMSE for energy production estimation with tilted measurement and estimated total tilted irradiaition amount were around 1-2%. This shows that accuracy of tilted radiation estimation and accuracy of energy production estimation differs from each other. %RMSE difference between most accurate and least accurate model was around 7% and if do not consider Muneer model which is the least accurate model, difference is less than 1% for most accurate and least accurate models. It can be concluded that to estimate energy production importance of models which estimates total irradiation on a tilted plate is getting smaller.

For the future, it can be suggested that with more DHI data collection, a better model to estimate DHI for Cyprus can be created. This created model can be used for Southern Turkey, North Africa, West of Middle East. These areas are rich by solar income and with accurate estimations more reliable and more economic power plants and grid can be built. Moreover, collecting data for a longer period can be suggested. With a longer data collection period estimation accuracy would be higher or created model to estimate DHI would give more accurate estimation results for Cyprus. Additionally, another suggestion for the future is that using another software to obtain curve fitting lines and equations of them. In this study, Microsoft Excel is used to do

curve fitting; however, Matlab software has more advanced tools to check these data, with that software more advanced equation and more accurate estimations can be obtained.

REFERENCES

[1] C. D. Woodroffe *et al.*, "Differences in benthic fauna and sediment among mangrove (Avicennia marina var. australasica) stands of different ages in New Zealand," *Estuar. Coast. Shelf Sci.*, vol. 56, no. May, pp. 581–592, 2007.

[2] N. L. Panwar, S. C. Kaushik, and S. Kothari, "Role of renewable energy sources in environmental protection: A review," *Renew. Sustain. Energy Rev.*, vol. 15, no. 3, pp. 1513–1524, 2011.

[3] H. Li, W. Ma, X. Wang, and Y. Lian, "Estimating monthly average daily diffuse solar radiation with multiple predictors: A case study," *Renew. Energy*, vol. 36, no. 7, pp. 1944–1948, 2011.

[4] S. Ibrahim, I. Daut, Y. M. Irwan, M. Irwanto, N. Gomesh, and Z. Farhana, "Linear regression model in estimating solar radiation in perlis," *Energy Procedia*, vol. 18, no. September 2015, pp. 1402–1412, 2012.

[5] R. Perez, R. Seals, P. Ineichen, R. Stewart, and D. Menicucci, "A new simplified version of the perez diffuse irradiance model for tilted surfaces," *Sol. Energy*, vol. 39, no. 3, pp. 221–231, Jan. 1987.

[6] L. Al-Ghussain, O. Taylan, and M. Fahrioglu, "Sizing of a Photovoltaic-Wind-Oil Shale Hybrid System: Case Analysis in Jordan," *J. Sol. Energy Eng. Trans. ASME*, vol. 140, no. 1, pp. 1–12, 2018.

[7] C. K. Pandey and A. K. Katiyar, "A comparative study to estimate daily diffuse solar radiation over India," *Energy*, vol. 34, no. 11, pp. 1792–1796, 2009.

[8] N. Bailek *et al.*, "A new empirical model for forecasting the diffuse solar radiation over Sahara in the Algerian Big South," *Renew. Energy*, vol. 117, pp. 530–537, 2018.

[9] M. Iqbal, "Correlation of average diffuse and beam radiation with hours of bright sunshine," *Sol. Energy*, vol. 23, no. 2, pp. 169–173, 1979.

[10] S. Barbaro, "Diffuse solar radiation statistics for Italy," *Sol. Energy*, vol. 26, no. 5, pp. 429–435, 1981.

[11] H. Aras, O. Balli, and A. Hepbasli, "Estimating the horizontal diffuse solar radiation over the Central Anatolia Region of Turkey," *Energy Convers. Manag.*, vol. 47, no. 15–16, pp. 2240–2249, 2006.

[12] T. E. Boukelia, M. S. Mecibah, and I. E. Meriche, "General models for estimation of the monthly mean daily diffuse solar radiation (Case study: Algeria)," *Energy Convers. Manag.*, vol. 81, pp. 211–219, 2014.

[13] JainP.C., "A model for diffuse and global irradiation on horizontal surfaces," *Sol. Energy*, vol. 45, no. 5, pp. 301–308, 1990.

[14] A. A. El-Sebaii and A. A. Trabea, "Estimation of horizontal diffuse solar radiation in Egypt," *Energy Convers. Manag.*, vol. 44, no. 15, pp. 2471–2482, 2003.

[15] Y. Jiang, "Estimation of monthly mean daily diffuse radiation in China," *Appl. Energy*, vol. 86, no. 9, pp. 1458–1464, 2009.

[16] S. Tarhan and A. Sari, "Model selection for global and diffuse radiation over the Central Black Sea (CBS) region of Turkey," *Energy Convers. Manag.*, vol. 46, no. 4, pp. 605–613, 2005.

[17] B. Y. H. Liu and R. C. Jordan, “The interrelationship and characteristic distribution of direct, diffuse and total solar radiation,” *Sol. Energy*, vol. 4, no. 3, pp. 1–19, 1960.

[18] K. Ulgen and A. Hepbasli, “Diffuse solar radiation estimation models for Turkey’s big cities,” *Energy Convers. Manag.*, vol. 50, no. 1, pp. 149–156, 2009.

[19] K. Gopinathan, “Diffuse radiation models and monthly-average, daily, diffuse data for a wide latitude range,” *Energy*, vol. 20, no. 7, pp. 657–667, 1995.

[20] P. JK., “The estimation of monthly mean values of daily total short-wave radiation on vertical and inclined surfaces from sunshine records for latitudes 40N-40S,” in *Proceedings of UN conference on new sources of energy*, 1961, pp. 378–90.

[21] B. S. C. G. C. S. L. C. S. E., “Diffuse solar radiation estimation models,” *Sol. Energy*, no. 26, pp. 429–435, 1981.

[22] K. Bakirci, “Models for the estimation of diffuse solar radiation for typical cities in Turkey,” *Energy*, vol. 82, pp. 827–838, 2015.

[23] C. Rensheng, K. Ersi, Y. Jianping, L. Shihua, Z. Wenzhi, and D. Yongjian, “Estimation of horizontal diffuse solar radiation with measured daily data in China,” *Renew. Energy*, vol. 29, no. 5, pp. 717–726, 2004.

[24] K. R. R. Supit I, “A simple method to estimate global radiation,” *Sol. Energy*, vol. 63, no. 3, pp. 147–60, 1998.

[25] D. Yang, “Solar radiation on inclined surfaces: Corrections and benchmarks,” *Sol. Energy*, vol. 136, pp. 288–302, 2016.

[26] Ralph C. Temps, “Solar radiation incident upon slopes of different orientations,” *Sol. Energy*, vol. 19, no. 2, pp. 179–184, 1977.

[27] J.W. Bugler, “The determination of hourly insolation on an inclined plane using a diffuse irradiance model based on hourly measured global horizontal insolation,” *Sol. Energy*, vol. 19, no. 5, pp. 477–491, 1977.

[28] JOHN E. HAY, “Estimating solar irradiance on inclined surfaces: a review and assessment of methodologies,” *Int. J. Sol. Energy*, vol. 3, no. 4–5, pp. 203–240, 1985.

[29] T.M. Klucher, “Evaluation of models to predict insolation on tilted surfaces.,” *Sol. Energy*, vol. 23, no. 2, pp. 111–114, 1979.

[30] M. Steven, “The diffuse solar irradiance of slopes under cloudless skies.,” *Q. J. R. Meteorol. Soc.*, vol. 105, no. 445, pp. 593–602, 1979.

[31] M. Steven, “The angular distribution and interception of diffuse solar radiation below overcast skies,” *Q. J. R. Meteorol. Soc.*, vol. 106, no. 447, pp. 57–61, 1980.

[32] J. E. Hay, “Calculating solar radiation for inclined surfaces: practical approaches,” *Renew. Energy*, vol. 3, no. 4–5, pp. 373–380, 1993.

[33] C. J. Willmott, “On the climatic optimization of the tilt and azimuth of flat-plate solar collectors,” *Sol. Energy*, vol. 28, no. 3, pp. 205–216, 1982.

[34] Pericles S. Koronakis, “On the choice of the angle of tilt for south facing solar collectors in the Athens basin area,” *Sol. Energy*, vol. 36, no. 3, pp. 217–225, 1986.

[35] R. Perez, “An anisotropic hourly diffuse radiation model for sloping surfaces: description, performance validation, site dependency evaluation,” *Sol. Energy*, vol. 36, no. 6, pp. 481–497, 1986.

[36] R. Perez, P. Ineichen, R. Seals, J. Michalsky, and R. Stewart, “Modeling daylight availability and irradiance components from direct and global irradiance,” *Sol. Energy*, vol. 44, no. 5, pp. 271–289, 1990.

[37] A. Skartveit and R. Olseth, “Modelling slope irradiance at high latitudes,” *Sol. Energy*, vol. 36, no. 4, pp. 333–344, 1986.

[38] C. Gueymard, “An anisotropic solar irradiance model for tilted surfaces and its comparison with selected engineering algorithms,” *Sol. Energy*, vol. 38, no. 5, pp. 367–386, 1987.

[39] T. Muneer, “Solar radiation model for Europe,” *Build. Serv. Eng. Res. Technol.*, vol. 11, no. 4, pp. 153–163, 1990.

[40] D. Reindl, W. A. Beckman, and J. A. Duffie, “Evaluation of hourly tilted surface radiation models,” *Sol. Energy*, vol. 45, no. 1, pp. 9–17, 1990.

[41] F. Olmo, J. Vida, I. Foyo, Y. Castro Diaz, and L. Alados-Arboledad, “Prediction of global irradiance on inclined surfaces from horizontal global irradiance,” *Energy*, vol. 24, no. 8, pp. 689–704, 1999.

[42] Y. Tian, R. Davies Collery, P. Gong, and B. Thorrold, “Estimating solar radiation on slopes of arbitrary aspect.,” *Agric. For. Meteorol.*, vol. 109, no. 1, pp. 67–74, 2001.

[43] V. Badescu, “3D isotropic approximation for solar diffuse irradiance on tilted surfaces,” *Renew. Energy*, vol. 26, no. 2, pp. 221–233, 2002.

[44] Z. Li, H. Xing, S. Zeng, J. Zhao, and T. Wang, “Comparison of Anisotropic Diffuse Sky Radiance Models for Irradiance Estimation on Building Facades,” *Procedia Eng.*, vol. 205, pp. 779–786, 2017.

[45] W. Yao, Z. Li, Q. Zhao, Y. Lu, and R. Lu, “A new anisotropic diffuse radiation model,” *Energy Convers. Manag.*, vol. 95, pp. 304–313, 2015.

[46] N. Igawa, Y. Koga, T. Matsuzawa, and H. Nakamura, “Models of sky radiance distribution and sky luminance distribution,” *Sol. Energy*, vol. 77, no. 2, pp. 137–157, 2004.

[47] K. N. Shukla, S. Rangnekar, and K. Sudhakar, “Comparative study of isotropic and anisotropic sky models to estimate solar radiation incident on tilted surface: A case study for Bhopal, India,” *Energy Reports*, vol. 1, pp. 96–103, 2015.

[48] C. K. Pandey and A. K. Katiyar, “Hourly solar radiation on inclined surfaces,” *Sustain. Energy Technol. Assessments*, vol. 6, pp. 86–92, 2014.

[49] J. E. Hay, “Study of short wave radiation on non-horizontal surfaces,” *Sol. Energy*, vol. 23, no. 4, pp. 301–307, 1979.

[50] A. M. Noorian, I. Moradi, and G. A. Kamali, “Evaluation of 12 models to estimate hourly diffuse irradiation on inclined surfaces,” *Renew. Energy*, vol. 33, no. 6, pp. 1406–1412, 2008.

[51] J. E. Hay, “Calculation of monthly mean solar radiation for horizontal and inclined surfaces,” *Sol. Energy*, vol. 23, no. 4, pp. 301–307, 1979.

[52] R. C. Temps and K. L. Coulson, “Solar radiation incident upon slopes of different orientations,” *Sol. Energy*, vol. 19, no. 2, pp. 179–184, 1977.

[53] B. Y. H. Liu, “The interrelationship and characteristic distribution of direct, diffuse and total solar radiation,” *Sol. Energy*, vol. 4, no. 3, pp. 1–19, 1960.

[54] S. Nijmeh and R. Mamlook, “Testing of two models for computing global solar radiation on tilted surfaces,” *Renew. Energy*, vol. 20, no. 1, pp. 75–81, 2000.

[55] J. A. Duffie and W. A. Beckman, *Solar engineering of thermal processes, 1991*. 2001.

[56] T. M. Kl, “EVALUATION OF MODELS TO PREDICT I N S O LATI O N ON TI L TED SURFACES Division of Solar Energy,” no. March, 1978.

[57] D. WŁODARCZYK and H. NOWAK, “Statistical analysis of solar radiation models onto inclined planes for climatic conditions of Lower Silesia in Poland,” *Arch. Civ. Mech. Eng.*, vol. 9, no. 2, pp. 127–144, 2012.

[58] P. G. Loutzenhiser, H. Manz, C. Felsmann, P. A. Strachan, T. Frank, and G. M. Maxwell, “Empirical validation of models to compute solar irradiance on inclined surfaces for building energy simulation,” *Sol. Energy*, vol. 81, no. 2, pp. 254–267, 2007.

[59] S. Dubey, J. N. Sarvaiya, and B. Seshadri, “Temperature dependent photovoltaic (PV) efficiency and its effect on PV production in the world - A review,” *Energy Procedia*, vol. 33, pp. 311–321, 2013.

[60] Axitec, “No Title,” 2017. [Online]. Available: https://www.axitecsolar.com/tr/ev.html.

APPENDIX

Appendix A: $\bar{R}_b$ values which was used for calculation of monthly average radiation on a tilted surface [55].

ϕ	Jan	Feb	Mar	Apr	May	Jun	Jul	Aug	Sep	Oct	Nov	Dec
0	0.59	0.69	0.83	1.00	1.13	1.20	1.17	1.05	0.90	0.74	0.61	0.56
5	0.62	0.72	0.84	0.98	1.09	1.14	1.12	1.03	0.90	0.76	0.65	0.59
10	0.67	0.75	0.86	0.97	1.06	1.10	1.08	1.01	0.90	0.79	0.69	0.64
15	0.72	0.79	0.88	0.97	1.03	1.06	1.05	0.99	0.91	0.82	0.74	0.70
20	0.79	0.85	0.91	0.97	1.02	1.04	1.03	0.99	0.93	0.87	0.80	0.77
25	0.88	0.91	0.95	0.98	1.01	1.02	1.01	0.99	0.96	0.93	0.89	0.87
30	1.00	1.00	1.00	1.00	1.00	1.00	1.00	1.00	1.00	1.00	1.00	1.00
35	1.16	1.11	1.07	1.03	1.00	0.99	0.99	1.02	1.05	1.10	1.15	1.18
40	1.39	1.26	1.15	1.06	1.01	0.98	0.99	1.04	1.11	1.22	1.35	1.43
45	1.72	1.46	1.26	1.11	1.02	0.99	1.00	1.07	1.19	1.39	1.64	1.81
50	2.24	1.75	1.41	1.17	1.04	0.99	1.01	1.11	1.30	1.62	2.08	2.44
55	3.16	2.19	1.60	1.25	1.06	1.00	1.03	1.16	1.44	1.95	2.83	3.63
60	5.17	2.91	1.88	1.34	1.09	1.00	1.04	1.22	1.62	2.47	4.30	6.64
ϕ	Jul	Aug	Sep	Oct	Nov	Dec	Jan	Feb	Mar	Apr	May	Jun